Ayşe DEMİR

M.S. Thesis In Chemistry

September-2010

SYNTHESIS AND BIOLOGICAL INVESTIGATION OF HYDROGENATED AND FLUORINATED AMINO ACID-BASED MOLECULES THAT MAY BIND SPECIFICALLY TO THE ALPHA5/BETA1 INTEGRIN

by

Ayşe DEMİR

September 2010

SYNTHESIS AND BIOLOGICAL INVESTIGATION OF HYDROGENATED AND FLUORINATED AMINO ACID-BASED MOLECULES THAT MAY BIND SPECIFICALLY TO THE ALPHA5/BETA1 INTEGRIN

by

Ayşe DEMİR

A thesis submitted to

the Graduate Institute of Sciences and Engineering

of

Fatih University

in partial fulfillment of the requirements for the degree of

Master of Science

in

Chemistry

September 2010
Istanbul, Turkey

APPROVAL PAGE

I certify that this thesis satisfies all the requirements as a thesis for the degree of Master of Science.

_____
Prof. Dr. Ayhan BOZKURT
Head of Department

This is to certify that I have read this thesis and that in my opinion it is fully adequate, in scope and quality, as a thesis for the degree of Master of Science.

_____	_____
Assist. Prof. Sedat COŞGUN Supervisor	Assist. Prof. Sevim IŞIK Co-Supervisor

Examining Committee Members

Assist. Prof. Dr. Sedat COŞGUN	_____
Assist. Prof. Dr. Sevim IŞIK	_____
Asst. Prof. Dr. Ali Ekrem MÜFTÜOĞLU	_____
Asst. Prof. Dr. Levent SARI	_____
Asst. Prof. Dr. Ramazan ÖZTÜRK	_____

It is approved that this thesis has been written in compliance with the formatting rules laid down by the Graduate Institute of Sciences and Engineering.

_____
Assoc. Prof. Dr. Nurullah ARSLAN
Director

September 2010

SYNTHESIS AND BIOLOGICAL INVESTIGATION OF HYDROGENATED AND FLUORINATED AMINO ACID-BASED MOLECULES THAT MAY BIND SPECIFICALLY TO THE ALPHA5/BETA1 INTEGRIN

Ayşe DEMİR

M.S. Thesis – Chemistry
September 2010

Supervisor: Assist. Prof. Dr. Sedat COŞGUN

Co-Supervisor: Assist. Prof. Dr. Sevim IŞIK

ABSTRACT

Integrins are cell surface receptors that take part in cell – cell adhesion and cell – extracellular matrix (ECM) adhesion events as well as in cell migration and cell signaling. $\alpha_5\beta_1$ integrins are expressed on a wide range among brain tumor cells.

In this study, an intermediate spiroisoxazolinopyrrole of the most specific $\alpha_5\beta_1$ integrin antagonist SJ749 was synthesized. Fischer esterification reaction, Swern oxidation, and Wittig olefination were performed. Next, fluorinated diaminopropionate molecules were synthesized for coupling to SJ749 instead of the (2,4,6-trimethylphenyl) diaminopropionate. At the end, biological evaluation of the molecules synthesized was performed. These assays included cytotoxicity and cell proliferation.

Keywords: SJ749, Peptidomimetic, Integrin, Diaminopropionate, RGD, Astrocytoma

ALFA5/BETA1 İNTEGRİNE BAĞLANMASI OLASI AMİNO ASİT BAZLI HİDROJENLİ VE FLORLU MOLEKÜLLERİN SENTEZİ VE BİYOLOJİK ÖZELLİKLERİNİN İNCELENMESİ

Ayşe DEMİR

Yüksek Lisans Tezi – Kimya
September 2010

Tez Danışmanı: Yrd. Doç. Dr. Sedat COŞGUN

Ortak Tez Danışmanı: Yrd. Doç. Dr. Sevim IŞIK

ÖZ

İntegrinler hücre – hücre adezyonunda ve hücre – ekstraselüler matriks (ESM) adezyonunda rol alan hücre yüzeyi respestörleridirler ki aynı zamanda hücre göçünde ve hücre haberleşmesinde (signaling) yer alırlar. $\alpha_5\beta_1$ integrinler beyin tümor hücrelerinde geniş bir yelpazede bulunur.

Bu çalışmada, en spesifik $\alpha_5\beta_1$ integrin antagonisti olan psödopeptit SJ749 molekülünün spiroizoksazolinopirol ara ürünü sentezlenmiştir. Fischer Esterleşme reaksiyonu, Swern oksidasyonu ve Wittig olefinasyonu reaksiyonları uygulanmıştır. Bunun ardından SJ749'daki (2,4,6-trimetilfenil)sülfonil alaninin olduğu yere kenetlenmek üzere florlu diaminopropiyonat molekülleri sentezlenmiştir. Son olarak da, sentezlenen moleküllerin biyolojik aktiviteleri gerçekleştirilmiştir. Biyolojik testler, A–172 ve U–87 astrositom hücre soylarında sitotoksisite, hücre proliferasyonu ve sitotoksisite mevcutsa apoptoz deneyleridir.

Anahtar Kelimeler: SJ749, Peptidomimetik, İntegrin, Diaminopropiyonat, RGD, Astrositom

This dissertation is dedicated to my dear Mom and Dad, without whom my terrorizing life in graduate school would not have been possible.

ACKNOWLEDGEMENT

I would like to express my appreciation to my supervisor Asst. Dr. Sedat Coşgun for his assistance in not only my research, but also all aspects of the graduate school life, and my co-advisor Asst. Dr. Sevim Işık for assisting me on the biological assays and giving me a new insight on what science actually is and how research is done.

My lab mate Melike Nur Türk deserves my gratitude for her enormous help and great friendship. She was there when I needed help. I also thank to Tuğba Sağır and Nihal Karakaş for performing biological assays, their friendship, and motivation.

Sümeyye Bahçeci has been a cool and awesome friend as well as being my reference book; I owe her great thanks for her contributions to my research by sharing her experiences and helpful thoughts.

Additionally, special thanks to Dr. Burak Esat, head of our neighboring research group for his assistance, and helpful discussions as well as other professors of our department.

I would also like to thank my former lab mates Hilal Doğan, and Muhammed Aydın, for their friendship, help and for sharing their glassware and chemicals.

I am very fortunate to have had the opportunity to be friends with Bahar Birsöz, Şeyda Karaman, Tuba Emnacar Kunduracı, Nebiyyeh Kamacı Dağdeviren, Gülsüm Arıkan, and Zehra Durmuş, who always have accompanied me in my hard and good times in addition to their scientific discussions; along with Nürüfe, Güzin, Ümran, Kuaybe, Beyza, Özge, Deniz, Serhat, Tuğba Ş, Hilal Ş, Esma, Rukiye, Hero and my friends at school, especially in the Departments of Chemistry and Biology

Finally I am grateful to my grandparents and my parents, especially my dear Mom who has always been with me, encouraged me to do better, and supported me; I could not do it without you.

This work was supported by TÜBİTAK (The Scientific and Technological Research Council of Turkey) Project No. 107T627.

TABLE OF CONTENTS

LIST OF SCHEMES

LIST OF TABLES

LIST OF FIGURES

LIST OF SYMBOLS AND ABBREVIATIONS

SYMBOL		ABBREVIATION
NMR	:	Nuclear Magnetic Resonance
FT-IR	:	Fourier Transform Infrared Spectroscopy
ATR	:	Attenuated total reflection infrared
UV	:	Ultraviolet
TLC	:	Thin Layer Chromatography
Ac	:	Acetyl-
$CDCl_3$	:	Deuterated chloroform
δ	:	Chemical shift
D	:	Deuterium
D_2O	:	Deuterated water
Et	:	Ethyl-
EtOAc	:	Ethyl acetate
Me	:	Methyl-
min.	:	minutes
mL	:	milliliter
mmol	:	millimol
ppm	:	Parts per million
T	:	Temperature in Celsius
TBDMS	:	Tert-butyldimethylsilyl
TBDMSCl	:	Tert-butyldimethylsilyl chloride
TFA	:	Trifluoroacetic acid
THF	:	Tetrahydrofuran
TMS	:	Tetramethyl silane
Z	:	Benzyloxy carbonyl-

d4	:	4 deuterated hydrogens
d6	:	6 deuterated hydrogens
s	:	singlet
d	:	doublet
t	:	triplet
q	:	quartet
m	:	multiplet
br	:	broad

CHAPTER 1

INTRODUCTION

1.1. BIOORGANIC AND MEDICINAL CHEMISTRY, RATIONAL DRUG DESIGN AND PEPTIDOMIMETICS

Bioorganic and medicinal chemistry targets understanding life at the molecular level of biological processes, and living organisms, checks the interaction of those with chemical agents and focuses on the molecular interactions in key biological targets such as receptors, channels, enzymes, nucleotides, lipids and saccharides. Medicinal chemistry is probably the oldest approach for the drug discovery. Many of the medicines we use today are products of the search through a best knowledge and application of bioorganic and medicinal chemistry (O'Connor 1993). Major requirements for drug discovery in medicinal chemistry include expertise in synthetic chemistry and pharmacology literature along with the capability of thinking originally; imagining beyond anyone else in this field. Medicinal chemistry, however, much reliance is placed on known compounds. So, a different point of view is needed to be complexed with medicinal chemistry-based drug design.

Apart from medicinal chemistry lies the rational drug design approach. Rational drug design is based on known structures of receptors and and their natural ligands; therefore something can be stated on what the mimic or antagonist molecule should look like. Analytical techniques and theory-based methods such as X-ray crystallography, high-field and high-resolution NMR, computer assisted molecular modeling and quantum mechanics are among these. In our study, however, we have focused on both on peptidic and non-peptidic ligands.

Peptides are small molecules that have numerous advantages from a drug design point of view when compared with proteins and have a wide range of physicochemical and biological properties. Peptides have been used for a very long time for the treatment and diagnosis of diseases. But the growing interest in peptides as therapeutic candidates increased dramatically after 1960s with the development of novel synthesis methods as well as the recombinant DNA (rDNA) technology. Especially after the sequencing methods became available, scientists started peptides synthesis programs based on the results of sequencing already-known peptides in addition to their isolation and characterization (O'Connor 1993).

Non-covalent protein-protein and peptide-protein interactions display a very important role in cellular signaling and immune response (Heckmann 2007). A huge variety of peptides have been discovered and characterized for the last thirty years (Ferrario 2002; Le, Wang et al. 2007). These peptides have antimicrobial properties (Wang YP 2010), anti-cancer characteristics (Lapis 2010), act as neuromodulators and so on. These features make peptides as important targets in drug discovery. Nevertheless, peptide usage has the some limitations:

(a) Side effects resulting from interactions with multiple receptors.

(b) Poor bioavailability because of their high molecular weight lack of transporters.

(c) Poor metabolic stability since peptides face proteolytic degradation in the serum and the gut.

(d) Extensive or moderate clearance by kidneys and the liver (Heckmann 2007).

Peptidomimetics are defined as compounds “whose essential elements (pharmacophore) mimic a natural peptide or protein in 3D space and which retain the ability to interact with the biological target and produce the same biological effect” (Vagner, Qu et al. 2008). Since the dominant position peptide and protein-protein interactions play in molecular recognition and signaling, especially in living systems, the design and synthesis of peptidomimetics are very important.

1.2. INTEGRINS

Since the introduction of the term integrin by Tamkun and Hynes (Tamkun, DeSimone et al. 1986), the field of cellular signaling targeting integrins has become a major search field. Integrins are heterodimeric cell surface glycoproteins that mediate

cell attachment to extracellular matrix (ECM) or to another cell (Barczyk, Carracedo et al. 2010). The main functions of integrins include providing cell adhesion of the cell to the ECM and signaling from the ECM to the cell (Zaidel-Bar, Itzkovitz et al. 2007) while also involved integrins are in binding to cells by certain types of viruses, immune patroling, and cell migration. Apart from their significant roles in cell adhesion and cell migration, signaling by a numerous other receptors such as GPRC (G-protein coupled receptors) and cytokines are governed by integrin mediated interactions. Accordingly, integrins also play roles in several human diseases and integrin antagonists have been designed and evaluated *in vivo* and *in vitro* for a number of diseases involving cancer, arthritis, and some of the antagonists even entered clinical trials (Huveneers, Truong et al. 2007). Integrins have become to be involved in targeting pathological pathways in order to cure diseases. It is thought that targeting integrins may be useful in the diagnosis and/or treatment of the disesase mentioned above.

In animal cells, the part which provides structural support to the cells is the extracellular matrix (ECM). Cells are able to communicate in a very precise manner over short distances by the instructive interface of ECM which act as a physical scaffold for cell positioning and an instructive interface (Heckmann 2007). The ECM in connective tissue is usually more abundant than the cells it surrounds. There are two classes of extracellular macromolecules make up the matrix: (1) polysaccharide chains of the class called glycosaminoglycans (GAGs), which are usually found covalently linked to protein in the form of proteoglycans, and (2) fiber forming “fibrous” proteins which have both structural and adhesive functions: collagen, elastin, fibronectin, laminin, and so on (Alberts 2002). GAGs are unbranched polysaccharide chains of repeating disaccharide units. The two sugars in the disaccharide repeating units are an amino sugar (*N*-acetylglucosamine or *N*-acetylgalactosamine), which is usually sulfated, and the other is a uronic acid (glucuronic or iduronic). GAGs are highly negatively charged. Fibrous proteins, on the other hand, are fibrils or networks on cell surface that produce them by a process that depends on the underlying actin cortex. Fibrous proteins support the matrix and provide surface areas for adhesion. Fibronectin and laminin are examples of large, multidomain matrix glycoproteins.

Cell surface receptors of the integrin family are mediated and integrated in the ECM-dependent communication. Among the several natural recognition motifs of integrin ligands has been the Arg-Gly-Asp (RGD) tripeptide the oldest and the most famous one (Ruoslahti and Pierschbacher 1986). It was even named as the “universal

recognition motif" due to its presence in many ECM proteins like fibronectin, fibrinogen, laminin, etc (Gurrath 2004). Integrin classification can be made based on their ECM: RGD-, LDV-, LDV-binding integrins (αA-domain-containing); αA-domain-containing β1 integrins; and non-αA-domain-containing laminin-binding integrins. In this part, however, we will concentrate on natural and artificial integrin ligands of the integrin α5β1 which either are peptides based on the RGD sequence or non-peptides, or peptidomimetics mimicking RGD.

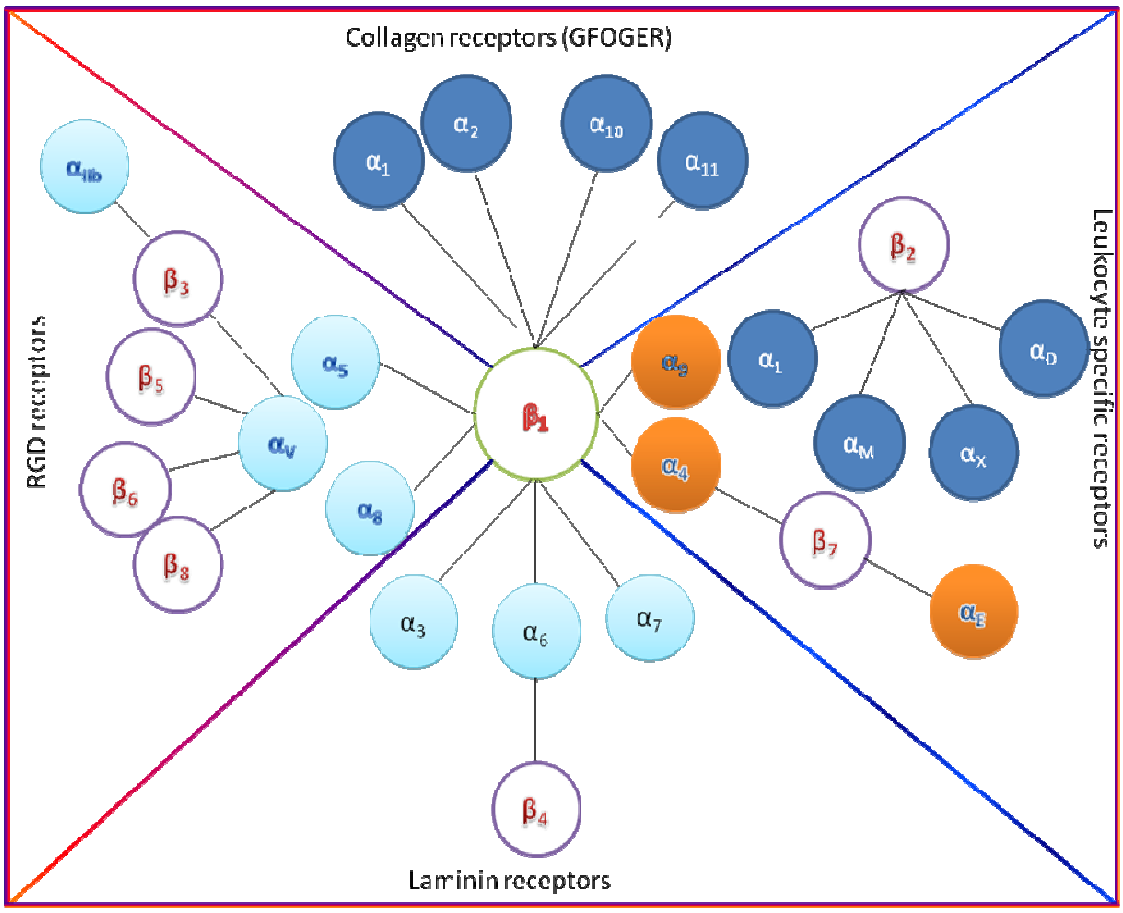

Figure 1.1 *The integrin family:* Combinations of α and β subunits that have been identified on cells up to now. Adapted from Hynes (2002) *Cell* 110: 673–687.

1.2.1.Integrin Structure

In vertebrates are there 18 α and 8 β subunits are encoded which 24 different functional integrin heterodimers bound with non-covalent interactions are known to be generated (Barczyk, Carracedo et al.). An overview on the possible combinations of α and β subunits is shown in Figure 1.1. The *α*- and *β*-subunit extracellular segments have up to 1104 residues and 778 residues respectively. Also, the N-terminal portions of each

subunit combine to form a globular ligand-binding "head" connected to the membrane by a long (~170 Aº) stalk (Arnaout, Mahalingam et al. 2005).

The integrin isoforms are characterized by 75% - 80% sequence identity. However, only a number of integrins (8 out of 24) recognize the RGD sequence in the native ligands.

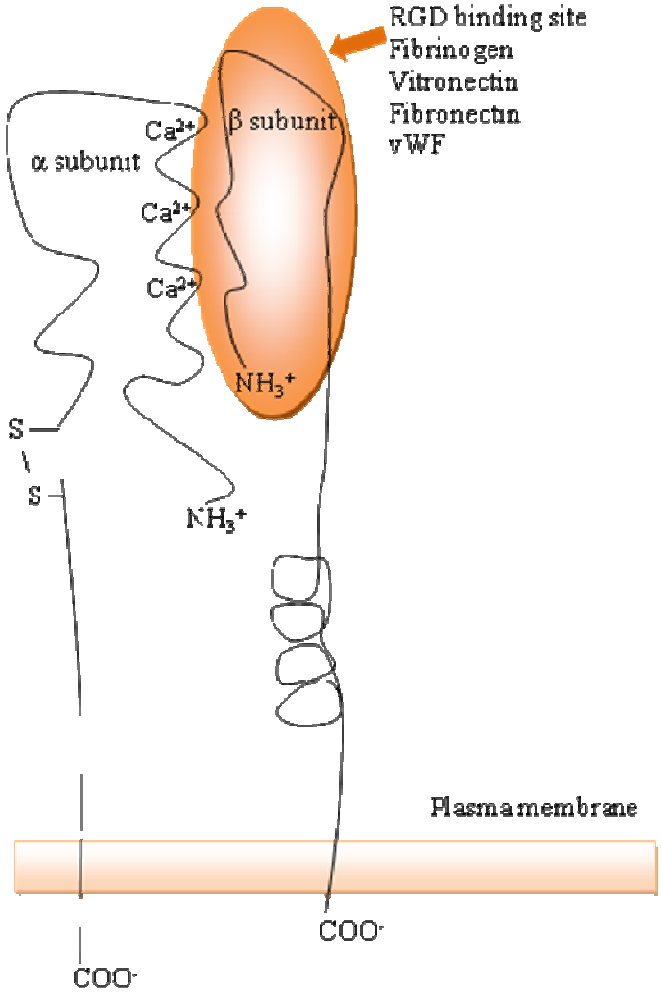

Figure 1.2 Schematic representation of the general structure of an integrin heterodimer and its binding units.

Glycoprotein IIb/IIIa (gpIIb/IIIa, also recognized as integrin αIIbβ3) is an integrin complex found on platelets. The activation of platelets causes changes in platelet shapes and conformational changes in gpIIb/IIIa receptors. Following the platelet activation, the platelet membrane gpIIb/IIIa receptors appear on the platelet surface; "adhesive macromolecule" fibrinogen or fibronectin. GpIIb/IIIa inhibitors are a class of antiplatelet agents used in treating patients who have unstable angina, certain types of

heart attacks such as acute coronary syndromes, acute ischaemic stroke and so on (Patrono and Rocca 2010). GpIIb/IIIa receptor antagonists are anticoagulant drugs that act by blocking platelets although a British group's recent finding has shown that the antiplatelets not only block integrins, but also cause integrin clustering triggered upon binding (Jones, Harper et al. 2010). Synthetic peptides containing the sequence Arg-Gly-Asp, which corresponds to the site of cell adhesion in fibronectin and is also present in the alpha chain of fibrinogen block the binding of gpIIb/IIIa to platelets (Mousa 2002).

Table 1.1 Integrin types, their ligands and their locations.

INTEGRIN	LIGAND	DISTRIBUTION
α5β1	fibronectin	ubiquitous
α6β1	laminin	ubiquitous
α7β1	laminin	muscle
αLβ2	Ig superfamily counterreceptors	white blood cells
α2β3	fibrinogen	platelets
α6β4	laminin	epithelial hemidesmosomes

1.2.2 Arginine-Glycine-Aspartic Acid (RGD)

Many integrin types such as α5β1, α8β1, αIIbβ3, αVβ3, αVβ5, αVβ6 and αVβ8 recognize an Arg-Gly-Asp (RGD) motif within their ligands (Figure 1.3). These ligands are ECM proteins such as fibrinogen, fibronectin, vitronectin, collagen, and laminin (Figure 1.2). RGD present on extracellular matrix proteins is known to be a requirement for binding to cell surface receptor proteins, the integrins. The RGD sequence is vastly recognized by integrins and involves a number of important cellular processes, such as cell anchorage to the extracellular matrix, cell-to-cell communication, cell growth and migration, blood clotting, etc. However, here are also unnatural processes like microbial invasion of cells and tumor metastasis related with some type of ligand-to-receptor binding via the RGD sequence. Small RGD peptides and pseudopeptides mimicking the RGD structure or the binding ligand sequence have been known to competitively bind to cell surface receptors just like the native extracellular matrix proteins do. Therefore,

small RGD peptides and peptidomimetics might be used as antagonists to the extracellular matrix proteins (Barczyk, Carracedo et al. ; Maglott, Bartik et al. 2006; Huveneers, Truong et al. 2007).

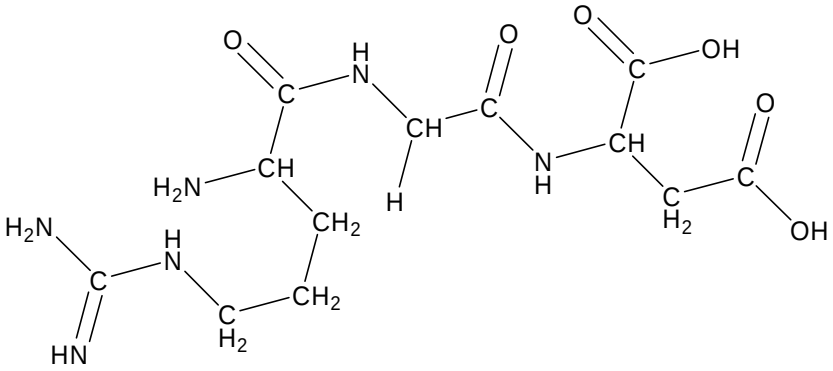

Figure 1.3 Structure of the RGD tripeptide.

The binding region of fibronectin to the integrin is known as Fn-10 (Figure 1.4). Studies have shown that the head piece of integrin α5β1 without a ligand is similar to the ECM region of integrin αVβ3; so based on this information, α5β1 has been modeled (Takagi 2004).

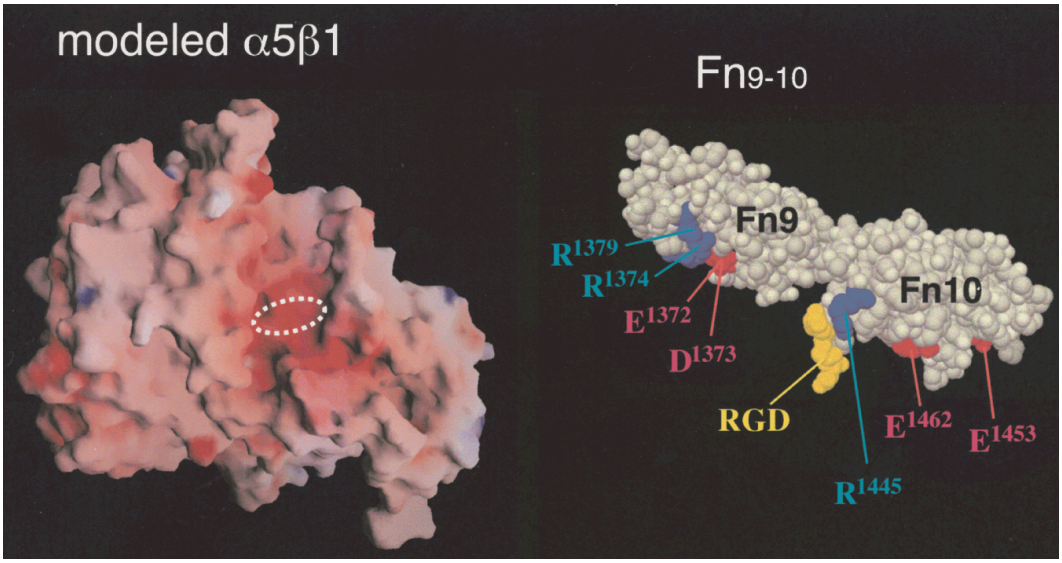

Figure 1.4 The distribution of charge in α5β1-Fibronectin interface. Left: A molecular surface of the α5β1 headpiece model created using the αVβ3 crystal structure as the template colored by electrostatic potential ranging from red (<-25 kT) to blue (>25 kT). The dotted oval is thought to be the approximate location of the RGD-docking site. Right: The structure of the Fn9-10 fragment in the CPK representation (conserved basic

(blue) and acidic (red) residues on the same face as the RGD loop (yellow)) (Takagi 2004).

1.2.3 SJ749 and its promise in gliomas

Gliomas are known as the most lethal brain tumors. The nontargeted conventional treatment of gliomas involves surgery, radiation therapy, and chemotherapy. However, these treatments remain inefficient due to some reasons such as drug resistance, toxicity, and poor blood-brain barrier diffusion. The inhibition of proliferation and migration or simultaneous inhibition of invasion and angiogenesis are multiple cell signaling pathways that might be crucial for modulating cell cycle progression and clonogenicity.

The integrin is of particular interest as a target for cancer, since the observation that integrin and its ligand fibronectin are found to be in excess amounts in tumor vessels of many solid malignancies. In some types of cancers, integrin, especially α5β1 is also seen to have direct roles in tumor cell migration, invasion, and survival.

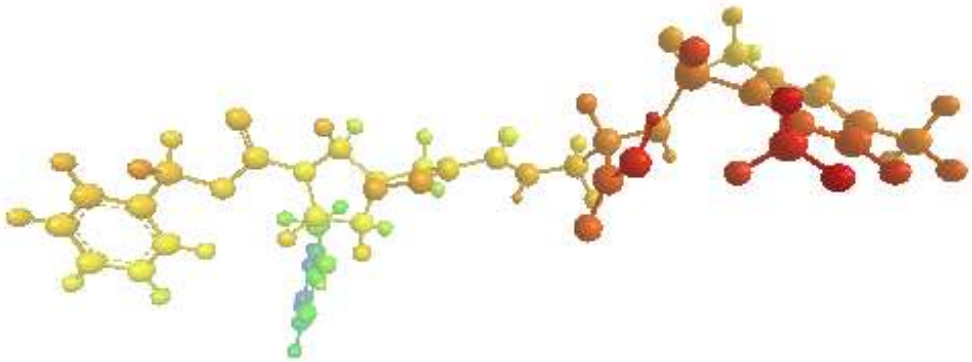

Figure 1.5 Optimized structure of SJ749 in Chem3D program with CS MOPAC® Pro computational method.

SJ749 is the most potent and selective nonpeptidic α5β1 integrin antagonist known so far (Maglott, Bartik et al. 2006). SJ749, {(S)-2-[(2,4,6-trimethylphenyl) sulfonyl] amino-3-[7-benzyloxycarbonyl-8-(2-pyridinylaminomethyl)-1-oxa-2,7-diazaspiro-(4,4)-non-2-en-3-yl] carbonylamino] propionic acid} (Figure 1.5), is a nonpeptidic integrin ligand derived from the most abundant natural tripeptide sequence, RGD. SJ749 specifically inhibits the α5β1-mediated cell adhesion to fibronectin. Not only is SJ749 an adhesion antagonist, but also it acts as a ligand mimetic and expresses

similar stimuli to the cell as for endogenous integrin ligands. Therefore, SJ749 plays an eminent role as an anticancer target effecting proliferation of tumor cells.

1.3. Fluorine

Fluorine is the most electronegative element in the periodic table. There are many interesting physicochemical characters of fluorine:

(1) relatively small atomic size,

(2) high carbon – fluorine bond energy,

(3) high electronegativity, and

(4) nuclear spin of ½,

(5) enhancement of lipophilicity.

These properties provide fluorine a wide range of use in the industry. On the other hand, there is considerable interest in the pharmaceutical uses of fluorine. Fluorinated compounds can probe the biochemical reaction mechanisms.

A wide range of biological functions are carried out by fluorinated organic molecules and fluorinated molecules are being designed and synthesized as anti-cancer agents. The number of fluorinated antitumor and antimitotic agents is increasing and the agents have now becoming available for cancer treatment (Isanbor and O'Hagan 2006). The most widely used ones are the 5-fluoropyrimidines, such as 5-fluorouracil (5-FU) 1, 5-fluoro-20- deoxyuridine (FdUrd), and their prodrug derivatives. Such prodrugs are converted to the bioactive molecules in laboratory conditions. Trifluoromethyl group is regarded as almost the same with its hydrogenated analog methyl group in biological systems (Zheng, Cao et al. 2003). However, $–CF_3$ and $–CH_3$ groups are chemically different from each other. Trifluoromethylated molecules have increased resistance towards biodegradation, higher susceptibility towards the action of nucleophilic agents, and improved lipophilicity. Therefore, these unique properties of the $–CF_3$ group brings out wide applications in pharmaceutical industry.

4-fluorophenyl group is being actively used in pharmaceuticals such as Bicalutamide/ Caso {*N* - [4 - cyano - 3 -(trifluoromethyl)phenyl] - 3 - [(4 - fluorophenyl) sulfonyl] - 2 - hydroxy - 2 - methyl - , (+/ −)}, Bromperidol/ Impromen Tesoprel Azuren, {4 - [4 - (4 - bromo - phenyl) - 4 - hydroxy - 1 - piperidyl] - 1 - (4 - fluorophenyl)butan - 1 – one}; Aprepitant/ Emend (5 - [[(2 R ,3 S) - 2 - [(1 R) - 1 - [3,5 - bis - (trifluoromethyl)phenyl] ethoxy] - 3 - (4 - fluorophenyl) - 4 -

morpholinyl]methyl] - 1,2 -dihydro - 3H - 1,2,4 - triazol - 3 - one), Atorvastatin Calcium/ Lipitor Caduet {[R - (R * , R *)] - 2 - (4 - fluorophenyl) - β , δ - dihydroxy - 5 - (1 - methylethyl) - 3 - phenyl - 4 - [(phenyl - amino)carbonyl] - 1 H - pyrrole - 1 – heptanoic acid,calcium salt (2 : 1) trihydrate}, Cisapride Monohydrate Δ / Propulsid (4 - amino - 5 - chloro - N - [1 - [3 - (4 - fluorophenoxy)propyl] - 3 - methoxypiperidin - 4 - yl] - 2 – methoxybenzamide hydrate), Citalopram Hydrobromide/ Celexa (1 - [3 - (dimethylamino) - propyl] -) - 1 - (p - fluorophenyl) - 5 – phthalancarbonitrile monohydrobromide), Droperidol *V* / Inaspine (3 - [1 - [4 - (4 - fluorophenyl) - 4 - oxobutyl] - 3,6 - dihydro - 2 *H* - pyridin - 4 - yl] - 1 *H* - benzimidazol - 2 - one), Escitalopram Oxalate/ Lexapro (S - (+) - 1 - [3 - (dimethylamino)propyl] - 1 - (p - fluorophenyl) - 5 - phthalancarbonitrile oxalate), and Ezetimibe/ Zetia Vytorin (1 - (4 - fluorophenyl) - 3(*R*) - [3 - (4 - fluorophenyl) - 3(*S*) - hydroxypropyl] - 4(*S*) - (4 - hydroxyphenyl) - 2 - azetidinone).

Statistics show that fluorine is the “ second - favorite heteroatom ” after nitrogen in drug design (Ojima 2009). All those characteristics listed above attribute to the high desire to use organofluorinated compounds. The replacement of a C – H or C – O bond with a C – F bond in biologically active compounds lead to higher metabolic stability, often increased binding to target molecules, and increased lipophilicity and membrane permeability. As a result, the rational design of fluoroorganic molecules will lead to the generation of new and effective biochemical tools (Ojima 2009).

CHAPTER 2

EXPERIMENTAL SECTION

2.1 MATERIALS AND METHODS

2.1.1 INSTRUMENTS AND MATERIALS

Melting points were determined on a Mettler FP 80 melting point apparatus and are uncorrected. ^{1}H, ^{13}C, and ^{19}F NMR spectra were recorded on a Bruker Ultra Shield Plus, Ultra long hold time 400 MHz NMR spectrometer; chemical shifts are expressed in δ ppm with reference to trimethylsilane (TMS). Following solvent peaks were used as internal standards: DMSO-d5: 2.50 ppm (^{1}H NMR) and 39.46 ppm (^{13}C NMR); acetone-d6: 2.05 ppm (^{1}H NMR) and 30.83 ppm (^{13}C NMR); chloroform-d3 ($CDCl_3$): 7.26 ppm (^{1}H NMR) and 77.0 ppm (^{13}C NMR); MeOH-d4: 3.31 ppm (^{1}H NMR) and 49.05 ppm (^{13}C NMR); and H_2O-d2: 4.80 ppm (^{1}H NMR). ^{1}H assignment abbreviations are as follows: s=singlet, d=doublet, t=triplet, q=quartet, m=multiplet and br=broad. FT-IR spectra were recorded on Perkin Elmer spectrophotometer in the range of 400–4000 cm^{-1} (abbreviations: m, s, br and w). Some of the prominent spectra were given behind the procedure as a numeric value. Thin-layer chromatography was performed on precoated (0.25-mm) silica gel plates; compounds were detected with a 254- and/or 366-nm UV lamp or by charging with I_2 vapor to visualize the amines. Silica gel (60-230 mesh) was employed for routine flash and column chromatography separations. Flash chromatography was performed on a Teledyne Isco Companion Flash Chromatographer. Absorbance was measured by ELISA reader (BioTek).

Reagent quality solvents were used without purification. Dichloromethane was distilled over molecular sieves, THF was dried over sodium with benzophenone and distilled prior to use. Triethylamine was distilled and kept over sodium hydroxide

before use. Amino acids were from Sigma, Fluka, Acros or Alfa Aesar. Other reagents were purchased from Fluka, Merck, or Sigma.

A–172 and U–87 cell lines were purchased from ATCC. DMEM and RPMI were purchased from Invitrogen, FBS was purchased from Gibco, LDH and WST–1 assays were purchased from Roche.

2.2. SYNTHESIS

2.2.1. Synthesis of the Intermediate Spiroisoxazolinopyrrole of SJ749 [3-[7-(Benzyloxycarbonyl)-8-(2-pyridinylaminomethyl)-1-Oxa-2,7-Diazaspiro[4.4]non-2-en-3-ylcarboxamido]-2(S)-(2,4,6-trimethylphenylsulfonylamino)propionic acid] and Its Fluorinated Analogs

The intermediate spiroisoxazolinopyrrole of SJ749 was synthesized as described in United States Patent 5760029.

2.2.1.1. Synthesis of *N*-Z trans-L-hydroxy proline (Z-Pro-OH) (1)

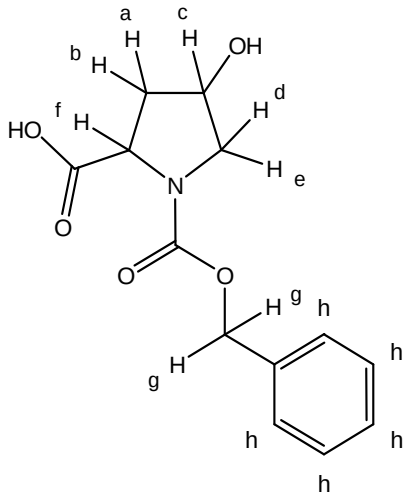

Figure 2.1 The Structure of *N*-Z Trans L-hydroxy proline (**1**).

$NaHCO_3$ (8.06 g) was dissolved in water and this solution was transferred into a three-neck angled round-bottom flask. Argon as an inert gas was introduced into the system Then, L-4-Hydroxyproline was added followed by the addition of benzyl chloroformate (45% solution in toluene) (ZCl) in a dropping funnel drop by drop within *ca.* 30 minutes while the contents of the round bottom flask were constantly being

stirred. The solution in the flask took a white aspect. After the addition of ZCl, the reaction was let to take place for 4 hours and 30 minutes at room temperature under constant stirring. The reaction mixture was then poured into a separatory funnel and washed 3 times with Et_2O. Using 6 N hydrochloric acid, the aqueous phases collected were acidified to pH=2 and extracted 3 times with EtOAc. In each extraction, the organic phase was collected in a flask and all of them were combined. The organic phase was once washed with H_2O and once with saturated NaCl solution (brine), dried with $MgSO_4$, and vacuum-filtered and evaporated *in vacuo* through a rotary-evaporator (Rotavap) (97%).

^{1}H NMR (400 MHz, D_2O-d_6) δ **h**: 7.25-7.56 (m, 5H), **g**: 5.10-5.14 (m, 2H), **f**: 4.47- 4.57 (m, 1H), **e**: 4.12–4.25 (m, 1H), **c and d**: 3.60 (d, broad J=4.4 Hz, 2H), **a and b**: 2.12-2.40 (m, 2H).

2.2.1.2. Reduction of *N*-Z 4-hydroxy proline with boranedimethylsulfide complex in THF (2)

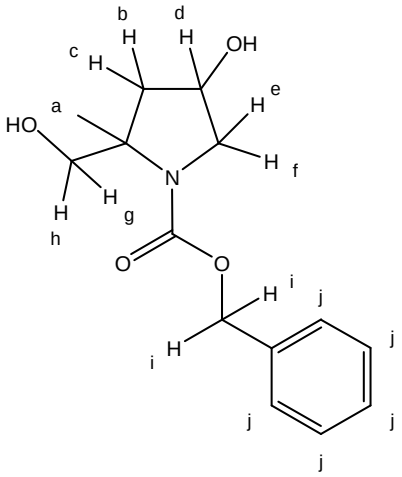

Figure 2.2 The Structure of *N*-Z-4-Hydroxy-L-prolinol (**2**).

N-Z trans-L-hydroxy proline **(1)** was dissolved in THF and this solution was transferred into a three-neck round-bottom flask. Argon as an inert gas was introduced into the system followed by placing a salt ice / acetone bath around it. Then, boranedimethylsulfide ($BH_3 \cdot Me_2S$) (2 M in THF) was added followed in a dropping funnel drop by drop within 30 minutes while the contents of the round-bottom flask were constantly being stirred. The solution in the flask took a white aspect. After the addition of $BH_3 \cdot Me_2S$, the reaction was let to take place for overnight at room temperature under constant stirring. The next morning, 0.2 equivalent of $BH_3 \cdot Me_2S$ was

added into the reaction vessel in which white solids had formed. Two hours later, a 1:1 mixture of MeOH:H_2O was added into the reaction flask during which white solid particles on the sides of the flask dissolved and a violent gas evaluation was observed. The reaction mixture was then poured into a separatory funnel and the aqueous phase extracted five times with EtOAc. In each extraction, the organic phase was collected in a flask and all of them were combined. The organic phase was twice washed with a saturated $NaHCO_3$ solution and brine, respectively, dried with $MgSO_4$, vacuum filtered, and evaporated through a rotary-evaporator (95%):

^{1}H NMR (400 MHz, DMSO-d_6) δ **a**: 1.60 (s, 1H), **b and c**: 2.03-2.11 (m,2H), **d, e and f**: 3.47-3.84 (m, 3H), **g**: 4.11 - 4.24 (m,1H), **h**: 4.42-54.50 (m,1H), **i**: 5.16 (s, 2H), **j**: 7.27-7.37 (m,5H).

2.2.1.3. Protection of the primary hydroxyl group in the diol N-Z-4-Hydroxy-L-prolinol by TBDMSCl (3)

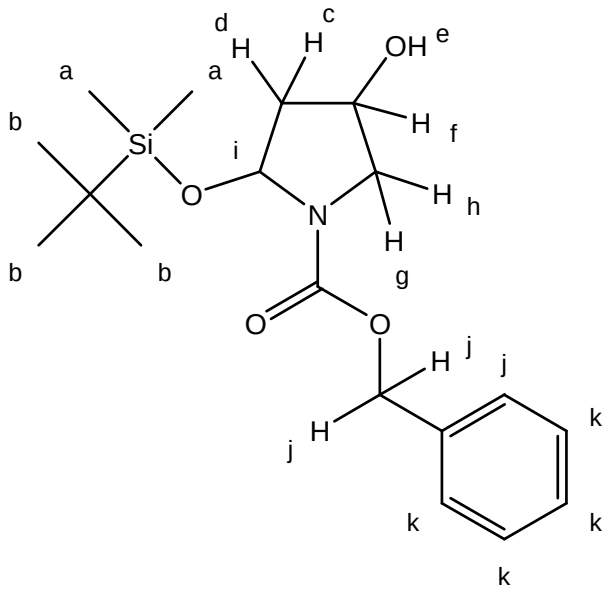

Figure 2.3 The Structure of L-Benzyloxycarbonyl-2-(S)-t-butyldimethylsilyloxymeth-yl-4-hydroxypyrrolidine (**3**).

The diol **(2)** was dissolved in sufficient amount of dry CH_2Cl_2 in a 250 ml three-neck round-bottom flask. The contents were stirred at 0°C under argon. After the reaction flask was placed in an ice-acetone bath, sufficient dry Et_3N and TBDMSCl were carefully added, respectively. The solution took a light orange color. The reaction

was let to take place for five days at room temperature. The progress of the reaction was monitored by TLC until all TBDMSCl was consumed. The solution was added sufficient amount of H_2O, and the organic phase was washed two times with water and once with brine. It was then dried over $MgSO_4$, filtrated, and evaporated *in vacuo*. The product was purified by flash chromatography on a silica gel using EtOAc5/Hexane5 as the eluting solvent to give dark yellow viscous oil (60%):

^{1}H NMR (400 MHz, $CDCl_3$) δ **k**: 7.35-7.27 (m, 5H), **j**: 5.22-3.55 (m, 2H, CH_2-Ph), **i**: 4.47 (s, 1H), **h**: 4.15-4.0 (m, 1H), **f and g**: 3.55-3.90 (m, 2H), **c, d and e**: 2.24-1.85 (m, 3H), **b**: 0.85 (m, 9H), **a**: 0.06-(-0.04) (s,6H)

2.2.1.4. Swern oxidation of the remaining secondary alcohol L-Benzyloxycarbonyl-2-(S)-t-butyldimethylsilyloxymethyl-4-hydroxypyrrolidine to ketone (4)

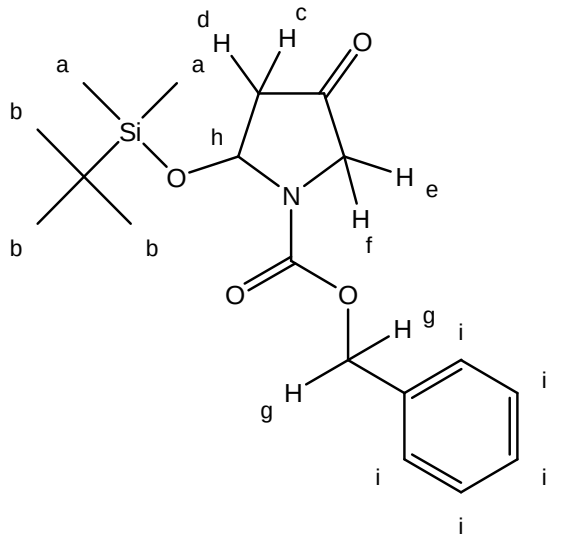

Figure 2.4 The Structure of L-Benzyloxycarbonyl-2-(S)-t-butyldimethylsilyloxymeth-yl-4-hydroxypyrrolidinone (**4**).

Oxalyl chloride was dissolved in a sufficient amount of dry CH_2Cl_2 in a three-neck round-bottom flask in a dry ice/acetone bath under argon gas environment while the contents were being constantly stirred. Next, DMSO dissolved in CH_2Cl_2 was added into the reaction media drop by drop through a dropping funnel connected to the middle neck of the reaction flask over a period of thirty minutes and that mixture was let to stir for an additional thirty minutes followed by the introduction of the remaining secondary alcohol through a cannula by purging its flask with Argon from a balloon into the

dropping funnel first, and then into the reaction media drop by drop at T<-65°C. After the addition of the starting material **(3)** finished, the mixture was stirred for another thirty minutes at T<-65°C. Triethylamine was then added drop by drop over 30 minutes again at T<-65°C. After that, the cooling bath was removed from the system while the temperature of the system was let to rise to 5-10°C for approximately 40 minutes. The reaction mixture was then quenched with 10% $KHSO_4$ solution, subsequently that mixture was transferred to a separatory funnel and layers separated. The aqueous phase was extracted with CH_2Cl_2 and the combined organic layers were washed three times with 10% citric acid solution and once with brine, then dried over anhydrous $MgSO_4$, filtered, and evaporated to yield orange oil. The product was used in the next step without further purification (93%):

^{1}H NMR (400 MHz, $CDCl_3$) δ **i**: 7.37 (s, 5H), **g**: 5.19-5.13 (s, 2H), **h**: 4.50-4.45 (m, 1H), **e and f**: 4.13-3.54 (m, 2H), **c and d**: 2.75-2.40 (m, 2H), **b**: 0.84 (m, 9H), **a**: 0.2 – (-0.01) (s, 6H).

2.2.1.5. Wittig olefination of the ketone 1-Benzyloxycarbonyl-2(S)-*tert*-butyldimethylsilyloxymethyl-4-pyrrolidinone to alkene with Methylene thylene triphenylphosphorane (5)

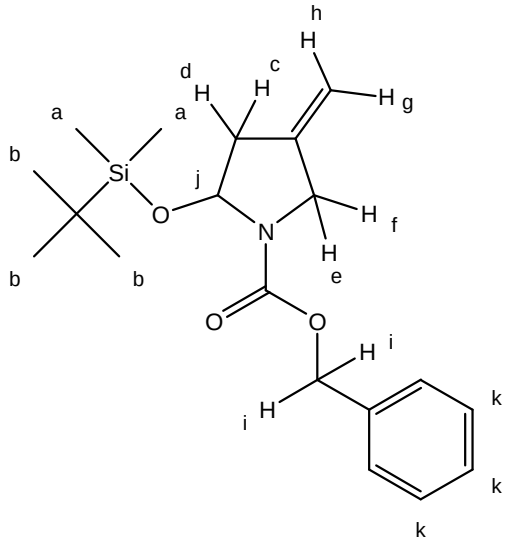

Figure 2.5 The Structure of nitrile oxide 1-Benzyloxycarbonyl–2(s)-*tert*-butyldimethylsilyloxymethyl–4-methylenepyrrolidine (**5**).

To a suspension of sufficient *t*-BuOK was added a sufficient amount of methyltriphenylphosphonium bromide in dry CH_2Cl_2 under argon and in an ice bath. A

light yellow solution formed and was stirred for 15 minutes, then to this mixture was introduced the starting material **(4)** in CH_2Cl_2 using a cannulation system through a cannula, Argon, and a dropping funnel. Then, the ice bath was removed and the contents were allowed to stir overnight. The next morning, the mixture was cooled in an ice bath followed by the quenching by using saturated aqueous NH_4Cl. The organic phase was extracted twice with ether followed by washing with water and brine, respectively. Finally, the organic phase was dried over $MgSO_4$, filtered and evaporated *in vacuo* (69%): ^{1}H NMR (400 MHz, $CDCl_3$) δ **k**: 7.36 (s, 5H), **i and j**: 5.15 (s, 2H), **g and h**: 5.04-4.86 (m, 2H), **e and f**: 4.10-3.41 (m, 2H), **c and d**: 2.55 (m, 2H), **b**: 0.84 (s, 9H), **a**: 0.09-(-0.02) (m, 6H).

2.2.1.6. 1,3-Dipolar cycloaddition of the alkene with the nitrile oxide 1-Benzyloxycarbonyl-2(s)-*tert*-butyldimethylsilyloxymethyl-4-methylenepyrrolidine generated from Chlorooximidoacetate and Triethylamine (6)

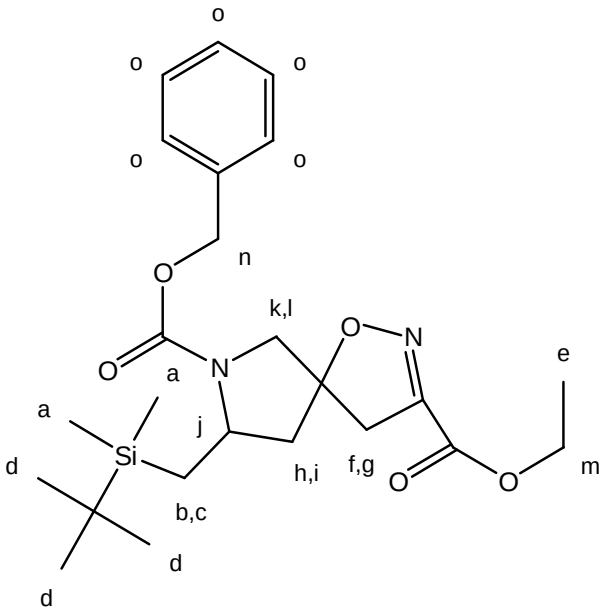

Figure 2.6 The Structure of Diazaspiro 1-Benzyloxycarbonyl–2(s)-*tert*-butyldimethylsilyloxymethyl–4-methylenepyrrolidine (**6**).

The alkene **(5)** (1.304 g, 3.6 mmol) was dissolved in a sufficient amount of dichloromethane (5 mL), treated with ethyl chlorooximidoacetate (0.818 g, 5.4 mmol, 1.5 equiv) and the resulting mixture was cooled to 0°C. Triethylamine was added drop by drop slowly (0.75 mL, 5.4 mmol, 1.5 equiv) and the mixture was let to stir for 24 h at room temperature followed by the introduction of dichloromethane. The organic

phase was washed three times with 10% aqueous citric acid, and once with brine and then dried over $MgSO_4$, filtered, and evaporated *in vacuo*. After eluting the crude through silica gel first with hexane/ether (80:20) by flash chromatography to eliminate the unreacted starting material, the mixture containing the product was subjected to classical column chromatography with hexane/ethyl acetate (75:25) to yield two diastereomers of the product as oil (12%):

^{1}H NMR (400 MHz, $CDCl_3$) δ **o**: 7.35 (s, broad, 5H), **n**: 5.19-5.05 (s, 2H), **m**: 4.41-4.30 (q, 2H), **k and l**: 4.18-4.14 (m, 2H), **j**: 3.67-3.62 (m, 1H), **g, h and i**: 2.47-2.25 (m, 3H), **b and c**: 1.50-1.41 (m, 2H) **e and f**: 1.41-1.34 (t, 2H), **d**: 0.87 (s, 9H), **a**: 0.04-(-0.04) (s, 6H).

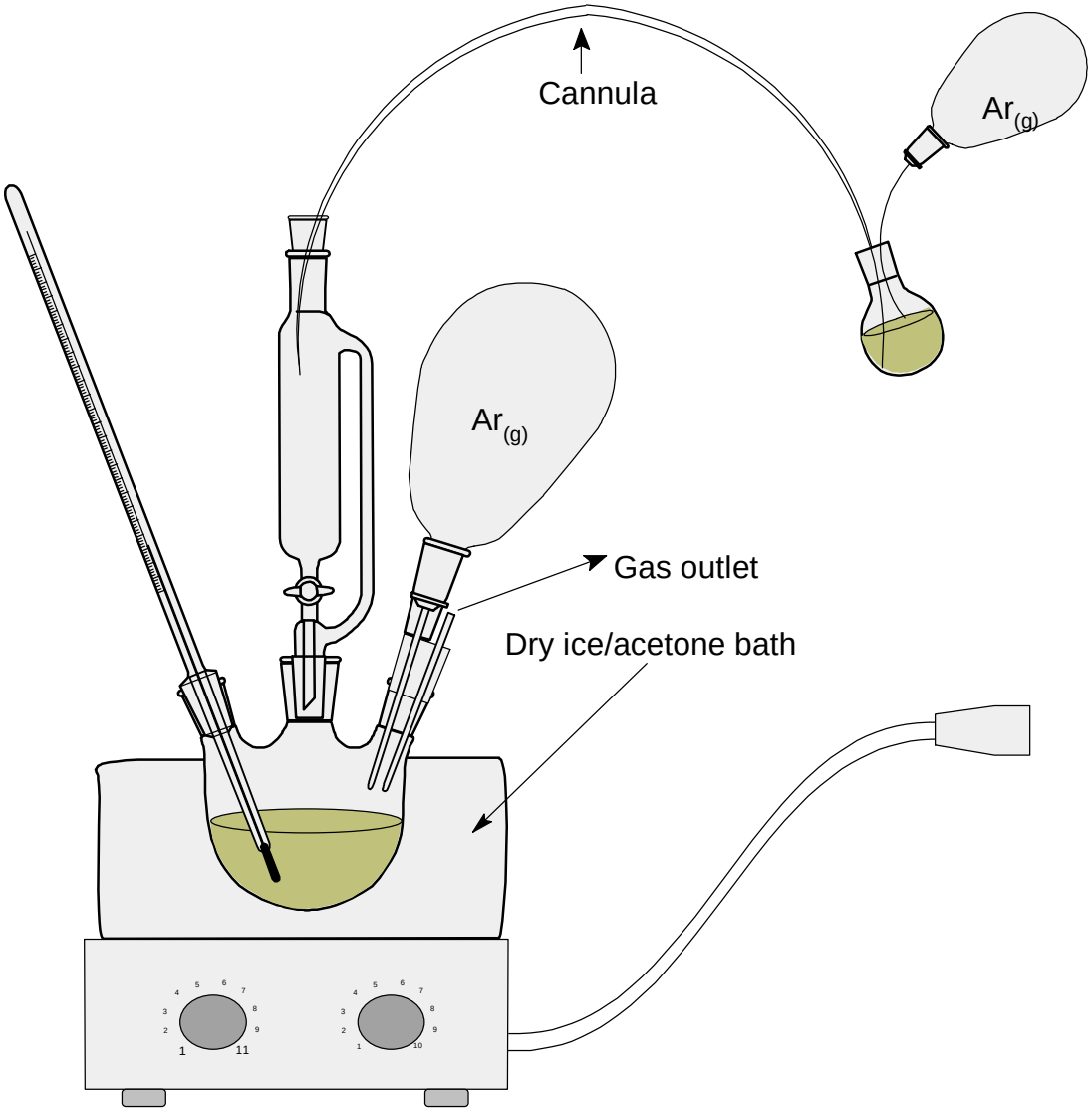

Figure 2.7 Experimental setup for Swern oxidation and Wittig olefination. Please note that dry ice is replaced with ice for Wittig olefination.

2.2.2. PREPARATION OF THE 2,3-DIAMINOPROPIONATE DERIVATIVES

The syntheses were started from L-Asparagine or Boc-L-Asparagine (Boc-Asn-OH) for substitution at the 3' position and 2' position, respectively (Pitts, Wityak et al. 2000) (Zhang, Kauffman et al. 1997). The Hofmann degradation of Asparagine before or after substitution of the hydrogens of one of the nitrogens led to the formation of diaminopropionic acid.

2.2.2.1. *N*-(2,4,6-trimethylphenyl)sulfonyl-L-asparagine (Mes-SO_2-Asn-OH) (7) (Pitts, Wityak et al. 2000)

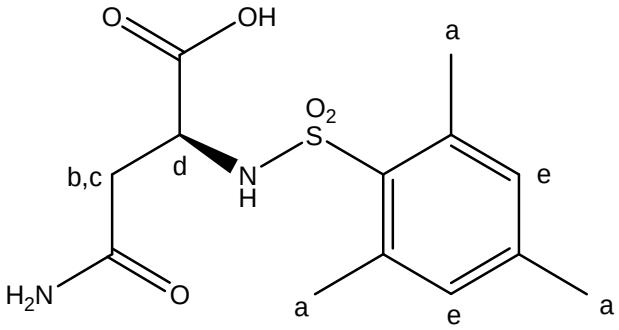

Figure 2.8 The Structure of *N*-(2,4,6-trimethylphenyl)sulfonyl-L-asparagine (**7**).

A slurry of L-Asparagine (10 g, 0.75 mol), THF (65 mL) and H_2O (125 mL) was added Et_3N (24.5 g, 0.24 mol) and (2,4,6-Trimethylphenyl)sulfonyl chloride (24.85 g, 0.114 mol), respectively. Subsequently the components became a homogenous yellow solution within 0.5 h. After the reaction was continued for 3 h at room temperature, the mixture was washed with diethyl ether and dichloromethane. Afterwards, the aqueous layer was separated and acidified to pH=1.5 with concentrated hydrochloric acid when an intense white precipitate occurred. The product was washed with water after 0.5 h and dried overnight (8.5 g, 85%): mp 194°C;

^{1}H NMR (400 MHz, MeOH-d_4) δ **e**: 6.94 (bs, 2H), **d**: 4.04 (t 1H), **a**: 2.58 (s, 8H), **a, b** and **c**: 2.28 (s, 3H).

2.2.2.2. 3-Amino-*N*-(2,4,6-trimethylphenyl)sulfonyl-L-alanine (8) (Mes-SO_2-Ala-OH) (Pitts, Wityak et al. 2000)

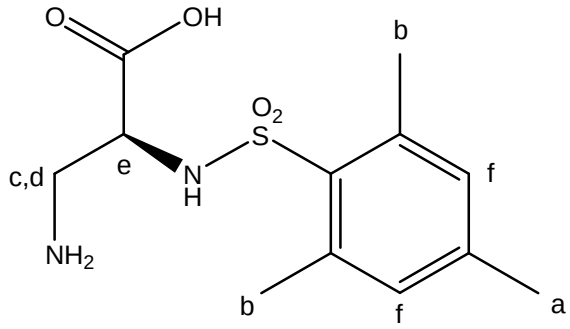

Figure 2.9 The Structure of 3-Amino-*N*-(2,4,6-trimethylphenyl)sulfonyl-L-alanine (**8**).

NaOH (3.2 g, 0.08 mol) was dissolved in water (20 mL) in an ice bath followed by the introduction of bromine (1.92 g, 0.01 mol) drop by drop within 5 min and the mixture which had a yellow color was stirred for 15 min. Next, *N*-(2,4,6-Trimethylphenyl)sulfonyl-l-asparagine (3.14 g, 0.01 mol) was added during 10 min while the yellow color was fading. Afterwards, the mixture was slightly heated to 85°C and the reaction components were refluxed for 1 h. The mixture was cooled down to room temperature and then more in an ice bath. The mixture was acidified to pH=6 with concentrated hydrochloric acid when a white solid evolved and a gas occurred followed by filtering, washing with cold water and drying overnight (1.77 g, 62%): mp 169°C;

^{1}H NMR (400 MHz, MeOH-d_4) δ **f**: 7.05 (s, 2H), **c**,**d**, and **e**: 3.67 – 3.22 (m, 3H), **b**: 2.69 (s, 6H), **a**: 2.30 (s, 3H).

2.2.2.3. *N*-(4-Fluorophenyl)sulfonyl-L-asparagine (F-Bn-SO_2-Asn-OH) (9)

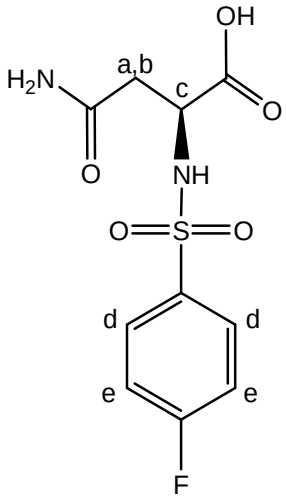

Figure 2.10 The Structure of *N*-(4-Fluorophenyl)sulfonyl-L-asparagine (**9**).

The title compound was synthesized from (4-Fluorophenyl)sulfonyl chloride following the general procedure for the preparation of *N*-(2,4,6-trimethylphenyl)sulfonyl-L-asparagine as yellow oil:

^{1}H NMR (400 MHz, CD_3OD) δ **a and b**: 2.4-2.70,(2H, t), **c**: 4.15 (1H, q.), **d**: 7.17-7.21 (m, 2H), **e**: 7.82-7.86 (m, 2H);

^{19}F NMR (400 MHz, CD_3OD) δ -104.96 (s, 1F).

2.2.2.4. 3-Amino-*N*-(4-fluorophenyl)sulfonyl-L-alanine (F-Bn-SO_2-Ala-OH) (10)

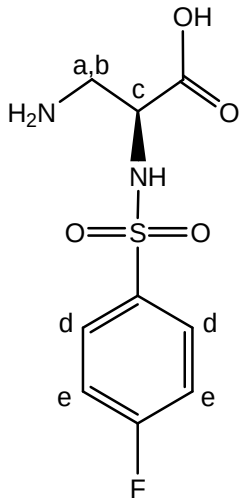

Figure 2.11 The Structure of 3-Amino-*N*-(4-fluorophenyl)sulfonyl-L-alanine (**10**).

The title compound was synthesized from *N*-(4-Fluorophenyl)sulfonyl-L-asparagine following the general procedure for the preparation of 3-Amino-*N*-(2,4,6-trimethylphenyl)sulfonyl-L-alanine to yield white powder:

^{1}H-NMR (400 MHz, CD_3OD) δ **a and b**: 2.9 (2H, m), **c**: 3.54 (1H, m), **d and e**: 8.0- 8.70 (m, 4H).

^{19}F NMR (400 MHz, CD_3OD) δ -105.3 (s, 1F).

2.2.2.5. *N*-(4-(Trifluoromethyl)phenyl)sulfonyl-L-asparagine (CF_3-Bn-SO_2-Asn-OH) (11)

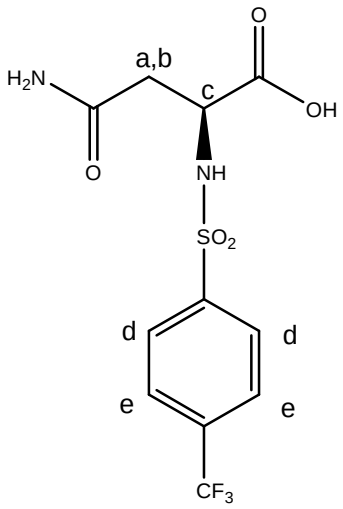

Figure 2.12 The Structure of *N*-(4-(Trifluoromethyl)phenyl)sulfonyl-L-asparagine (**11**)

The title compound was prepared from *N*-(4-(Trifluoromethyl)phenyl)sulfonyl chloride and L-Asparagine following the same procedure for *N*-(2,4,6-trimethylphenyl)sulfonyl-L-asparagine yielded white powder:

^{1}H NMR (400 MHz, D_2O) δ **d and e**: 7.95-7.76 (m, 4H), **c**: 3.21-3.20 (t, 1H), **a and b**: 3.14-3.09, 2.63-2.51 (dq, 2H).

^{19}F NMR (400 MHz, D_2O) δ -64.51 (s, 1F)

2.2.2.6. 3-Amino-N-(4-(trifluoromethyl)phenyl)sulfonyl-L-alanine (CF_3-Bn-SO_2-Ala-OH) (12)

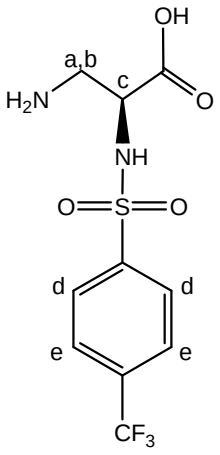

Figure 2.13 The Structure of 3-Amino-N-(4-(trifluoromethyl)phenyl)sulfonyl-L-alanine (**12**).

The title compound was prepared from *N*-(4-(Trifluoromethyl)phenyl)sulfonyl-L-asparagine using the same method for the preparation of 3-Amino-*N*-(2,4,6-trimethylphenyl)sulfonyl-L-alanine to yield white cream:

^{1}H NMR (400 MHz, D_2O) δ **d and e**: 7.86-7.73 (m, 4H), **c**: 3.73 (t, 1H), **a and b**: 3.27-3.02 (dq, 2H).

^{19}F NMR (400 MHz, D_2O) δ -104.9 (s, 1F)

2.2.2.7. *N*-(Heptafluorobutyryl)-L-asparagine (C_3F_7-C(=O)-Asn-OH) (13)

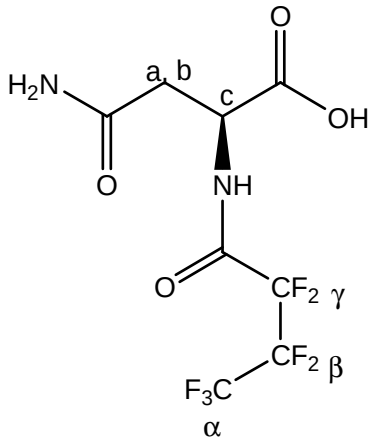

Figure 2.14 The Structure of *N*-(Heptafluorobutyryl)-L-asparagine (**13**).

The title compound was prepared from Heptafluorobutyryl chloride and L-Asparagine following the same procedure for *N*-(2,4,6-trimethylphenyl)sulfonyl-L-asparagine afforded white powder:

^{1}H NMR (400 MHz, CD_3Cl_3) δ **c**: 3.8 (q, 1H), **a**+**b**: 2.73 – 2.61 (dq, 2H);

^{19}F NMR (D_2O) δ **α**: -81.2 (t, 3F), **β**: -118.8 (m, 2F), **γ**: -128.8 (s, 2F).

2.2.2.8. 3-Amino-*N*-(heptafluorobutyryl)-L-alanine (C_3F_7-C(=O)-Ala-OH) (14)

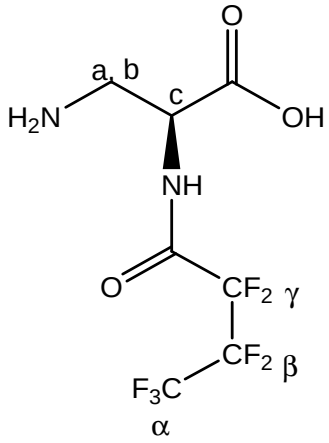

Figure 2.15 The Structure of 3-Amino-*N*-(heptafluorobutyryl)-L-alanine (**14**).

The title compound was prepared from *N*-(Heptafluorobutyryl)-L-asparagine following the same procedure for *N*-(2,4,6-trimethylphenyl)sulfonyl-L-asparagine afforded white hygroscopic solid:

^{1}H NMR (400 MHz, D_2O) δ **c**: 3.40 (q, 1H), **a**+**b**: 2.31 and 1.47 – 1.44 (m, 2H).

^{19}F NMR (400 MHz, D_2O) δ **α**: -81.7 (s, 3F), **β**: (-115) – (-123) (m, 2F), **γ**: -126.7, (m, 2F).

2.2.2.9. *N*-(*tert*-Butoxycarbonyl)-diaminopropionic acid (Boc-Dpr-OH) (15)

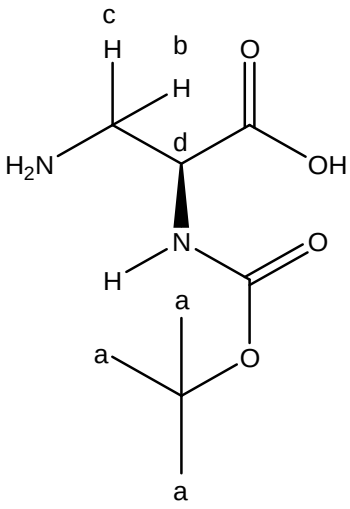

Figure 2.16 The Structure of *N*-(*tert*-Butoxycarbonyl)-diaminopropionic acid (**15**).

N-(*tert*-Butoxycarbonyl)-diaminopropionic acid (Boc-Dpr-OH) was prepared starting from Boc-Asn-OH (*N*-(*tert*-Butoxycarbonyl)-L-asparagine)as described in

Zhang *et al. (Zhang, Kauffman et al. 1997)* and Stanfield *et al.* (Stanfield, Felix et al. 1990). Basically, a mixture of N_{α}-*t*-Boc-L-asparagine (5.0 g, 0.022 mol) with iodosobenzene diacetate (PIDA, 8.32 g, 0.026 mol) in ethyl acetate, acetonitrile, and water (24/24/12 v/v/v) was stirred at 16°C for 30 min, reacted with cooling at 20°C for 4 h, cooled to 0°C and N_{α}-*t*-Boc-β-amino-L-alanine **(4)** was obtained by filtering, washing with ethyl acetate (10 mL) and drying (1.43 g, 65%): mp 213-217 °C;

^{1}H NMR (400 MHz, D_2O) δ **d**: 4.10 (t, 1H), **b and c**: 3.39 – 3.19 (dq, 2H), **a**: 1.42 (s, 9H).

2.2.2.10. *N*-(*tert*-Butoxycarbonyl)-3-(2,4,6-trimethylphenylsulfonyl)amino-L-alanine (Boc-Dpr(Mes-SO_2)-OH) (16)

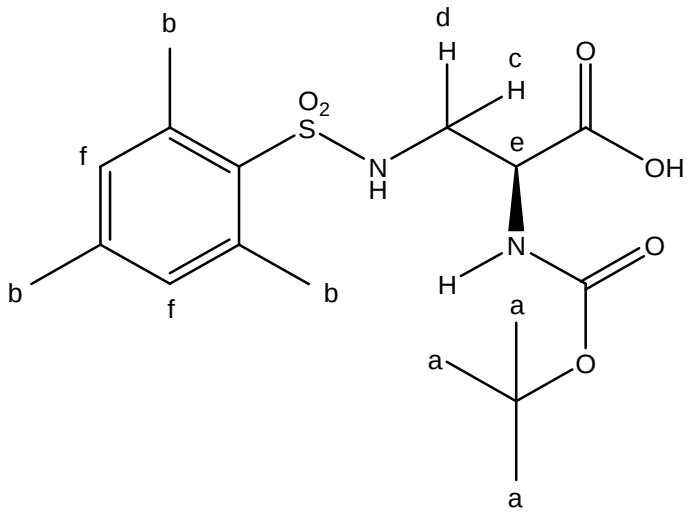

Figure 2.17 The Structure of *N*-(*tert*-Butoxycarbonyl)-3-(2,4,6-trimethylphenylsulfonyl)amino-L-alanine (**16**).

(0.204 g, 1 mmol) was suspended in a mixture of THF (0.87 ml) and H_2O (1.67 ml). Et_3N (0.327 g, 3.2 mmol) and (2,4,6-Trimethylphenyl)sulfonyl chloride (0.219 g, 1.5 mmol) were then added, respectively to yield a yellow mixture after 0.5 h. The reaction mixture was stirred for 3 h at room temperature. Next, the organic phase was washed with brine and distilled water, respectively, filtered and evaporated *in vacuo* (0.17 g, 45%): mp 110 – 116°C;

^{1}H NMR (400 MHz, $CDCl_3$) δ **f**: 6.89 (m, ar, 2H), **e and d**: 3.09 (q, 2H), **c and b**: 2.65 – 2.25 (m, 1H + 9H), **a**: 1.27 (m, 9H).

2.2.2.11. *N*-(*tert*-Butoxycarbonyl)-3-(4-fluorophenylsulfonyl)amino-L-alanine (17)

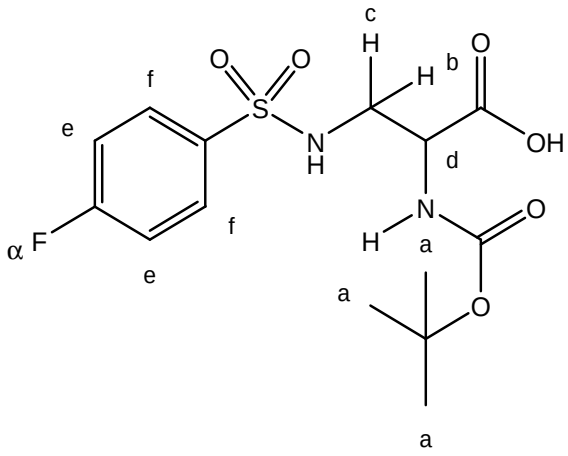

Figure 2.18 The Structure of *N*-(*tert*-Butoxycarbonyl)-3-(4-fluorophenylsulfonyl)amino-L-alanine **(Boc-Dpr(F-Bn-SO_2)-OH)** (**17**).

The same procedure to obtain *N*-(*tert*-Butoxycarbonyl)-3-(2,4,6-trimethylphenylsulfonyl)amino-L-alanine **(16)** was applied to yield yellow oil:

^{1}H NMR (400 MHz, $CDCl_3$) δ **f**: 8.08 (m, 2H), **e**: 8.07 (m, 2H), **b, c and d**: 3.34 (m, 2H + 1H), **a**: 1.44 (m, 9H).

^{19}F NMR (400 MHz, $CDCl_3$) δ **α**: -106.69 (s, 1F).

2.2.2.12. *N*-(*tert*-Butoxycarbonyl)-3-(4-(trifluoromethyl)phenylsulfonyl)-amino-L-alanine (Boc-Dpr(CF_3-Bn-SO_2)-OH) (18)

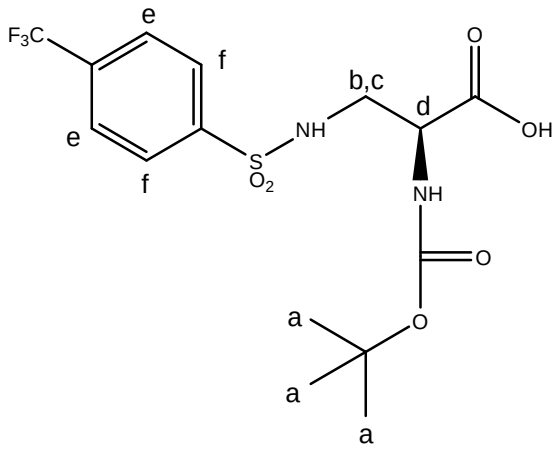

Figure 2.19 The Structure of *N*-(*tert*-Butoxycarbonyl)-3-(4-(trifluoromethyl)phenylsulfonyl)amino-L-alanine (**18**)

The title compound was prepared from 4-(trifluoromethyl)phenylsulfonyl chloride and Boc-Dpr-OH following the same procedure for **(17)** yielded light yellow powder:

^{1}H NMR (400 MHz, $CDCl_3$) δ **e and f**: 7.92-7.17 (m, 4H), **b, c and d**: 3.44 – 3.0 (dq, 2H + 1H), **a**: 1.23 (s, 9H).

^{19}F-NMR (400 MHz, $CDCl_3$) δ -63,132 (s, 3F)

2.2.2.13. *N*-(*tert*-Butoxycarbonyl)-3-(heptafluorobutyryl)amino-L-alanine (Boc-Dpr(C_3F_7-C(=O))-OH) (19)

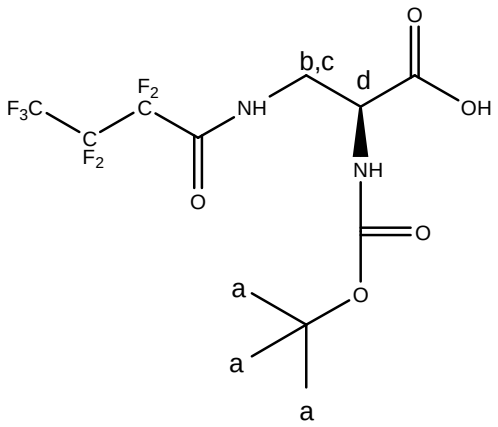

Figure 2.20 The structure of *N*-(*tert*-Butoxycarbonyl)-3-(heptafluorobutyryl)amino-L-alanine (**19**).

The title compound was prepared from 3-(heptafluorobutyryl chloride and Boc-Dpr-OH following the same procedure for *N*-(*tert*-Butoxycarbonyl)-3-(4-fluorophenylsulfonyl)amino-L-alanine **(17)** yielded (**19**) as yellow oil.

2.3. CULTURE OF A-172 AND U-87 CELLS

A-172 and U-87 cell lines were cultured in DMEM (Dulbecco's Modified Eagle Medium from GIBCO) medium containing 10% (v/v) fetal calf serum, 1% penicillin-streptomycin, in a humidified atmosphere of 95% air and 5% CO_2 at 37°C.

2.4. PROLIFERATION ASSAY

A-172 and U-87 cell lines were seeded in 96 well plates (1×10^4 cells / well) 24 hours before the experiment. Serial dilutions were made at the following ratios: 1.1, 1:10, 1:25, 1:50, and 1:100. Water soluble diaminopropionate derivatives were added. 24 hours later ten (10) µl of WST-1 reagent (ROCHE) was added into each well and their absorbance values were measured at 450 nm using an ELISA reader.

2.5. CYTOTOXICITY ASSAY

A-172 and U-87 cell lines were seeded in 96 well plates (1×10^4cells / well) 24 hours before the experiment. Serial dilutions were made at the following ratios: 1:1, 1:10, 1:125, 1:50, and 1:100. The diaminopropionate derivatives were added. The cytotoxicity within 8 and 24 hours were determined with the lactate dehydrogenase leakage assay (LDH) (ROCHE), respectively. One hundred (100) µl of the LDH solution was added into each well. Cells were incubated for 30 minutes at room temperature. Their absorbance values were measured at 490 nm using an ELISA reader.

CHAPTER 3

RESULTS AND DISCUSSION

The spiropisoxazolinopyrrole of SJ749 was synthesized as described in United States Patent 5760029 in six steps (**Scheme 3.2**). Firstly, the amine group in trans-L-4-hydroxyproline was protected with benzyl carbamate to afford *N*-Z- 4-Hydroxy – L-proline and the reaction was quite easy to perform. Afterwards, the carboxylic acid group was reduced to primary alcohol using borane dimethyl sulfide complex. The secondary alcohol on the proline was protected with tert-butyl dimethyl silyl chloride followed by Swern oxidation of the remaining alcohol group on the molecule. The ketone was converted to alkene by Wittig olefination. Finally, the alkene was spirocoupled with chlorooximidoacetate to yield the intermediate spiropisoxazolinopyrrole.

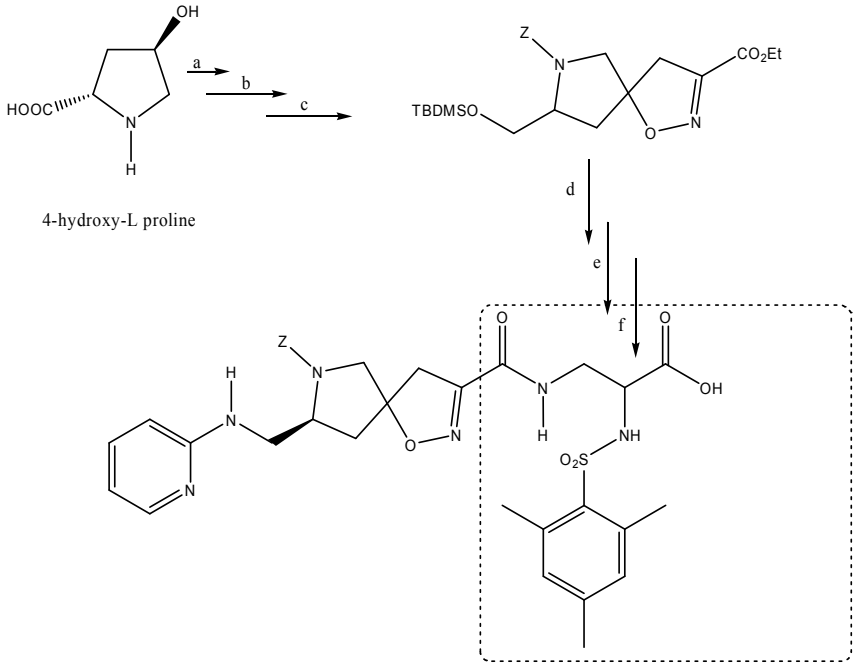

Scheme 3.1 A brief synthesis scheme for the synthesis of SJ749. The dotted areas denote the regions where modifications take place.

The modifications on SJ749 are on the diaminopropionate moiety as shown in **Scheme 3.1**. In this study, fluorine-based diaminopropionic acid derivatives were synthesized and these molecules are to be coupled with the rest of SJ749. Hydrogen substitutions both on N_{α} and N_{β} positions were made. The synthesis of 2,4,6-trimethylphenyl sulfonyl amino group in SJ749 was performed and novel fluorinated analogs of diaminopropionic acid were synthesized.

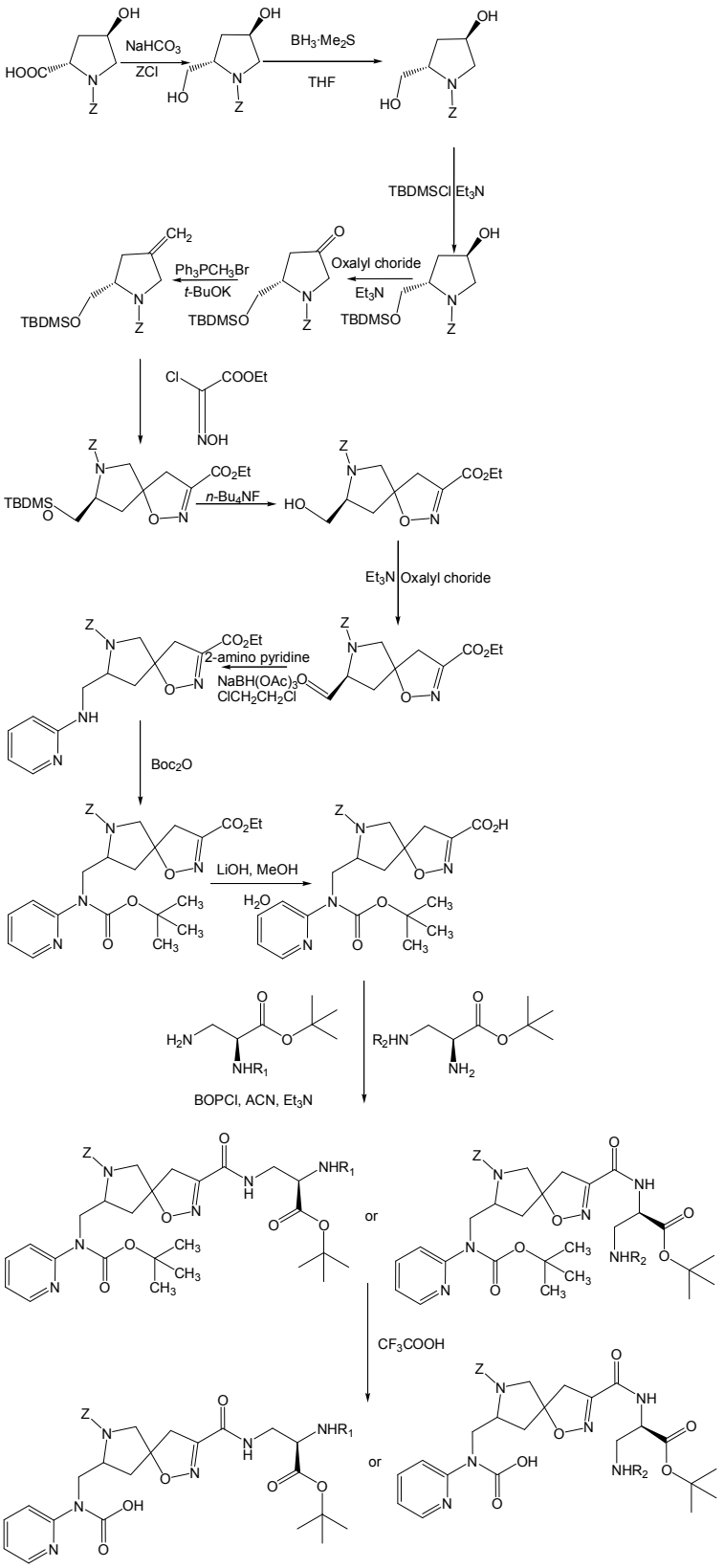

Scheme 3.2 Synthesis scheme for the synthesis of SJ749.

3.1 Synthesis of the spiroisoxazolinopyrrole of SJ749

3.1.1. *N*-Z- 4-Hydroxy – L- proline

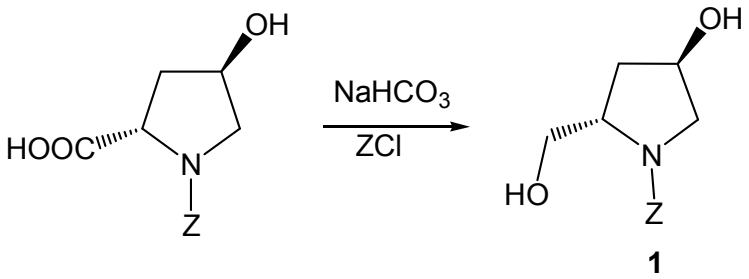

1

Scheme 3.3 Synthesis of *N*-Z- 4-Hydroxy – L- proline (**1**).

Commercially available L-Hydroxyproline (Merck) was protected as its *N*-Z derivative with the well-known group benzyloxy carbamate (Z) of benzylchloroformate (ZCl) in the presence of sodium bicarbonate and water at room temperature for 4.5 h as mentioned in the literature (Liu, Stephen et al. 2008; Grygorenko, Komarov et al. 2009).

The amine group in trans-L-4-hydroxyproline was protected with benzyloxy carbamate. Benzyloxy carbamate (Z) is one of the best groups for the protection of amines. The substitution of the amine hydrogen with Z was confirmed with NMR spectroscopy and ATR. The proton NMR of N-Z-hydroxy proline as shown in **Figure 3.1** is consistent with the one in the literature (SDBS – The Spectral Database of the Organic Compounds, Japan). The formation of the benzyloxycarbonyl (Z) protecting group is clearly seen in the proton NMR. The benzyloxycarbonyl (Z) protecting group appears as chemical shifts at 7.25-7.56 for the aromatic ring (h) and 5.80-6.30 ppm for the aliphatic CH_2 (g). Deuterated chloroform which is the solvent lies on the same chemical shift with that of the aromatic protons. The CH_2 protons on the ring have chemical shifts at 2.12-2.40 ppm for a and b, 3.60 ppm for c and d, and 4.47-4.57 ppm for e and f, respectively.

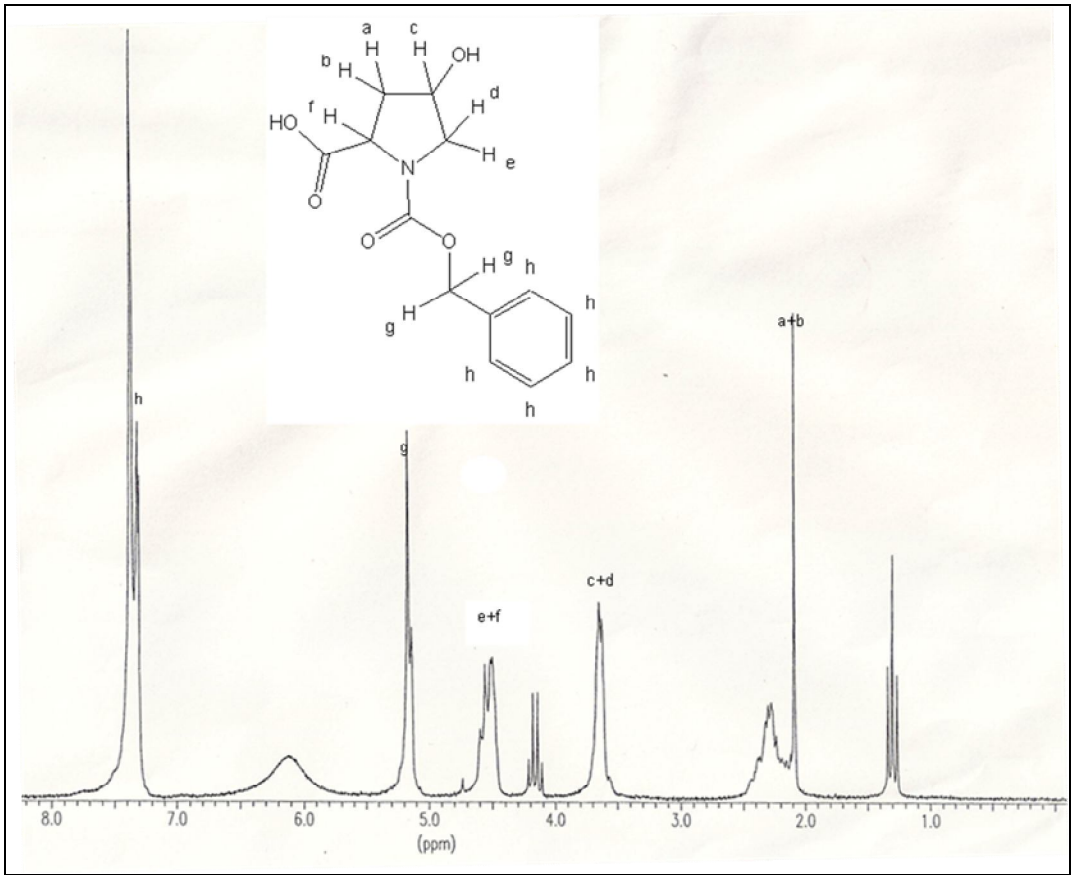

Figure 3.1 ^{1}H NMR spectrum of *N*-Z trans-L-hydroxy proline (Z-Pro-OH) **(1).** Solvent: D_2O.

In the ATR spectrum as depicted in **Figure 3.2**, the neat peak at 1674 cm^{-1} indicates the presence of the carboxyl group of the benzyloxy carbamate. This band belongs to C=O stretching. The aromatic CH stretch has a broad peak at 2950 cm^{-1} while the aromatic CC stretch band is about 1418 cm^{-1}. The O-H stretching appears as a broad peak at 3405 cm^{-1} and the amine N-H stretching is around 3000 cm^{-1}. There are also troughs between 1000 and 1100 cm^{-1} one of which is due to the C-O bond.

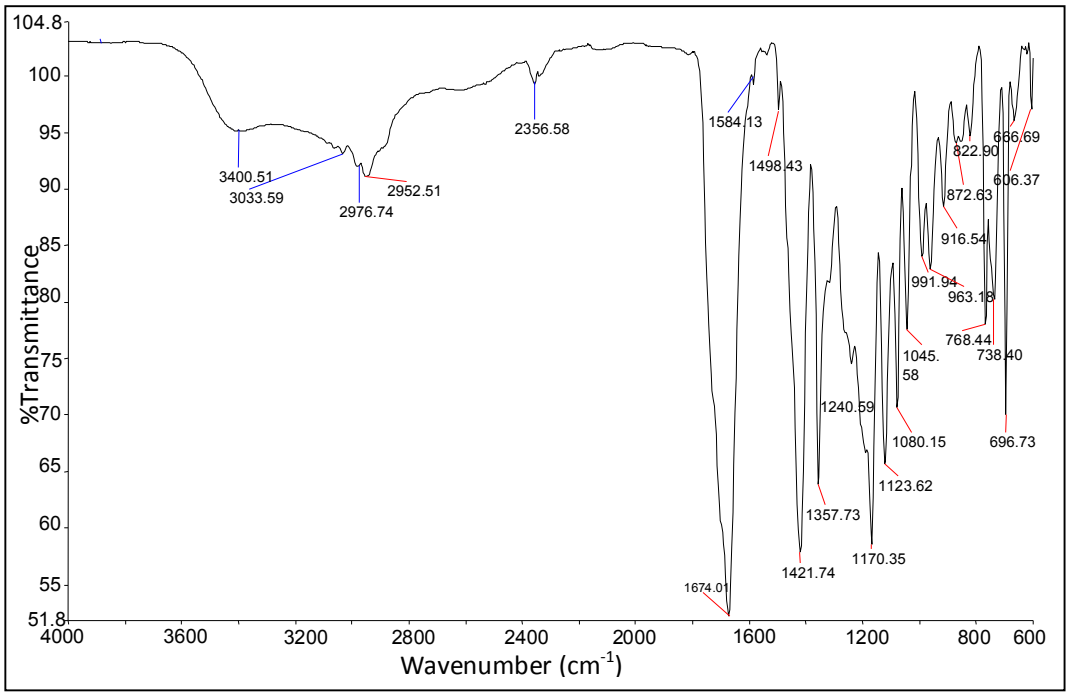

Figure 3.2 ATR spectrum of *N*-Z trans-L-hydroxy proline (Z-Pro-OH) **(1).**

3.1.2. The reduction of the carboxyl group on *N*-Z-4-Hydroxy–L-proline to alcohol (2)

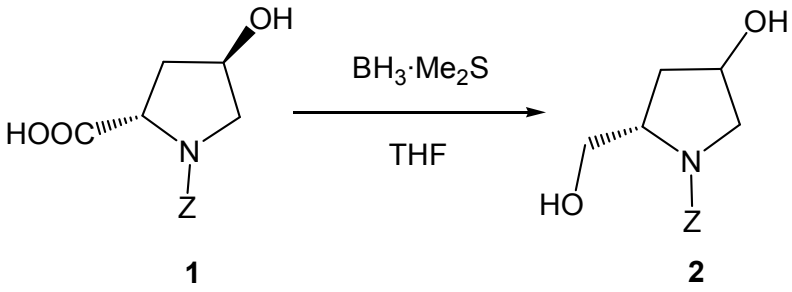

1 **2**

Scheme 3.4 Synthesis of *N*-Z-4-Hydroxy-L-prolinol (**2**).

In this reaction, the carboxyl group in N-Z- 4-Hydroxy – L- proline was reduced to primary alcohol by borane dimethyl sulfide complex in THF for overnight (Shanmugham and White 2004; Archambaud, Legrand et al. 2010). Attention should be paid while adding the borane dimethyl sulfide complex into the reaction vessel in ice bath since this complex solidifies in contact with air and the dropping may stop during the addition of it.

The reduction of the carboxylic acid to a secondary alcohol results in the formation of two protons in the carbon where the reduction has occurred as seen in **Figure 3.3**. We can see the chemical shifts of these protons, g and h, at 4.11-4.24 ppm and 4.42-4.50 ppm, respectively. There is also a significant change in the chemical shift of the single proton (a) which belongs to the ring carbon which has the newly formed secondary alcohol. The reduction is proven by the upfield shift for this proton to 1.60 ppm. The chemical shifts of the CH_2 protons b+c and e+f on the proline ring are located at 2.03-2.11 ppm and 3.47-3.84 ppm along with the one of the proton (d) on the carbon of the tertiary alcohol, respectively. The singlet at 5.16 ppm and the multiplet at 7.37 ppm are assigned to CH_2 (i) and phenyl (j) protons of the Z group, respectively.

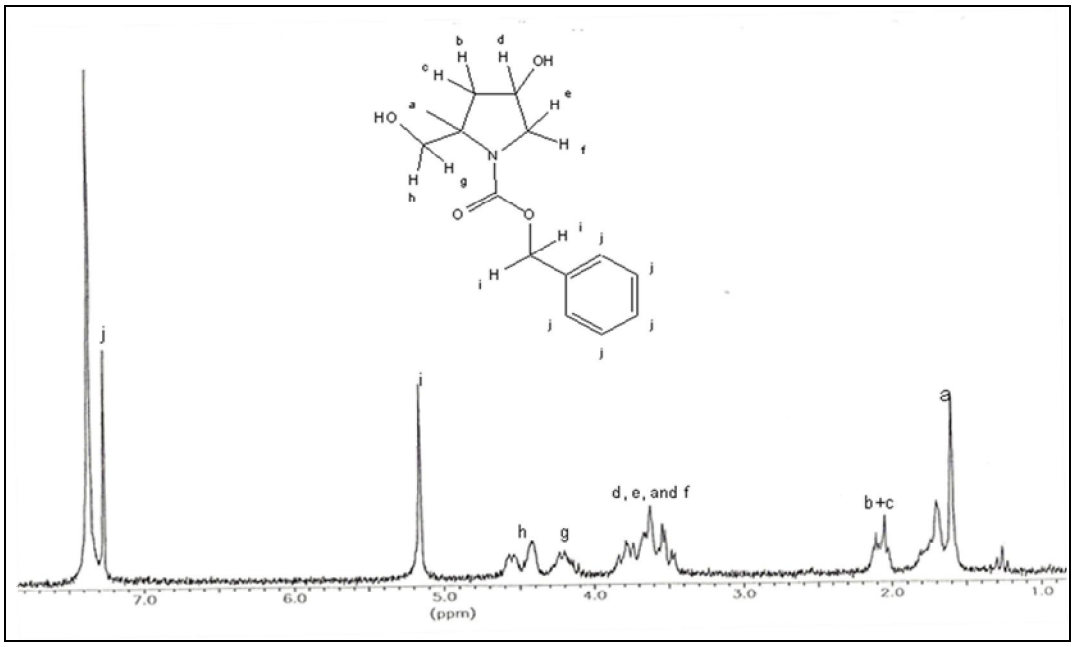

Figure 3.3 ^{1}H NMR spectrum of *N*-Z trans-L-hydroxy prolinol **(2).** Solvent: $CDCl_3$.

3.1.3. The protection of the primary alcohol in *N*-Z-4-Hydroxy–L-prolinol with TBDMSCl (3)

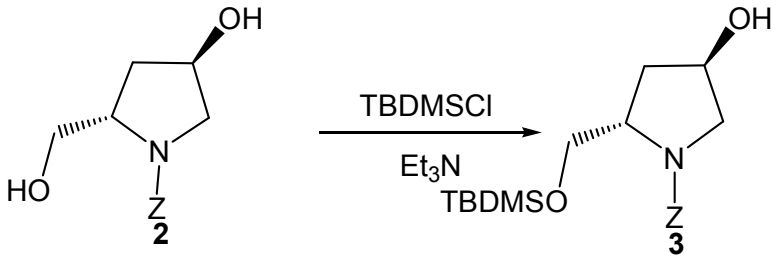

Scheme 3.5 Synthesis of L-Benzyloxycarbonyl-2-(S)-t-butyldimethyl-silyloxymethyl-4-hydroxypyrrolidine (**3**).

The primary alcohol group was protected with TBDMS- group since the other alcohol group was going to be subjected to Swern oxidation in the next step. Although TBDMS- group prefers binding to primary alcohol initially, special attention should be payed for the molar equivalents of the reactants and the reaction time in order the oxygen of the tertiary alcohol not to bind the TBDMS group. Otherwise, both of the alcohol groups might be protected.

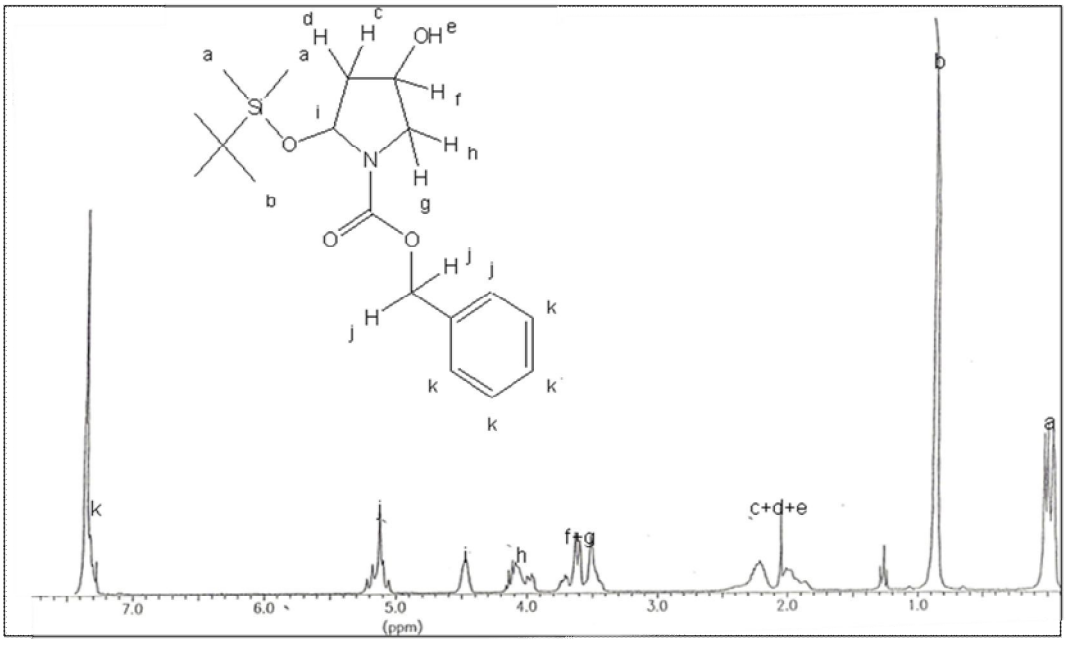

Figure 3.4 ^{1}H NMR spectrum of L-Benzyloxycarbonyl-2-(S)-t-butyldimethylsilyloxymethyl-4-hydroxypyrrolidine (*N*-Z trans-L-TBDMS-hydroxy proline) (Z-TBDMS-Pro-OH) **(3).** Solvent: $CDCl_3$.

The protection of the secondary alcohol is proven by the formation of silyl-methyl proton peaks in the proton NMR spectrum **Figure 3.4**: The chemical shifts at -0.04 – 0.06 ppm and 0.85 ppm are assigned to six protons (a) of the two methyl groups and nine protons (b) of the three methyl groups, respectively. There is a downfield shift in the single hydrogen (i) of the carbon where the TBDMS- groups is bound at 4.47 ppm when compared with the previous molecule (2). The chemical shifts for CH_2 protons on the proline ring are 1.85-2.24 ppm for c,d, and e; 3.55-3.90 ppm for f and g, and 4.0-4.15 ppm for h. The Z group's aliphatic and aromatic protons have chemical shifts of 5.0-5.22 ppm and 7.27-7.35 ppm, respectively.

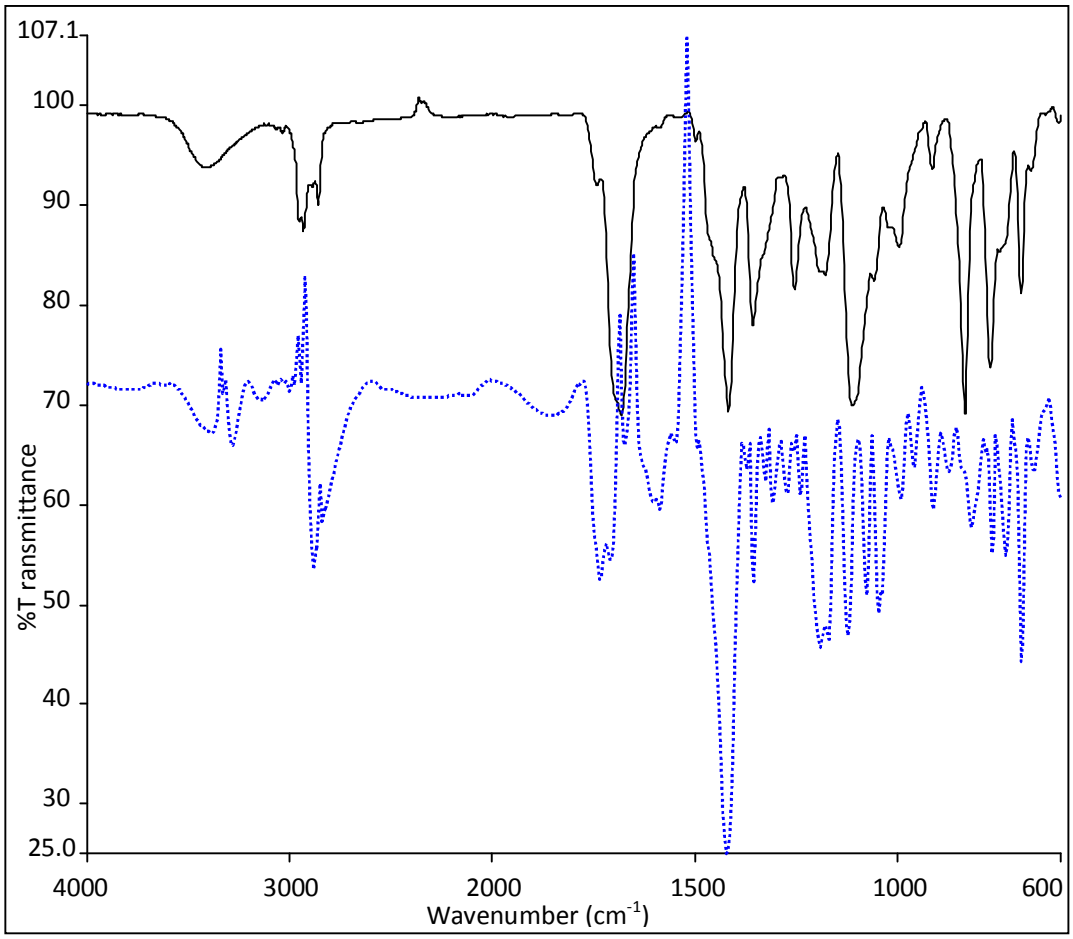

Figure 3.5 ATR spectra comparison of (**1**) and (**3**). The dotted lines above represent the ATR-IR spectrum of **(1)** while the straight line represents the one of **(3).**

3.1.4. The oxidation of the secondary alcohol in the protected N-Z-4-Hydroxy-L-Proline with Swern oxidation (4)

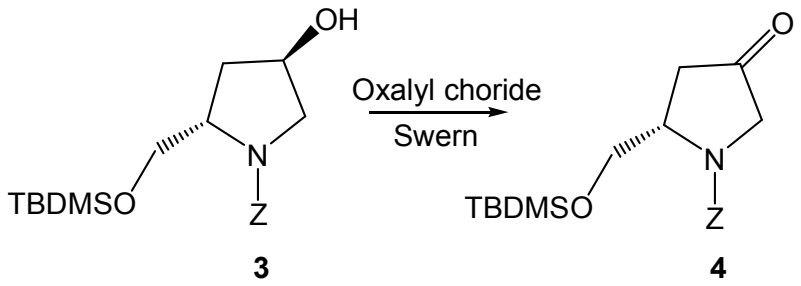

Scheme 3.6 Synthesis of L-Benzyloxycarbonyl-2-(S)-t-butyldimethyl-silyloxymethyl-4-hydroxypyrrolidinone (**4**).

Swern oxidation is another important point during the synthesis. The reaction time, the setup and temperature is an essential while conducting the experiment. Swern oxidation was applied to oxidize the free alcohol to ketone using oxalyl chloride as the dehydrating agent, DMSO which combines with the alcohol to yield alkoxysulfonium ion intermediate, and triethylamine to deprotonate the alkoxysulfonium ion to give the sulfur ylide. The transition state sulfur ylide decomposes to give dimethyl sulfide and the ketone 1-Benzyloxycarbonyl-2(S)-tert-butyldimethylsilyloxymethyl-4-pyrrolidinone. However, during Swern oxidation the temperature must be kept below -60°C to avoid side reactions such as the formation of a mixture of thioacetals. When the reaction is controlled in a good manner, the yield is good and the product obtained is pure.

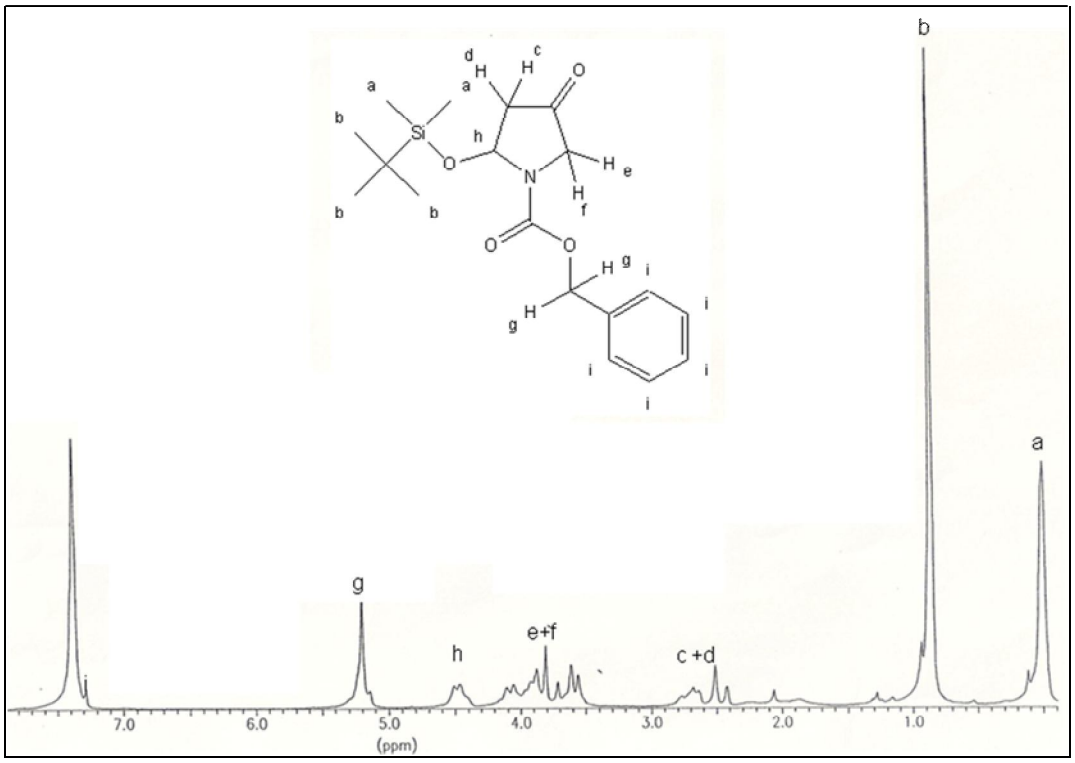

Figure 3.6 ^{1}H NMR spectrum of the ketone 1-Benzyloxycarbonyl-2(S)-*tert*-butyldi-methylsilyloxy-methyl-4-pyrrolidinone (**4**).

Swern oxidation results in the disapperance of the hydrogen which was previously bound to the same carbon with that of the tertiary alcohol as depicted in **Figure 3.6**. The chemical shifts at -0.01 – 0.02 ppm and 0.84 ppm are assigned to six protons (a) of the two methyl groups and nine protons (b) of the three methyl groups, respectively. The single hydrogen atom (h) of the carbon atom on the ring to which the –TBDMSO group is attached has a chemical shifts of 4.45-4.50 ppm. The phenyl protons (i) are assigned a chemical shift of 7.37 ppm whereas the CH_2 protons (g) neighbors to the phenyl group are assigned a chemical shift of 5.13-5.19 ppm as singlets. The chemical shifts of the other CH_2 protons of the ketone (4) are assigned at 2.40-2.75 ppm for c and d, and 3.54-4.13 for e and f.

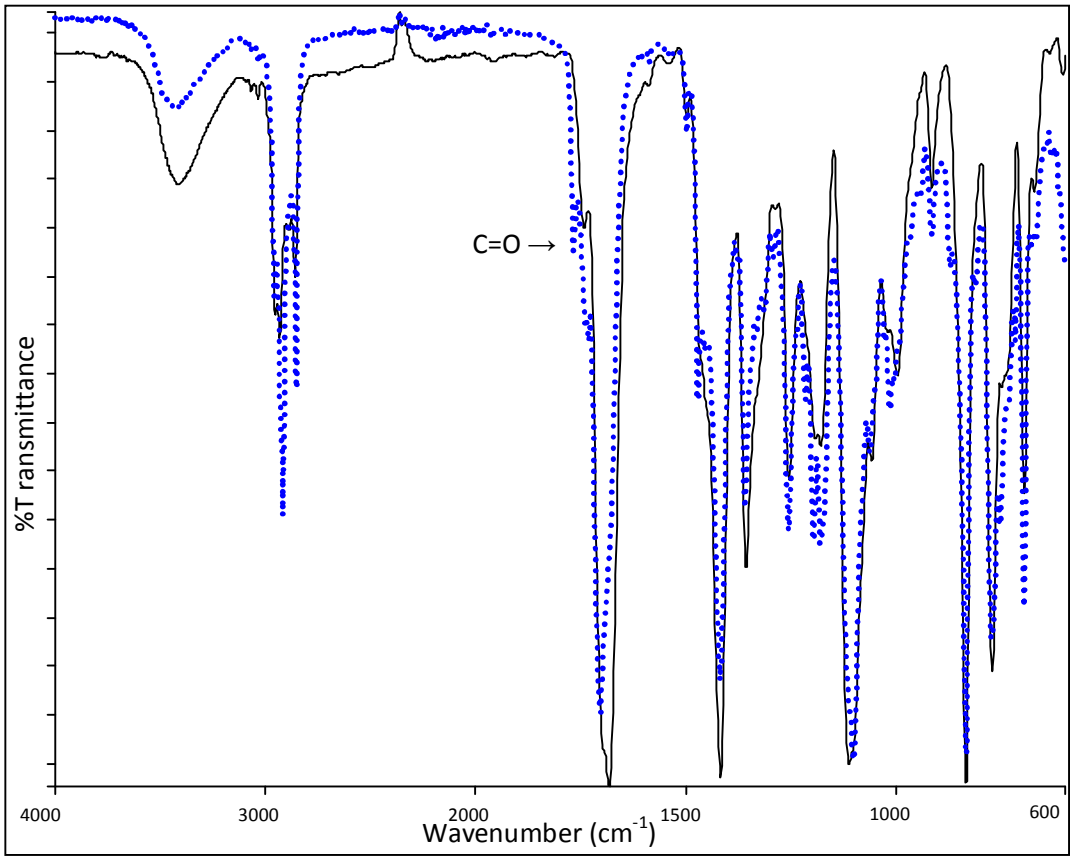

Figure 3.7 Comparison of the ATR spectra of (**3**) and (**4**). The dotted lines above represent the ATR-IR spectrum of **(4)** while the straight line represents the one of **(3).**

3.1.5. Wittig olefination of the ketone N-Z- 4-Hydroxy – L- Proline

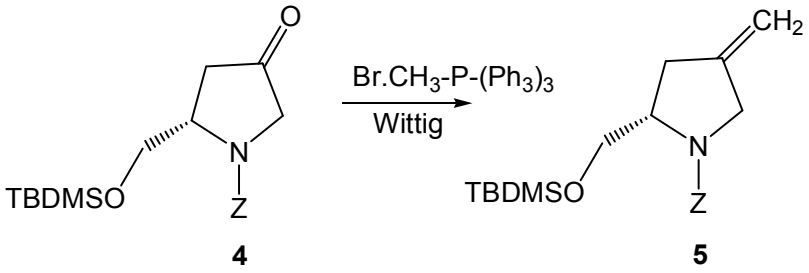

4 **5**

Scheme 3.7 Synthesis of 1-Benzyloxycarbonyl–2(s)-*tert*-butyldimethylsilyloxymethyl–4-methylenepyrrolidine (**5**).

The chemical reaction of an aldehyde or ketone with a triphenyl phosphonium ylide to yield an alkene and triphenylphosphine oxide is known as Wittig olefination. A methylene group was introduced using methylenetriphenylphosphorane (($Ph_3P=CH_2$))

For Wittig olefination, almost the same setup with that of Swern oxidation was used except that ice is used instead of dry ice.

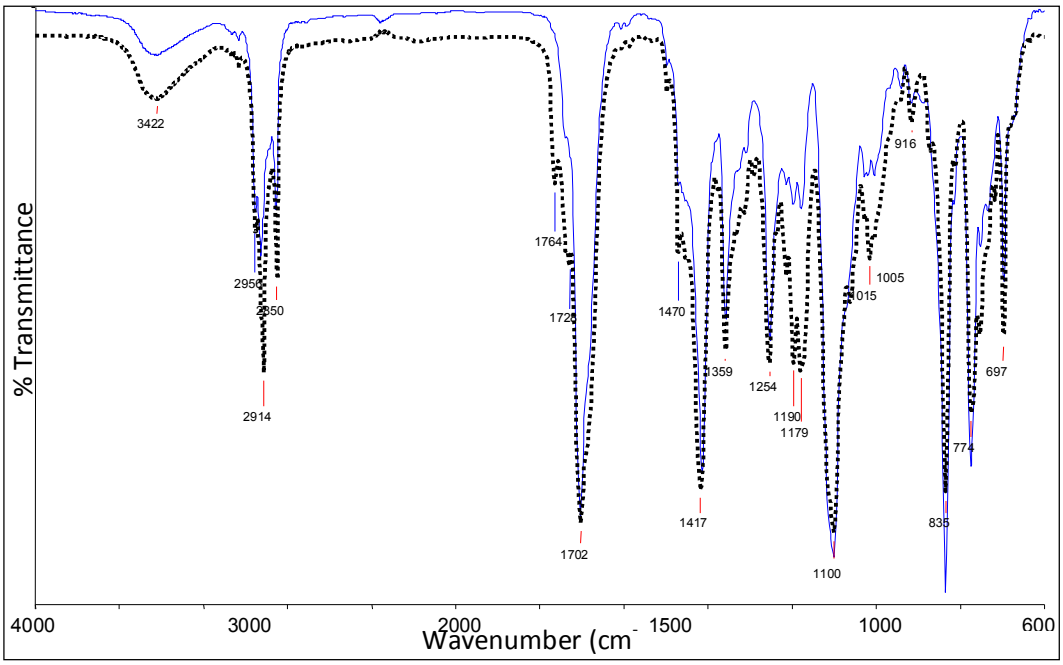

Figure 3.8 Comparison of the ATR spectra of (**4**) and (**5**). The dotted lines above represent the ATR-IR spectrum of **(4)** while the straight line represents the one of **(5).**

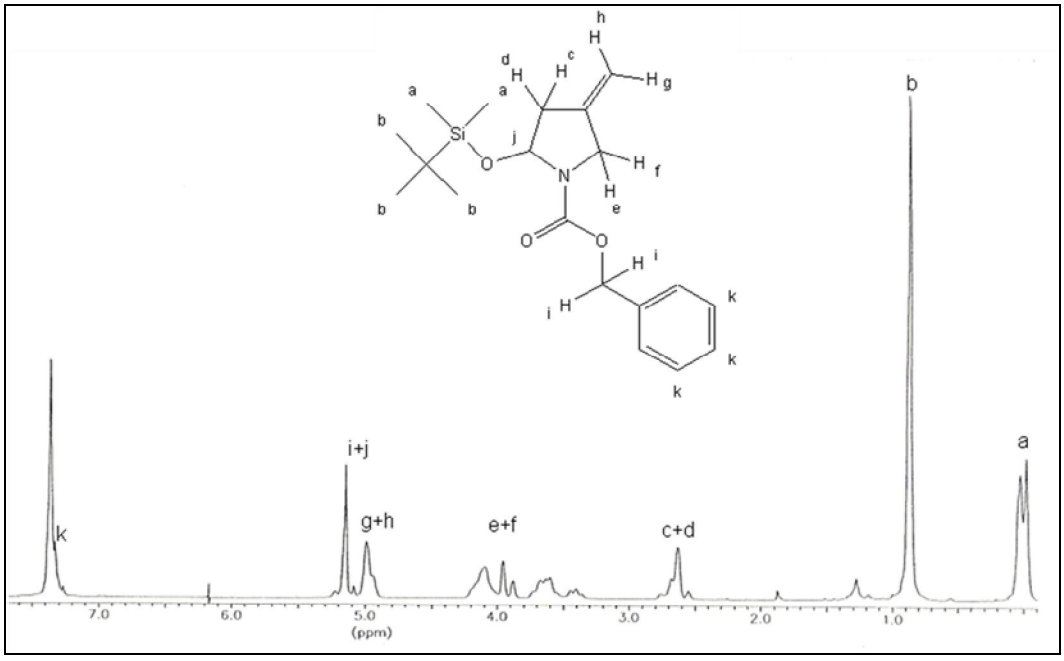

Figure 3.9 ^{1}H NMR spectrum of the nitrile oxide 1-Benzyloxycarbonyl–2(s)-*tert*-butyldimethylsilyloxy-methyl–4-methylenepyrrolidine (**5**). Solvent: $CDCl_3$.

The protons of the ketone (g and h) formed in Wittig olefination have a chemical shift of 4.86-5.04 ppm as a multiplet in the ^{1}H NMR spectrum as seen in **Figure 3.9**. The other -CH_2- and -CH- protons on the ring where ketone has formed appear at 2.55 ppm (c and d), 3.41-4.10 ppm (e and f) and 5.15 ppm (j), respectively. The nine and six methyl protons surrounding the silyl group have shifts at -0.02 – 0.09 ppm (a) and 0.84 ppm (b), respectively. The aliphatic (i) and aromatic (k) protons of the benzylcarboxy group (Z) are observed at 5.15 ppm and 7.36 ppm, respectively as multiplets.

The comparison of the ATR spectra of (**4**) and (**5**) reveals that Wittig olefination of the ketone (**4**) has occurred successfully (**Figure 3.8**). The carbonyl peak of (**4**) at 1765 cm^{-1} is absent in the spectrum of (**5**).

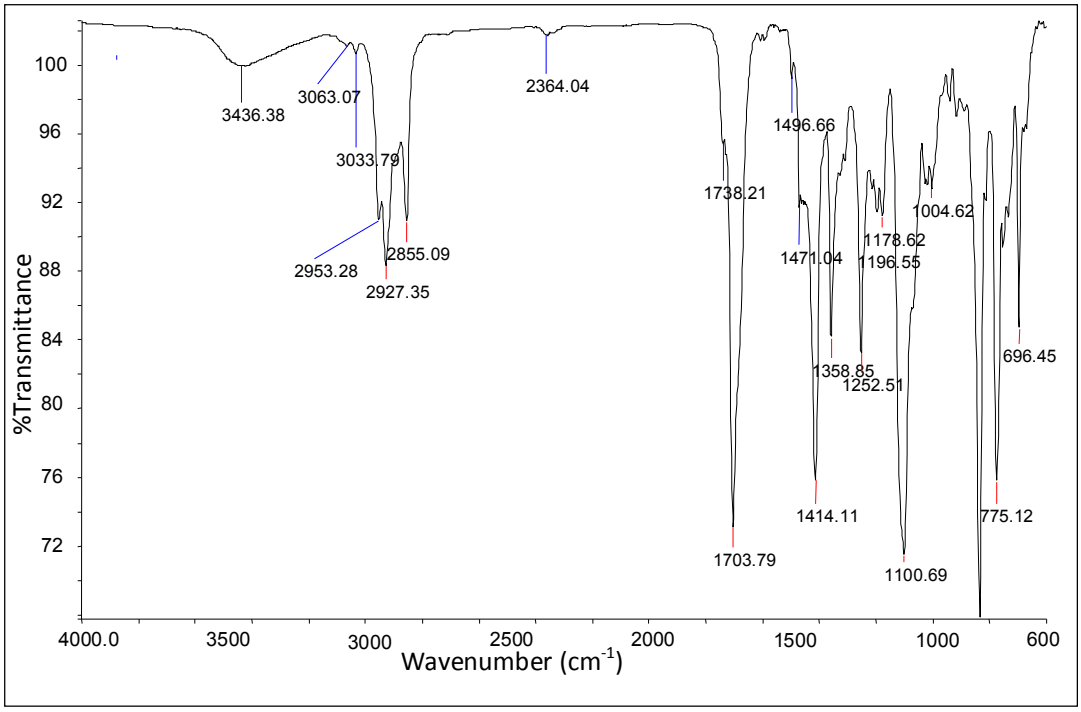

Figure 3.10 ATR spectrum of the nitrile oxide 1-Benzyloxycarbonyl–2(s)-*tert*-butyldi-methylsilyloxy-methyl–4-methylenepyrrolidine (**5**).

3.1.6. Spirocyclization

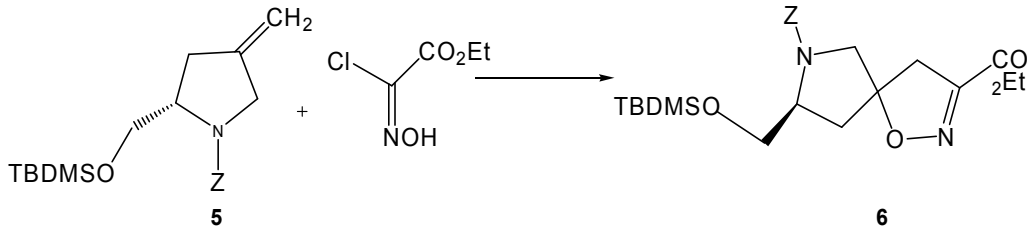

Scheme 3.8 Synthesis of Diazaspiro 1-Benzyloxycarbonyl–2(s)-*tert*-butyldimethylsilyloxymethyl–4-methylenepyrrolidine (**6**).

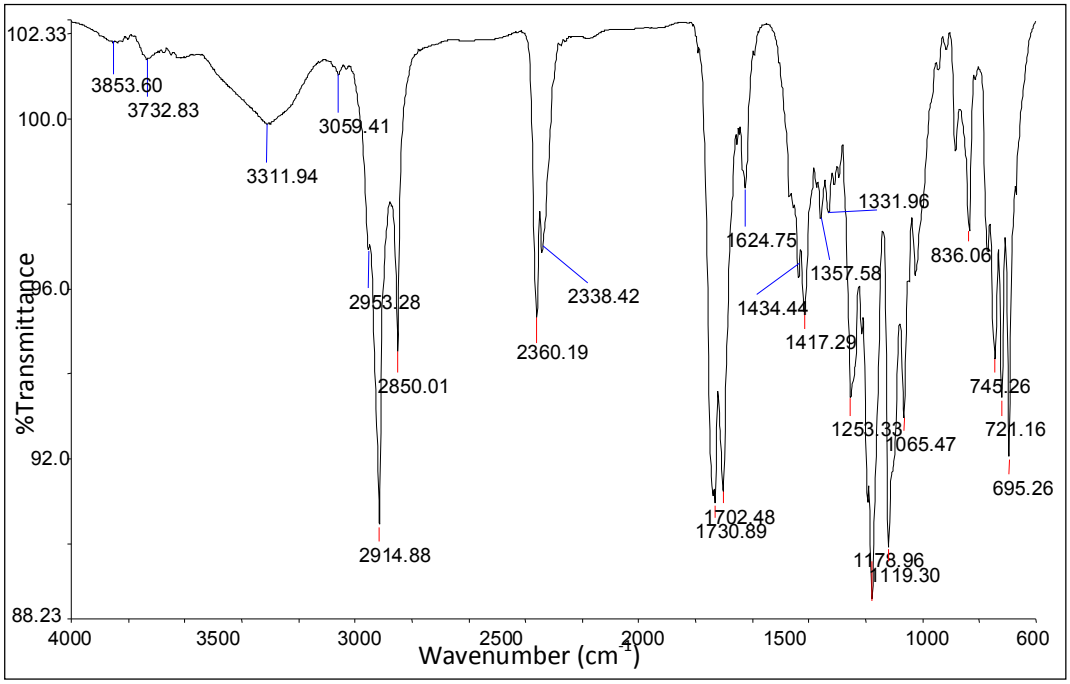

Figure 3.11 ATR spectrum of Diazaspiro 1-Benzyloxycarbonyl–2(s)-*tert*-butyldimethylsilyloxymethyl–4-methylenepyrrolidine (**6**).

The Wittig product was spirocoupled with ethyl chlorooximidoacetate. The resulting mixture included not reacted starting material as well as diastereomers. However, the separation of the diastereomers was very hard probably due to their close molecular structure helped them bind the silica in a similar manner.

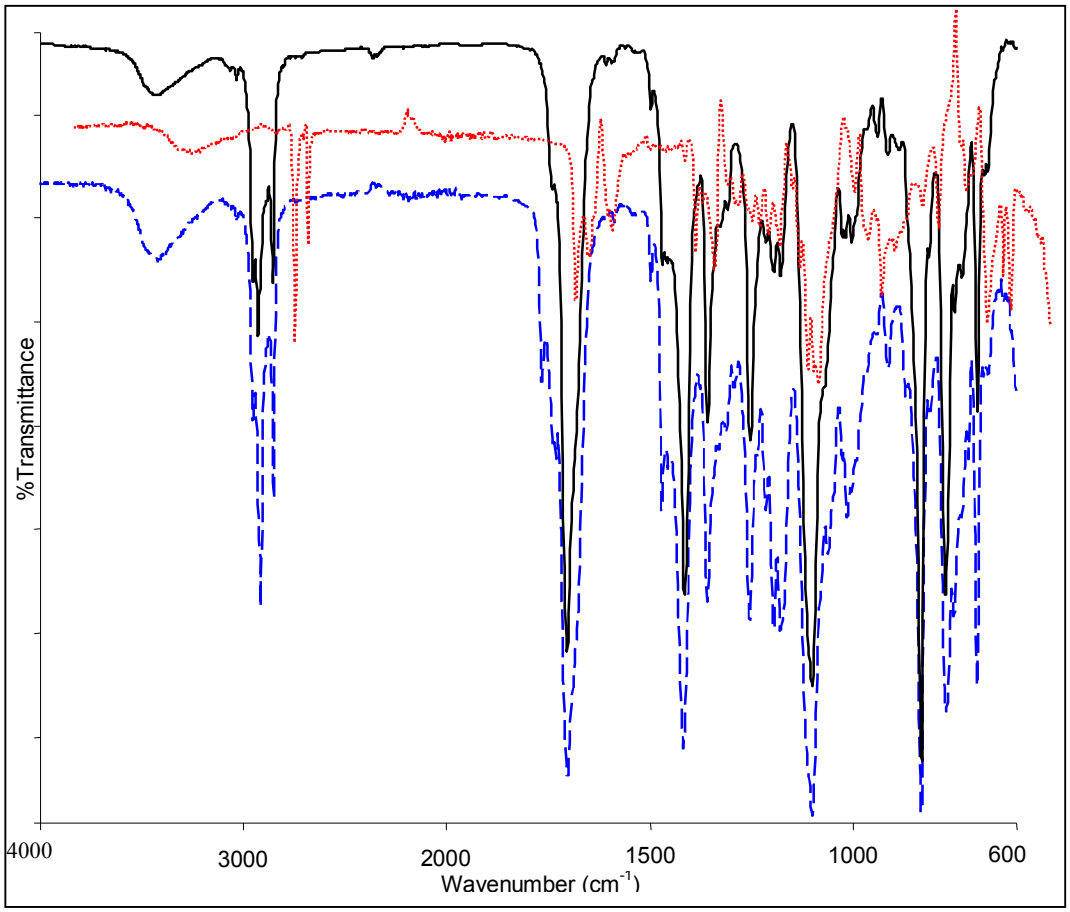

Figure 3.12 ATR spectra of (**4**), (**5**), and (**6**). The straight, dashed, and dotted lines denote the spectrum for (**4**), (**5**), and (**6**), respectively.

In the proton NMR of compound (**6**) as shown in **Figure 3.11, s**ilyl methyl protons appear close to 0 ppm which is the standard set by TMS, another silicium-containing molecule because of the shielding effect of the silicium. The nine protons of the three CH_3 groups (d) give a single peak sharply at 0.87 ppm and the shift of the six protons of the two CH_3 groups (a) is almost zero. However, we cannot see the two protons that belong to CH_2 next to Si (b and c) before 1 ppm. The peaks of the other CH_2 protons in the spirocycle itself (f, g, h, and i) are located at 1.34-1.40 ppm and 2.25-2.47 ppm along with the CH_3 protons of the ethyl group whereas the remaining CH_2 protons which is on the alpha position to the protected nitrogen group (k and l) appear at 4.14-4.18 ppm due to the deshielding effect of the nitrogen and maybe the oxygen which is not very far away from that CH_2 group. The hydrogen of the tertiary carbon (j) on the other alpha position to the nitrogen protected by Z group gives a peak

at 3.78-4.09 ppm. The CH_2 protons in the ethyl group (m) are neighbor to the deshielding oxygen atom and the chemical shift of these hydrogens are located at 4.30-4.41 ppm as quartet due to the CH_3 group next to it. Two CH_2 protons connected to aromatic ring (n) have a chemical shift of 5.05-5.19 ppm while the phenyl protons are located at 7.35 ppm in a broad single peak which is very close to the solvent's chemical shift.

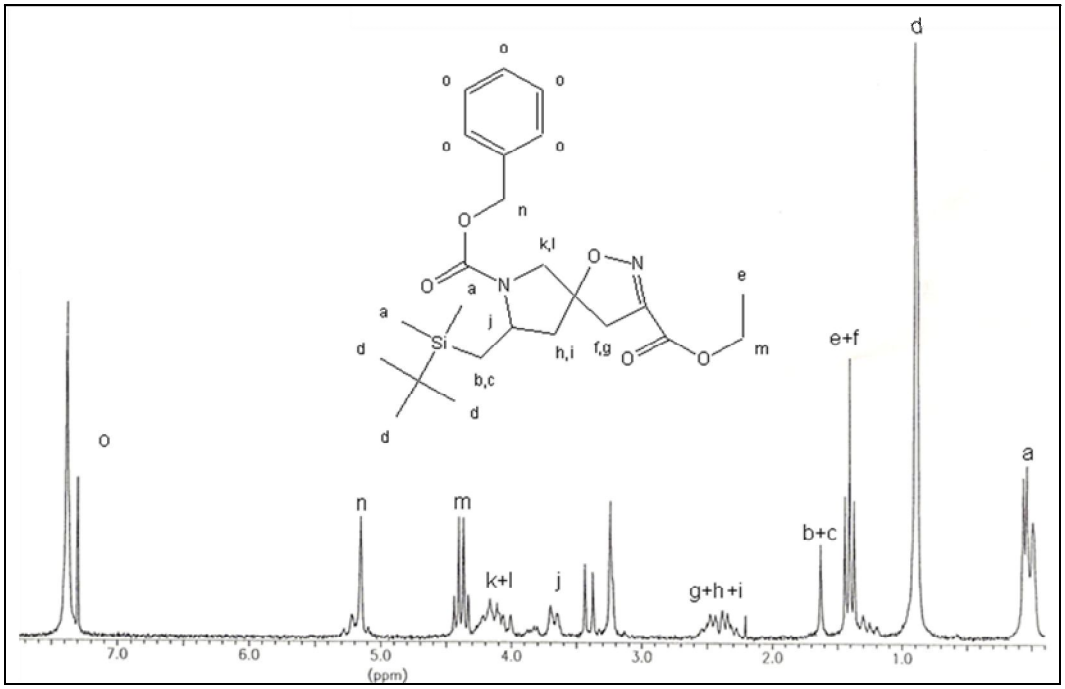

Figure 3. 11 ^{1}H NMR spectrum of the diazaspiro 1-Benzyloxycarbonyl–2(s)-*tert*-butyldimethylsilyloxy-methyl–4-methylenepyrrolidine (**6**). Solvent: $CDCl_3$.

Table 3. 1 Some physical properties of products **1-6**.

Product No.	Physical State	TLC, R_f	% Yield
1	Light yellow oil	EtOAc 9/ MeOH 1: 0.20	97
2	Yellow oil	EtOAc 9/ MeOH 1: 0.63	95
3	Viscous, yellow	EtOAc 4/ Hexane 6: 0.3	60
4	Viscous, yellow	EtOAc 3/ Hexane 7: 0.5	93
5	Viscous-solid	Ether 2/ Hexane 8: 0.40	69
6	Viscous, yellow	EtOAc 4/ Hexane 6: 0.36	20

3.2. Diaminopropionic acid derivatives

2,3-diaminopropionic acid (Dpr-OH), or *N*-Boc-3-amino-l-alanine has been frequently utilized for peptide synthesis or protein design (Englund, Gopi et al. 2004). For example, Dpr-OH-based chelators were used small and strong tripod ligands for the labelling of biomolecules with ^{99m}Tc (Liu, Oliveira et al. 2010). Dpr-OH is also substituted for Lysine to show the stability of α helix formation in simple polypeptides is affected by side chain length (Venkataramanarao, Sudarshan et al. 2007). L-Asparagine was the starting material for N_α-substituted diaminopropionic acids and Boc-L-asparagine was for N_β-substituted diaminopropionic acids. Either the fluorinated molecules or the control molecule were coupled followed by Hofmann degradation (**Scheme 3.9**) of the resulting compounds, or Boc-Asn-OH (Boc-L-asparagine) was degraded to Boc-Dpr-OH *via* Hofmann degradation using DIPA (iodosobenzene diacetate), and then coupled with the fluorinated molecules or the control molecule.

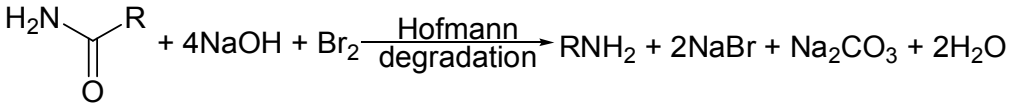

Scheme 3.9 A schematic representation of Hofmann degradation via sodium hypobromite.

3.2.1. N_α-substituted diaminopropionic acids

N_α-substituted diaminopropionic acids were synthesized as described by Pitts et al. (Pitts, Wityak et al. 2000). L-asparagine and the fluorinated or the control molecule were coupled (**Scheme 3.10**) followed by Hofmann degradation of the resulting compounds *via* sodium hypobromite composed of sodium hydroxide and bromine (**Scheme 3.11**).

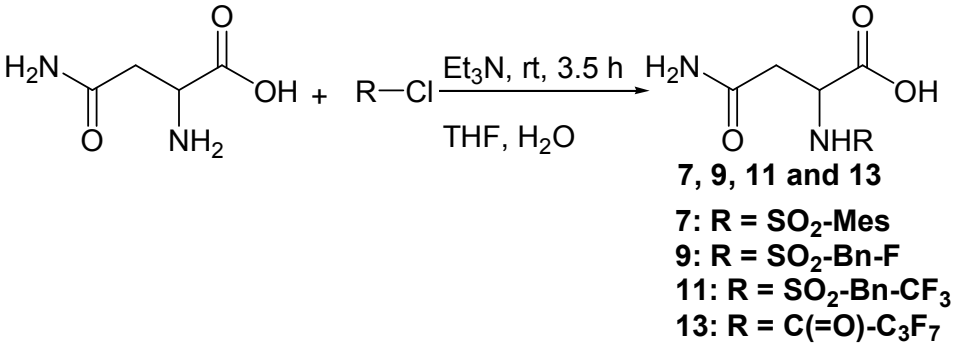

Scheme 3.10 Synthesis of N_{α}-substituted diaminopropionic acids.

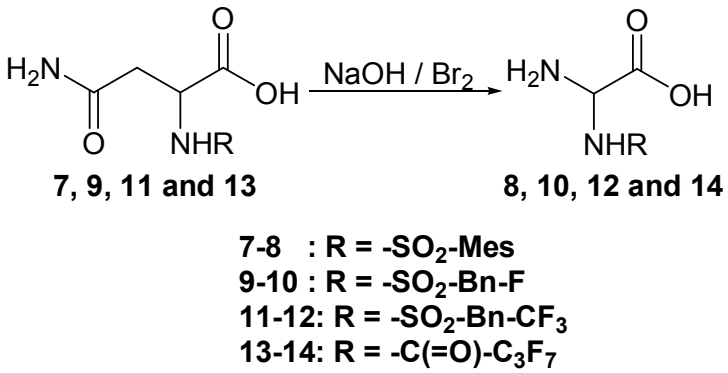

Scheme 3.11 Hofmann degradation of N_{α}-substituted Asparagine moieties.

In the ATR spectra of compound (**7**) in **Figure 3.13**, the C-H band stretching of the benzene ring is present to the left of 3000 cm^{-1}. The bands for C-H bends appear at 1000 cm^{-1} and for the in-plane bends in the aromatic ring at 659 cm^{-1}. The absorptions at 1667 and 1717 cm^{-1} are for the C=O double bond stretching. Above 3000 cm^{-1} we observe the N-H stretching as well as the O-H bonding. The C-H aromatic stretching is at 1590 cm^{-1}. The CH_3 bend band for the methyl groups attached to the aromatic ring is present at about 1400 cm^{-1}.

The proton NMR of compound (**7**) is on **Figure 3.14**. The singlets at 2.33 and 2.71 ppm belong to hydrogens **a** and **b**, respectively while hydrogens **c, d and e** appear as a multiplet between 3.34 and 3.70 ppm, and the aromatic hydrogens **f** have a singlet at 7.08 ppm.

When the ATR spectra of compounds (**7**) **Figure 3.13** and (**8**) **Figure 3.15** are compared, the absence of the second peak at around 1600-1700 cm^{-1} as seen in **Figure 3.16** confirms Hofmann degradation has occurred.

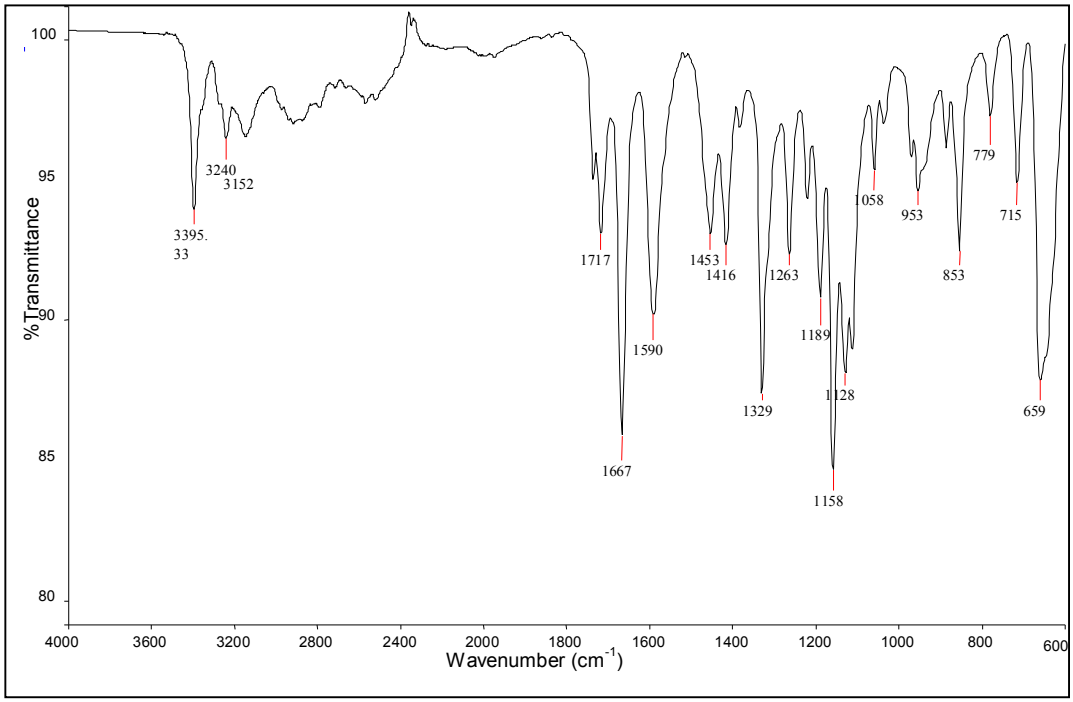

Figure 3.13 ATR-IR spectrum of Mes-Asn-OH **(7).**

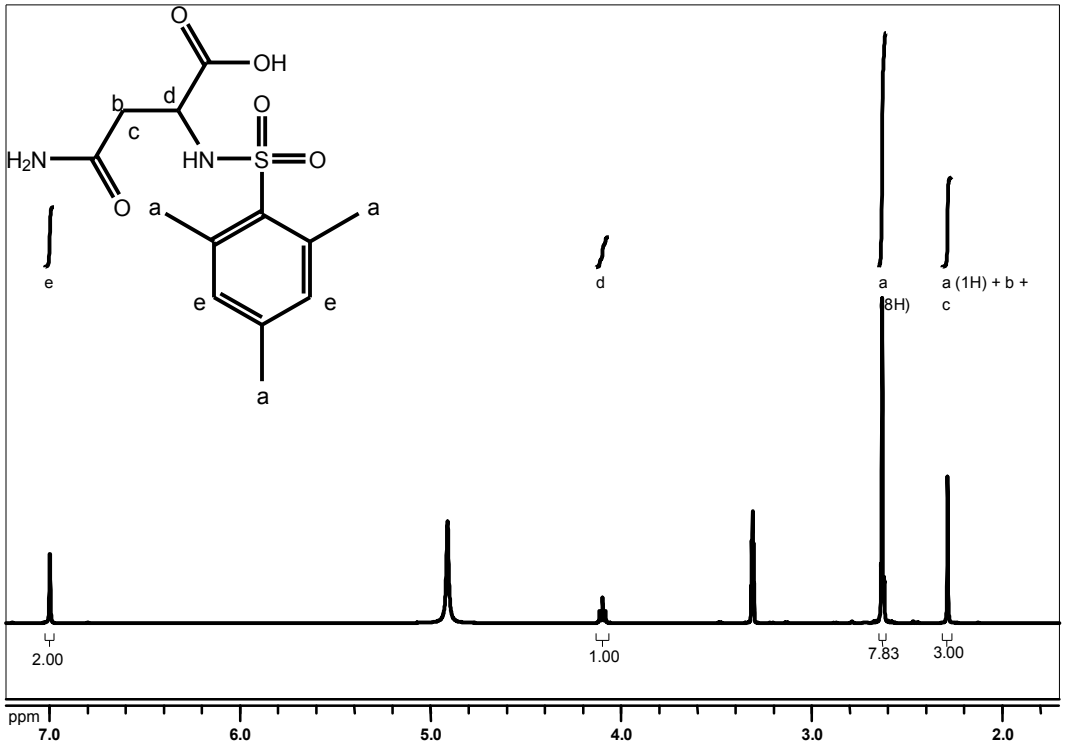

Figure 3.14 ^{1}H NMR spectrum of Mes-Asn-OH, **(7).** Solvent: MeOH – d4.

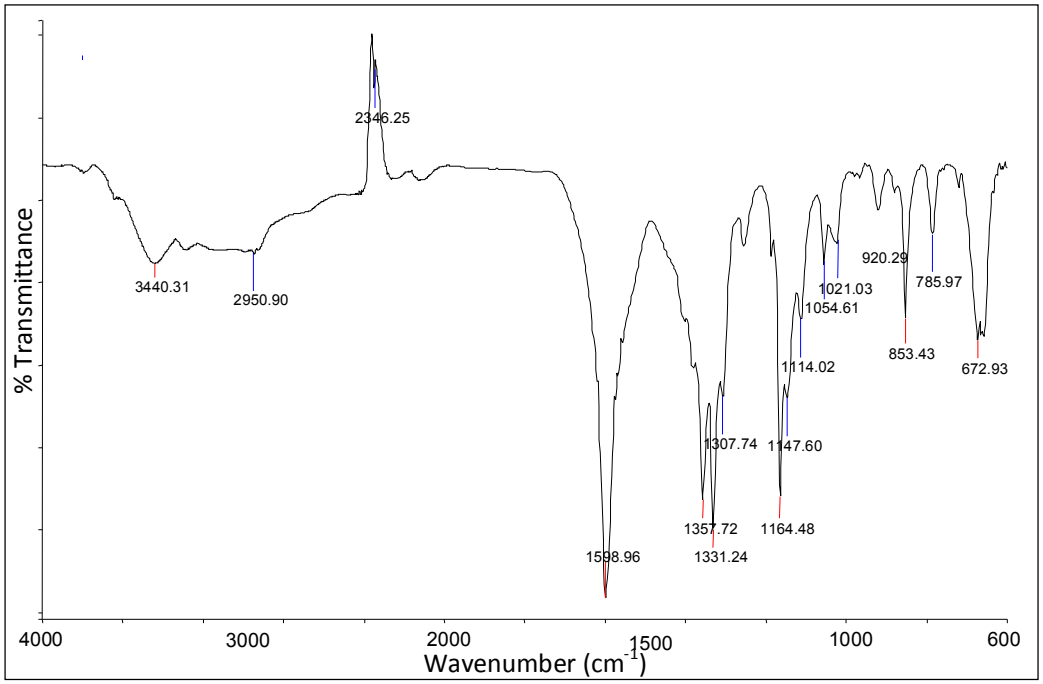

Figure 3.15 ATR-IR spectrum of Mes-Ala-OH **(8).**

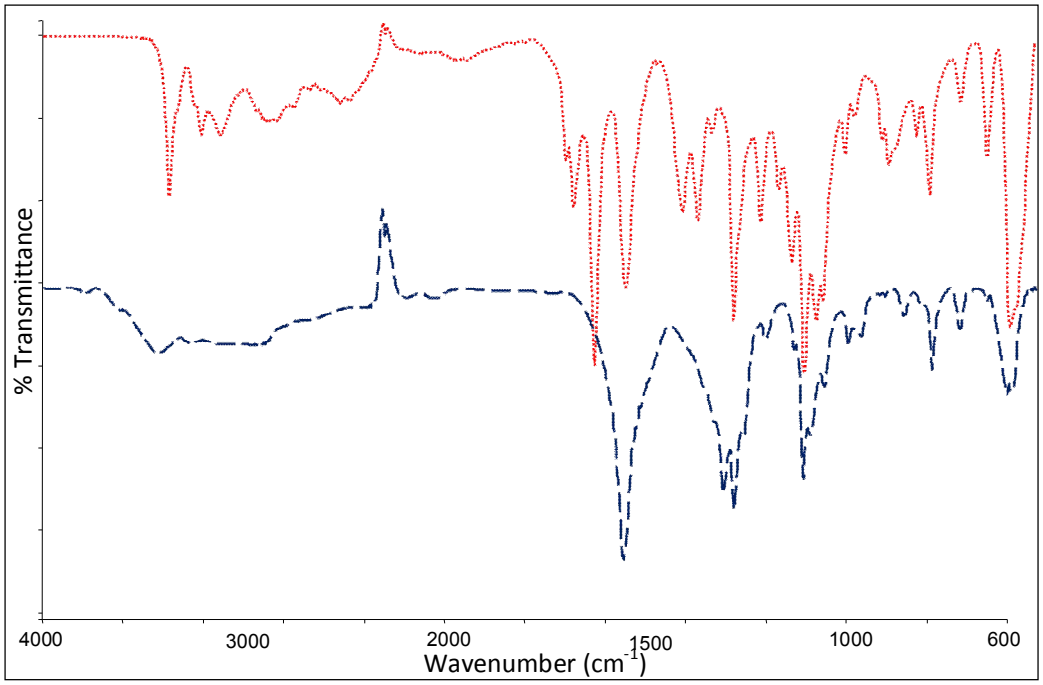

Figure 3.16 Comparison of the ATR-IR spectra of Mes-Asn-OH **(7)** and Mes-Ala-OH **(8)**. The dotted lines above represent the ATR-IR spectrum of **(7)** while the dashed lines represent the one of **(8).**

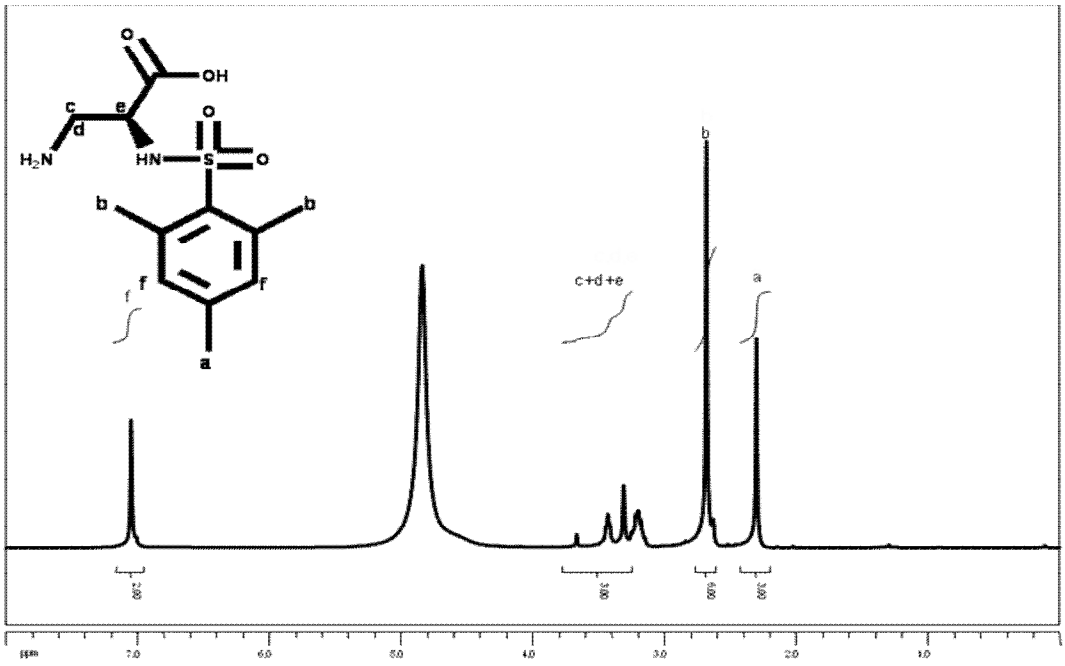

Figure 3.17 ^{1}H NMR spectrum of Mes-Ala-OH, **(8).** Solvent: MeOH – d4.

The ^{1}H NMR spectrum of compound (**8**) is shown in **Figure 3.17**. The singlets at 2.30 and 2.68 are assigned to methyl protons in para position and ortho position in the aromatic ring, respectively. The chemical shift of the -CH_2- protons in the alpha position to and the single proton in the beta position the primary amine appear between 3.18 and 3.43 as a multiplet. The protons which belong to the aromatic ring have a chemical shift at 7.05 as a singlet.

The ^{13}C NMR of the compound (**8**) is depicted in **Figure 3.18**. The signals at 19.72 and 21.86 ppm are assigned to the carbon atoms of the methyl groups that are on the para and ortho substitutions on the benzene ring, respectively. The carbon atoms in the –CH_2- and –CH- groups in the alpha and beta position to the primary amine group give chemical shifts at 38.86 and 42.13 ppm, respectively. The chemical shifts of the unsubstituted carbons (e) of benzene ring are at 132.70 ppm while the ortho (f) and para (g) substituted carbon atoms have chemical shifts at 132.28 and 142.79 ppm, respectively.

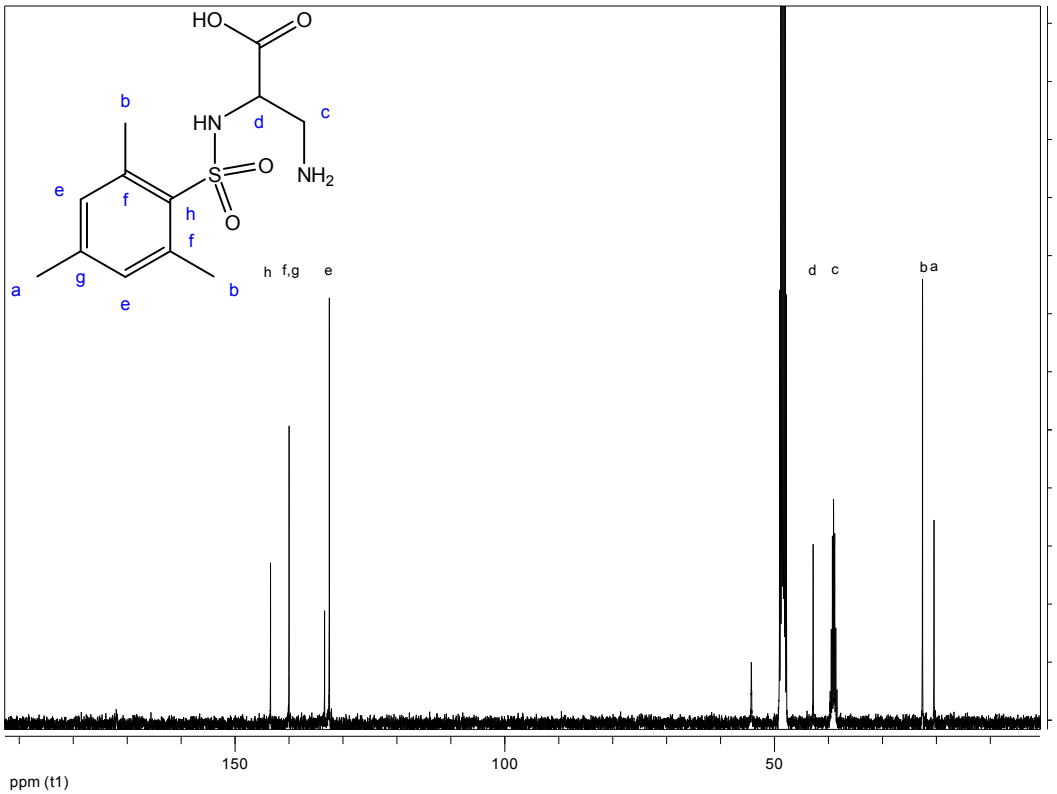

Figure 3.18 ^{13}C NMR spectrum of Mes-Ala-OH, **(8).** Solvent: MeOH – d4.

The ATR-IR spectra in **Figures 3.19** and **3.20** belong to compounds (**9**) and (**10**), respectively. The peaks around 3000 cm^{-1} represent the O-H stretching whereas the peaks around 1700 cm^{-1} confirm the presence of carboxyl groups. However, as seen in **Figure 3.21** has shown that Hofmann degradation has taken placed.

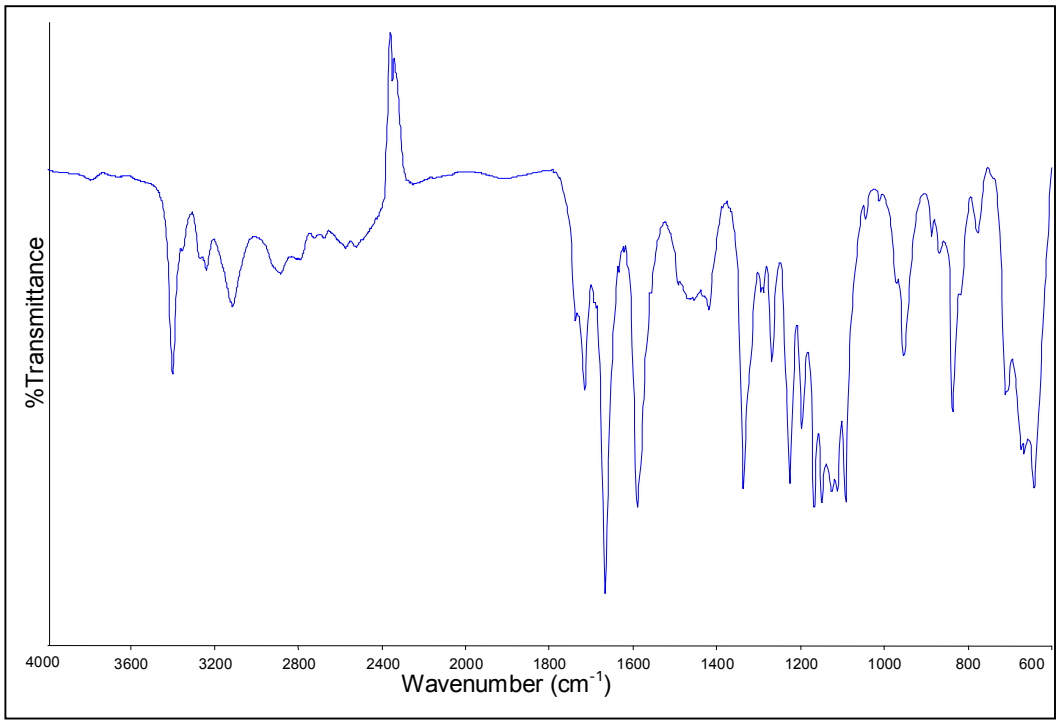

Figure 3.19 ATR-IR spectrum of F-Bn-SO_2-Asn-OH **(9).**

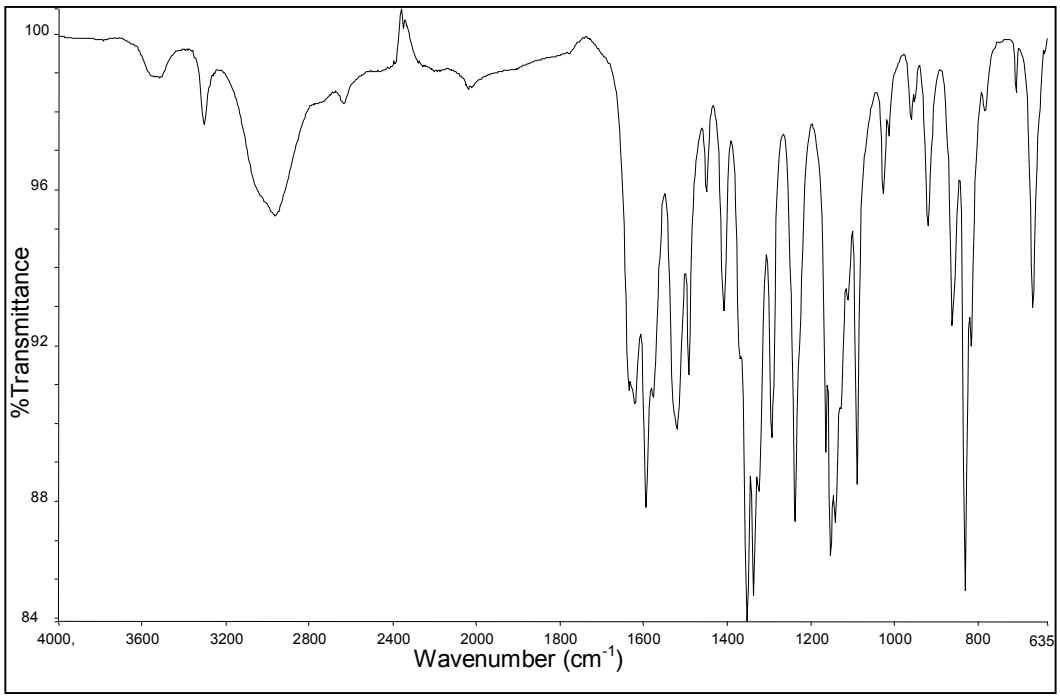

Figure 3.20 ATR-IR spectrum of F-Bn-SO_2-Ala-OH **(10).**

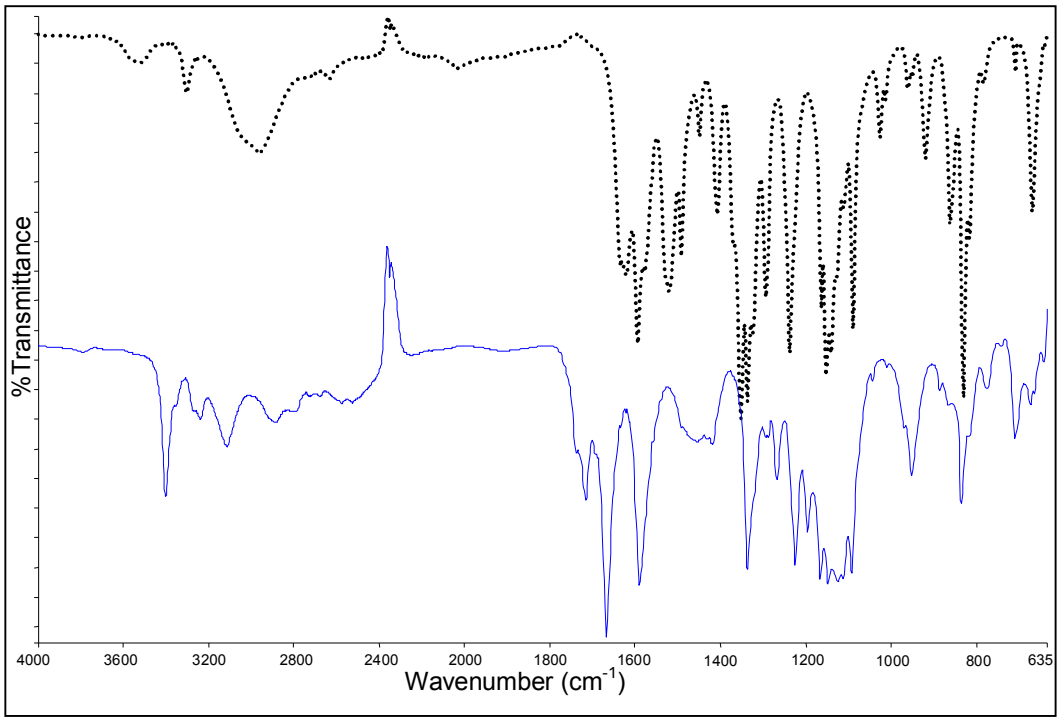

Figure 3.21 Comparison of ATR-IR spectra of F-Bn-SO_2-Asn-OH **(9)** and F-Bn-SO_2-Ala-OH **(10).** The dotted lines above represent the ATR-IR spectrum of **(9)** while the spectrum in the straight line belongs to **(10).**

In ^{1}H NMR of compound (**9**), the multiplet between 2.63 – 2.68 ppm is assigned to protons **a** and **b**. The singlet at 4.14 ppm belongs the hydrogen **c** of the tertiary carbon in the alpha position to the substituted amino group. The aromatic protons **d** and **e** have chemical shifts at 7.22 ppm and 7.86 ppm, respectively. The other chemical shifts not mentioned here belong to the solvent deuterated acetone.

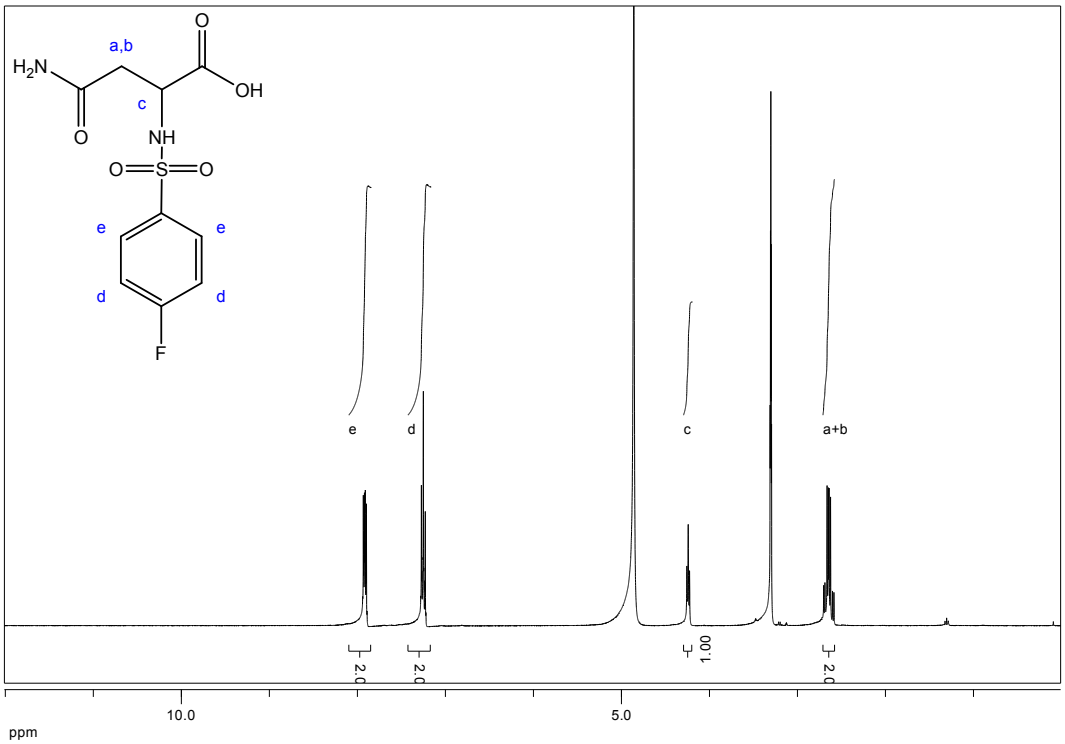

Figure 3.22 ^{1}H NMR spectrum of F-Bn-SO_2-Asn-OH, **(9).** Solvent: Acetone – d6

The ^{13}C NMR of compound (**9**) as in **Figure 3.23** shows the chemical shifts of the carbon atoms in (**9**) 10.84 ppm. Carbon (**a)** has a chemical shift at 38.78 ppm. The chemical shift of the tertiary carbon atom (**b**) is at 53.18 ppm. The chemical shifts of the carbon atoms in *ortho* and *meta* positions in the aromatic ring are located at 116.89 ppm and 131.01 ppm, respectively. The shift of the aromatic carbon atom bonded to the sulfonamide group is at 138.52 ppm whereas carbon (**f**) where the fluorine atom is bonded is assigned a chemical shift of 171.85 ppm. The peak at 172.65 ppm is assigned for the carbons of the two carboxyl groups present. The fluorine chemical shift is at -104.71 ppm in the ^{19}F NMR spectrum of compound (**9**) in **Figure 3.24.**

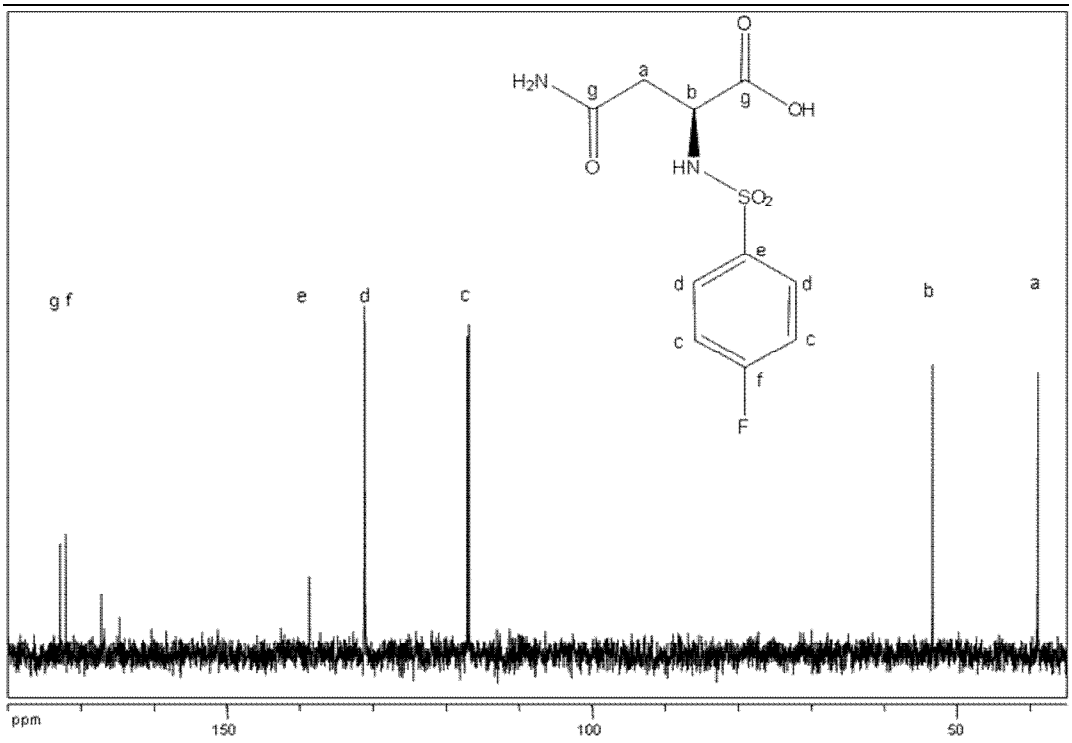

Figure 3.23 ^{13}C NMR spectrum of F-Bn-SO_2-Asn-OH, **(9).** Solvent: Acetone – d6.

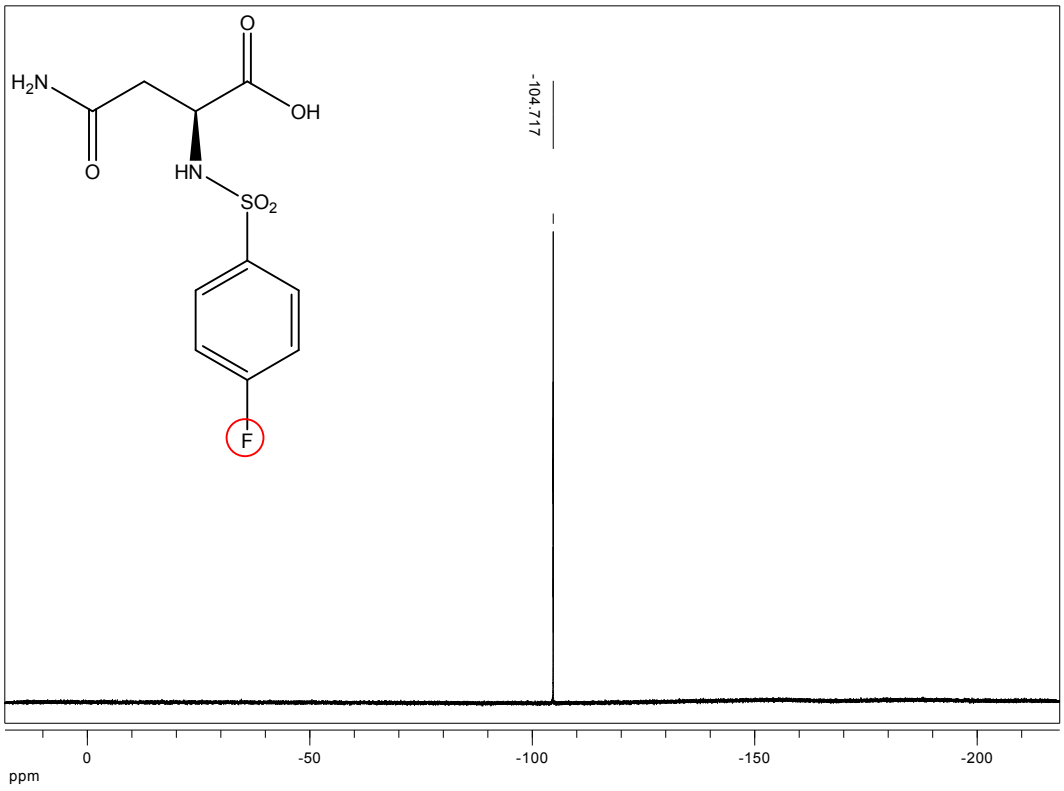

Figure 3.24 ^{19}F NMR spectrum of F-Bn-SO_2-Asn-OH, **(9).** Solvent: Acetone – d6.

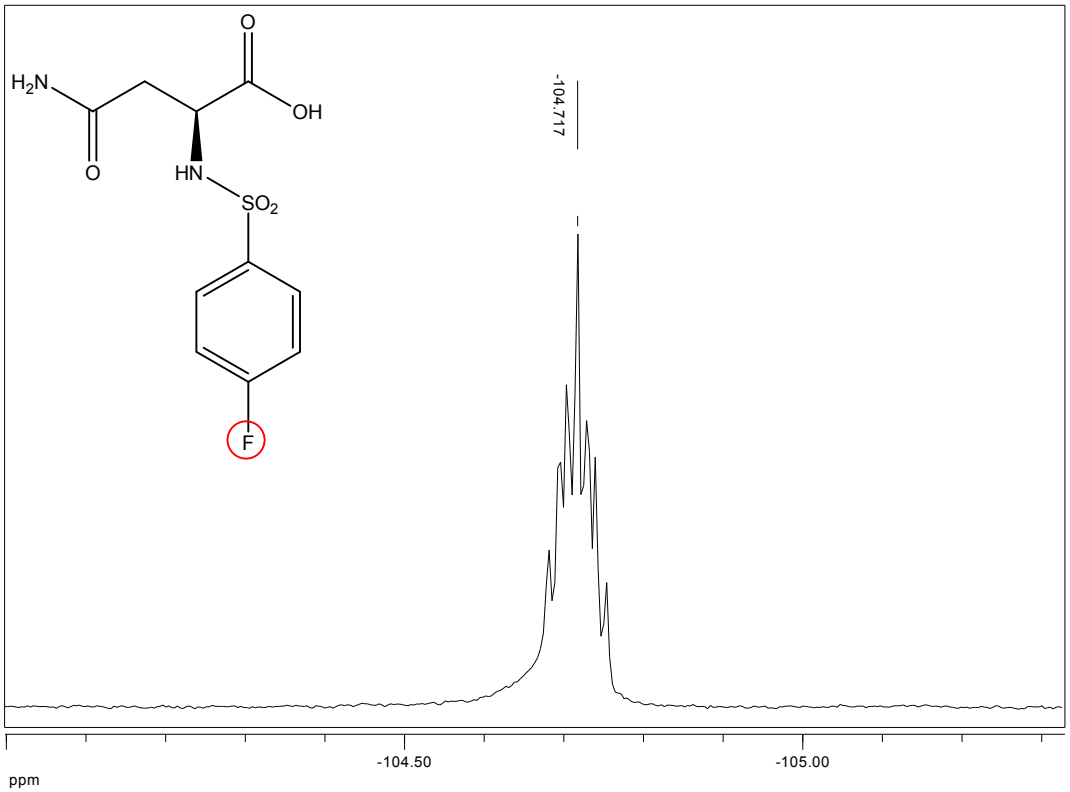

Figure 3.25 ^{19}F NMR spectrum of F-Bn-SO_2-Asn-OH, **(9).** Solvent: Acetone – d6.

^{1}H NMR spectrum of the compound (**10**) is shown in **Figure 3.26**. The chemical shifts of the aromatic protons **d** and **e** are located at 7.24 – 7.30 ppm and 7.85 – 7.89 ppm as multiplets, respectively. Proton **c** of the tertiary carbon atom has a multiplet between 3.79 – 3.82 ppm. Although the theoretical values for the chemical shifts of the methine protons **a** and **b** are 3.02 and 3.27 ppm, respectively as two quartets; the practical data which looks like the four multiplets between 3.33 ppm and 3.01 ppm suggests the presence of the R- enantiomer of compound (**10).** The peak at -104.41 ppm corresponds to the ^{19}F resonance of 4-fluorobenzene of (**10**) as shown in **Figure 3.27**.

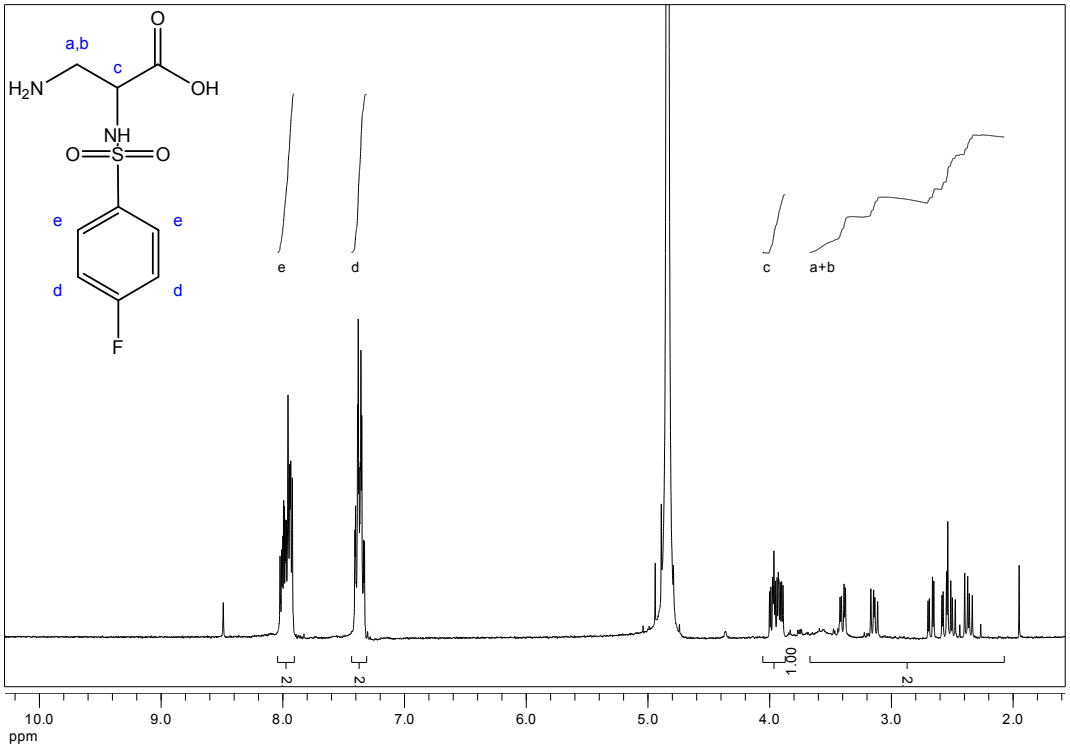

Figure 3.26 ^{1}H NMR spectrum of F-Bn-SO_2-Ala-OH, **(10).** Solvent: MeOH – d4.

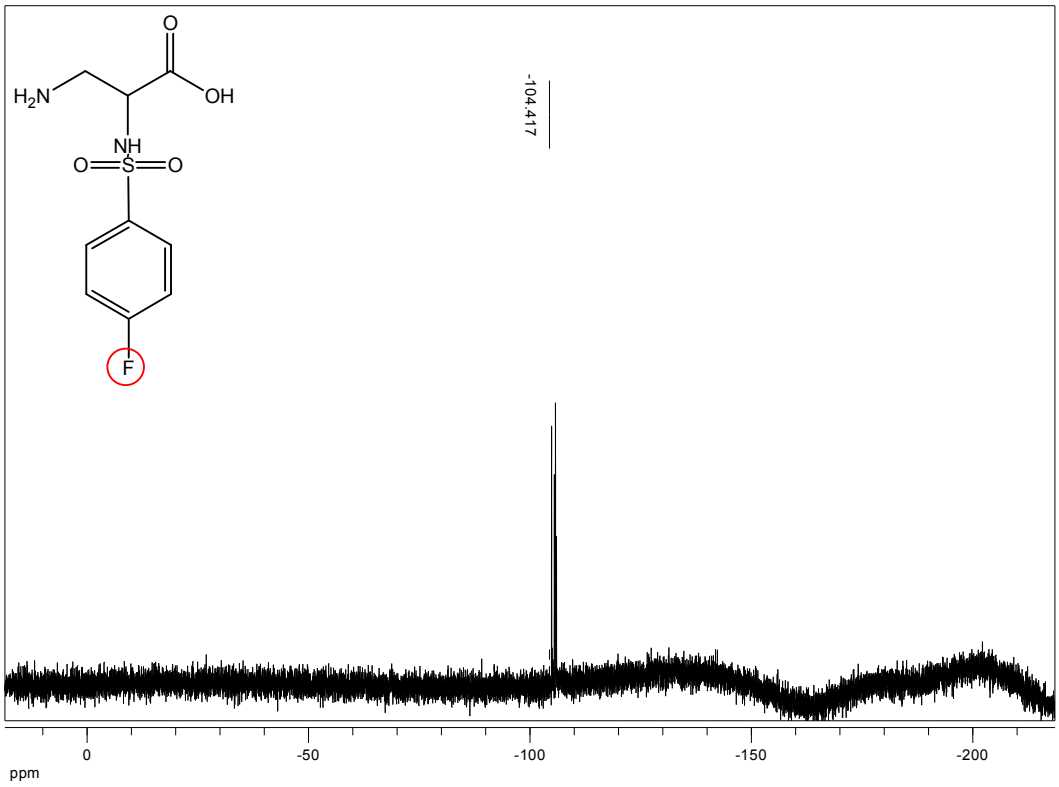

Figure 3.27 ^{19}F NMR spectrum of F-Bn-SO_2-Ala-OH, **(10).** Solvent: MeOH – d4.

The ATR spectra of compounds (**13**) and (**14**) are represented in **Figure 3.28** and **2.29**, respectively. When these spectra are compared as in **Figure 3.30**, we see the loss of one of the carbonyl group stretching in the spectrum of (**14**) when compared to the one of (**13**). This reveals that Hofmann degradation has occurred successively.

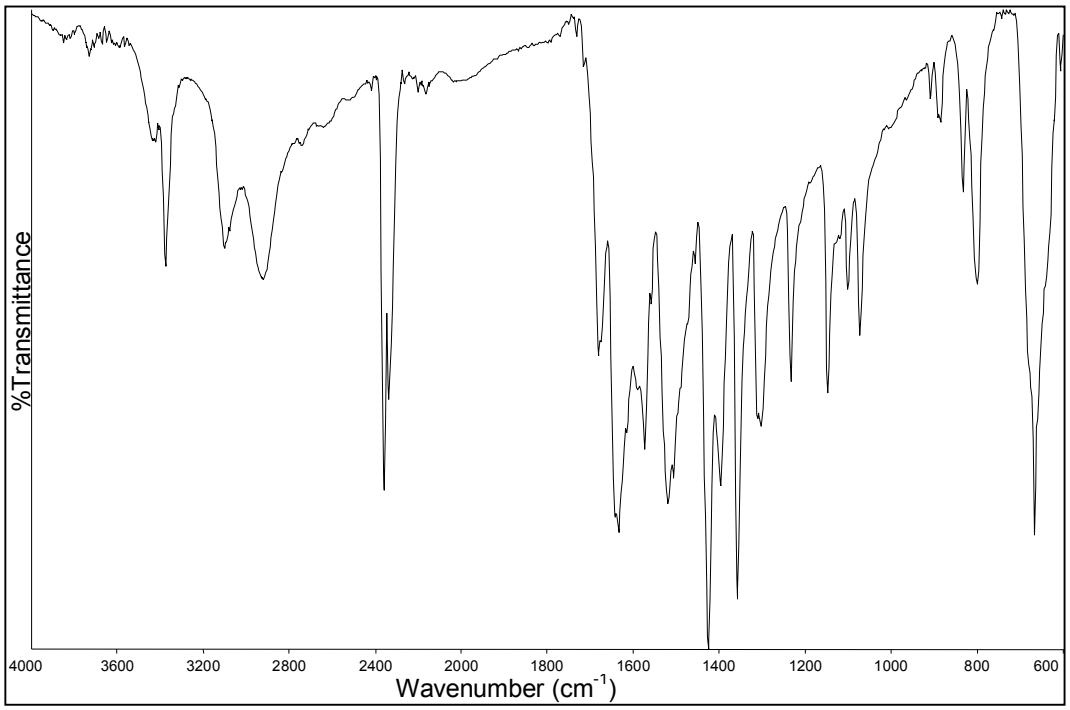

Figure 3.28 ATR-IR spectrum of C_3F_7-C(=O)-Asn-OH **(13).**

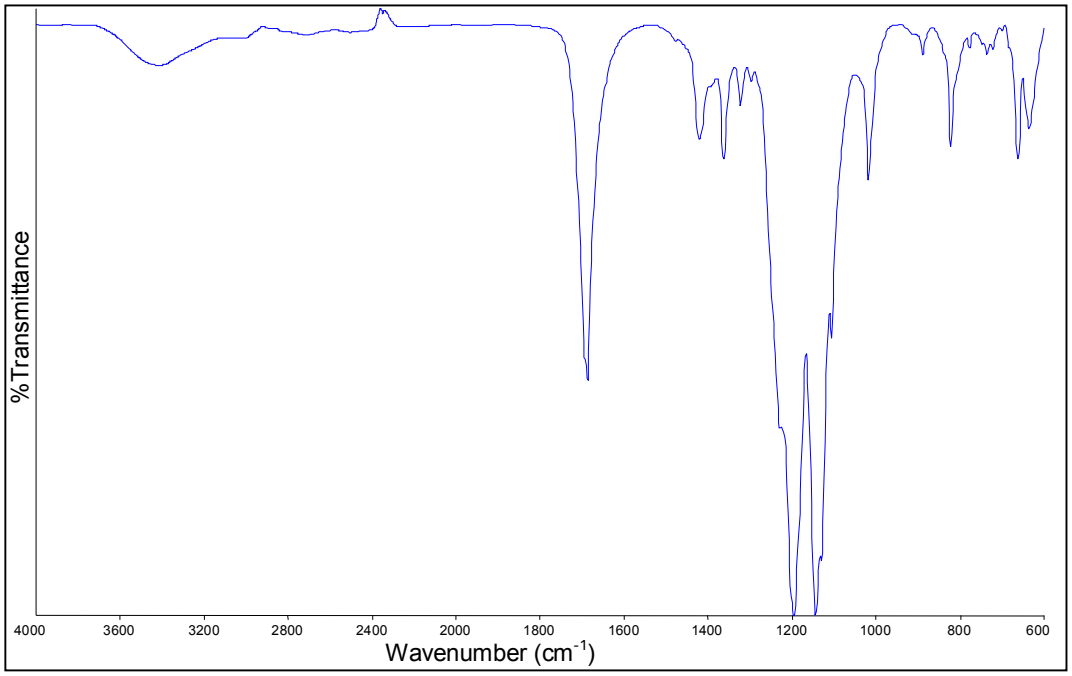

Figure 3.29 ATR-IR spectrum of C_3F_7-C(=O)-Ala-OH **(14).**

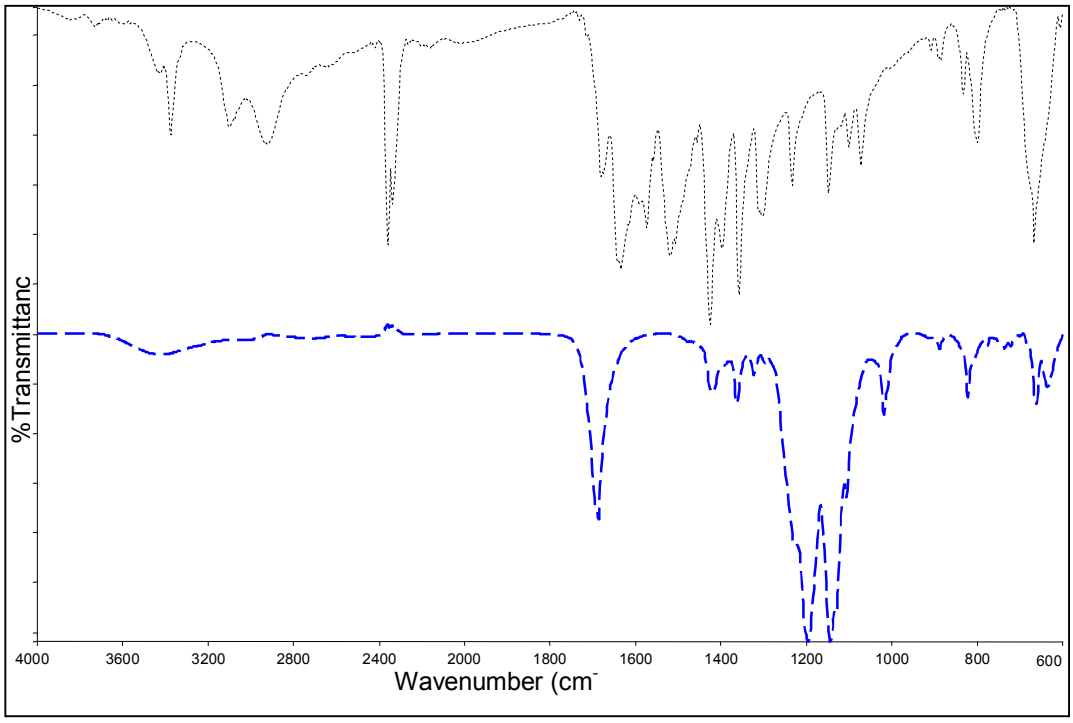

Figure 3.30 Comparison of ATR-IR spectra of C_3F_7-C(=O)-Asn-OH **(13)** and C_3F_7-C(=O)-Ala-OH **(14).** The dotted lines above represent the ATR-IR spectrum of **(13)** while the spectrum in the dashed line belongs to **(14).**

The ^{1}H and ^{19}F NMR spectra of compound (**13**) are represented in **Figure 3.31** and **2.32**, respectively. The doublet of quartet between 2.73 – 2.61 ppm is assigned for the protons (**a**) and (**b**), respectively while the quartet at 3.8 ppm is assigned for proton (**c**). The ^{19}F resonances of the fluorine atoms **α**, **β** and **γ** are observed at -81.2 ppm as a triplet, -118.8 ppm as a multiplet, and -128.8 as a singlet, respectively in the ^{19}F NMR spectrum of compound (**13).**

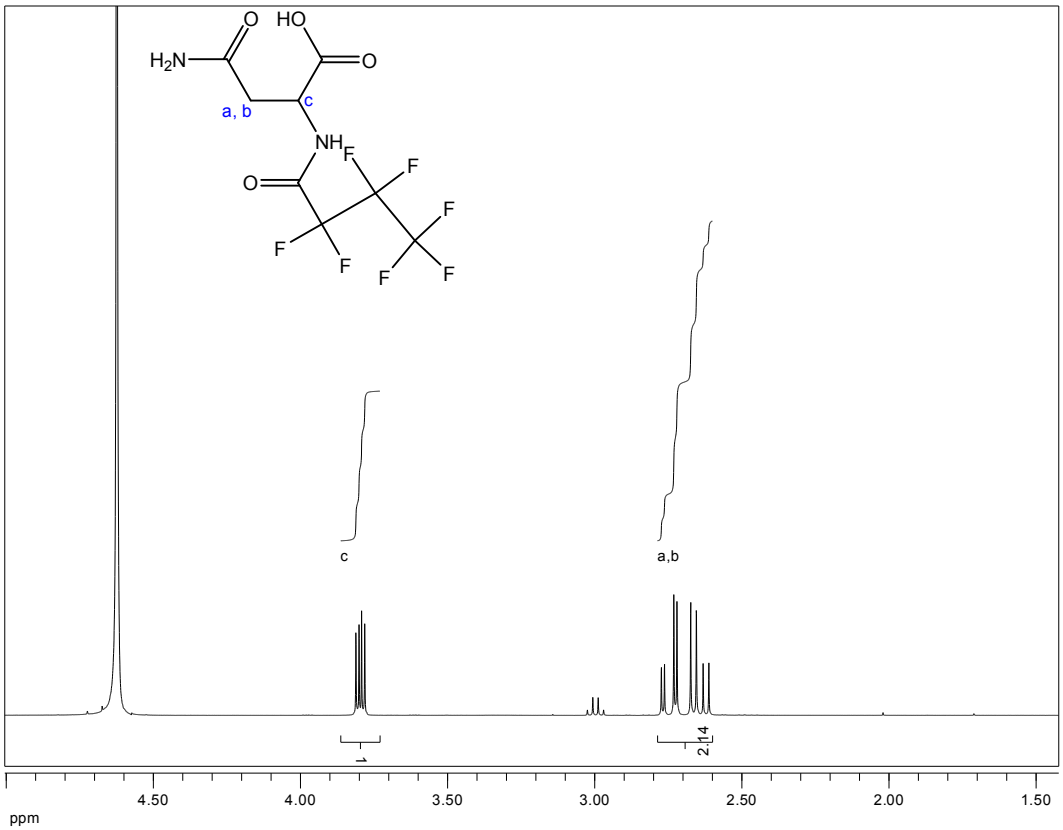

Figure 3.31 ^{1}H NMR spectrum of C_3F_7-C(=O)-Asn-OH, **(13).** Solvent: D_2O

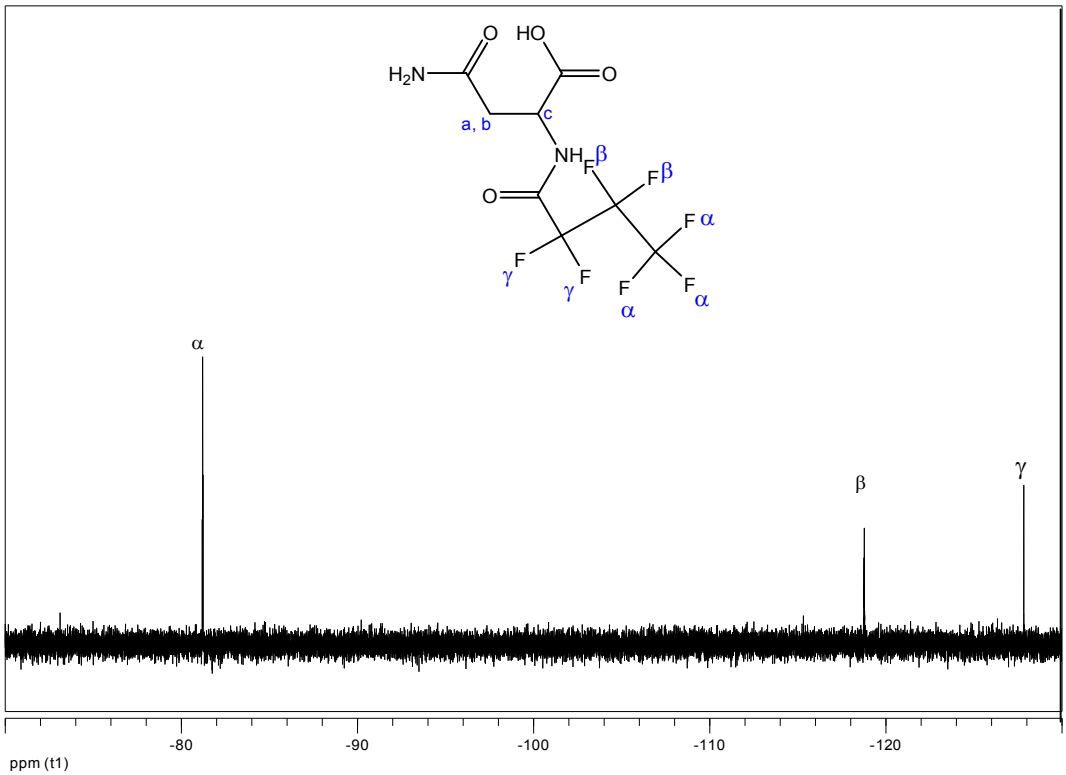

Figure 3.33 ^{19}F NMR spectrum of C_3F_7-C(=O)-Asn-OH, **(13).** Solvent: D_2O

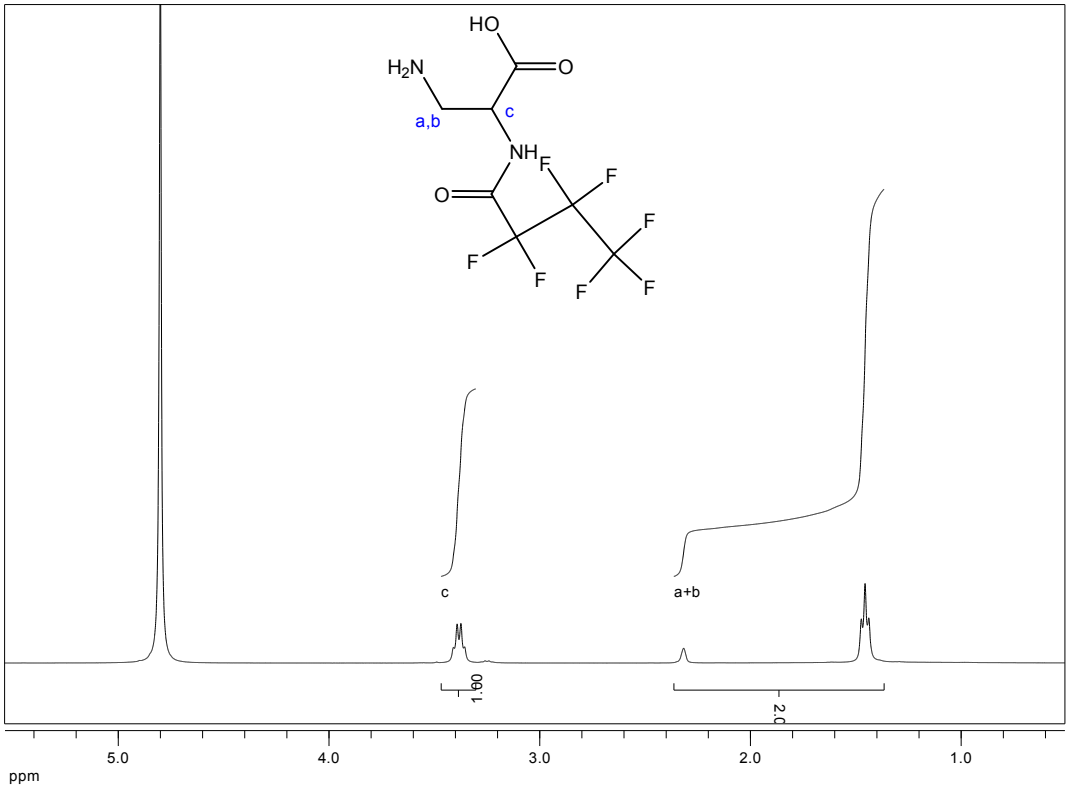

Figure 3.34 ^{1}H NMR spectrum of $C_3F_7C(=O)$-Ala-OH, **(14).** Solvent: D_2O.

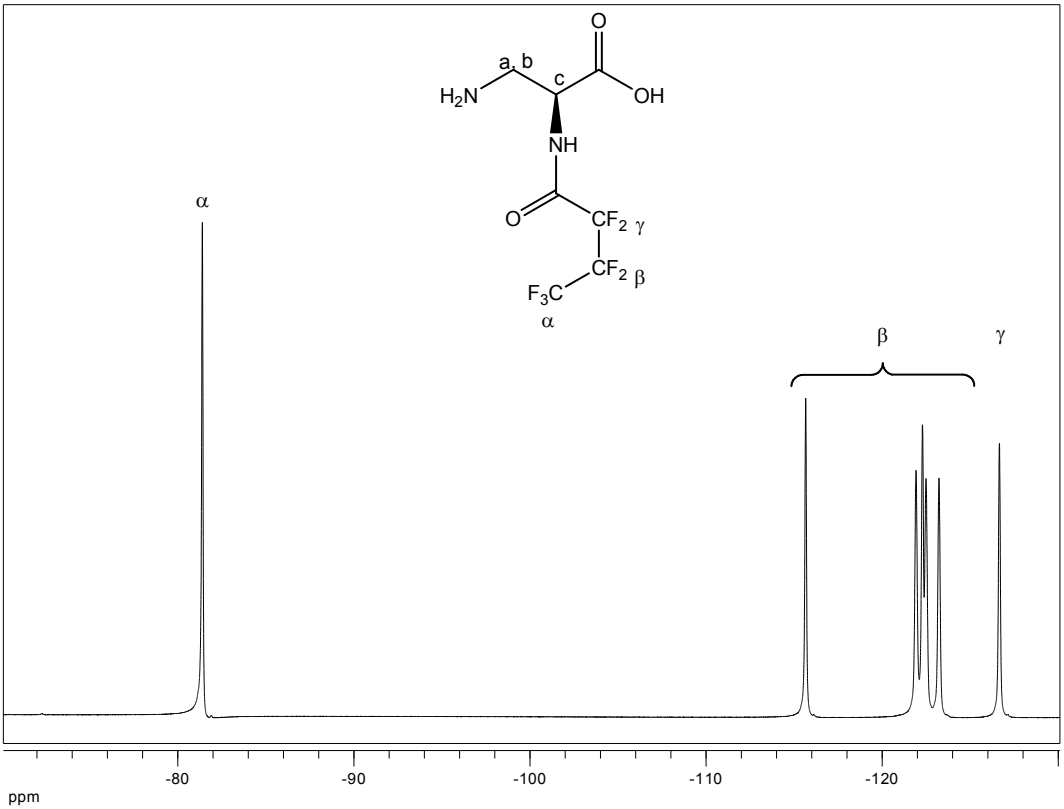

Figure 3.35 ^{19}F NMR spectrum of $C_3F_7C(=O)$-Ala-OH, **(14).** Solvent: D_2O.

Table 3. 2 Physical properties of N_α-substituted Asparagine and Dpr-OH moieties.

Molecule No.	Physical State	Melting Point (°C)	TLC, R_f (Butanol 1/ Toluene 1/ Acetic acid 1/ Water 0.5 unless stated otherwise)	% Yield
7	White powder	194	0.60	85
9	White powder	-	0.71	75
11	White powder	-	0.60	65
13	White powder	-	0.70	80
8	White powder	169	0.40	62
10	White powder	226	0.50 (EtOAc 5/Hexane 5)	80
12	White powder, hygroscopic	198-205	0.60	35
14	Viscous solid, white	195	0.60 (EtOAc 5/Hexane 5)	75

3.2.2. N_β-substituted diaminopropionic acids

N_β-substituted diaminopropionic acids were prepared after Hofmann degradation of Boc-Asn-OH as described in Zhang et al. (1997) since sodium hypobromite approach failed to obtain Boc-Dpr-OH from Boc-Asn-OH ((Zhang, Kauffman et al. 1997)). Basically, a mixture of N_α-*t*-Boc-L-asparagine with iodosobenzene diacetate in ethyl acetate, acetonitrile, and water (24/24/12 v/v/v) was was stirred at 16°C for 30 min, reacted with cooling at 20°C for 4 h, cooled to 0°C and N_α-*t*-Boc-β-amino-L-alanine (Boc-Dpr-OH) was obtained by filtering, washing with ethyl acetate and drying. Next, chloride salts of the fluorinated molecules or the control molecule were coupled with Boc-Dpr-OH to yield their corresponding products.

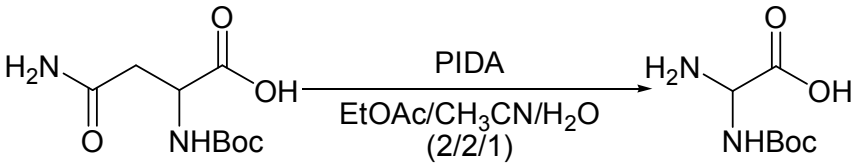

15

Scheme 3.12 Synthesis of N_α-*t*-Boc-L-diaminopropionic acid moieties. Conditions: PIDA (1.2 equiv.), EtOAc/CH_3CN/H_2O (24/24/12 v/v/v), 16°C for 30 min, then 20°C for 4 h

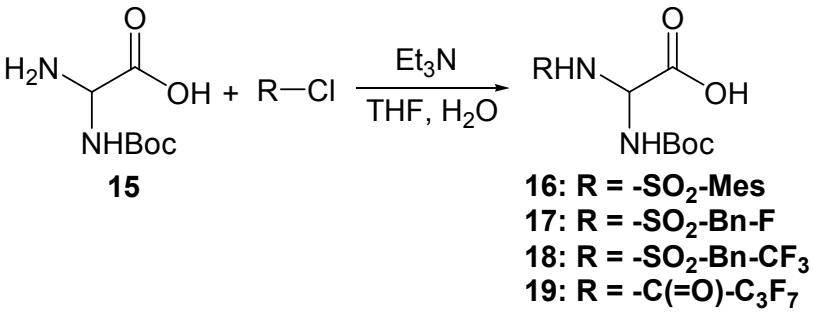

Scheme 3.13 Synthesis of N_{β}-substituted diaminopropionic acid moieties. Conditions: R-Cl (1.2 equiv.), Et_3N (3 equiv), THF, and H_2O, rt for 3.5 h

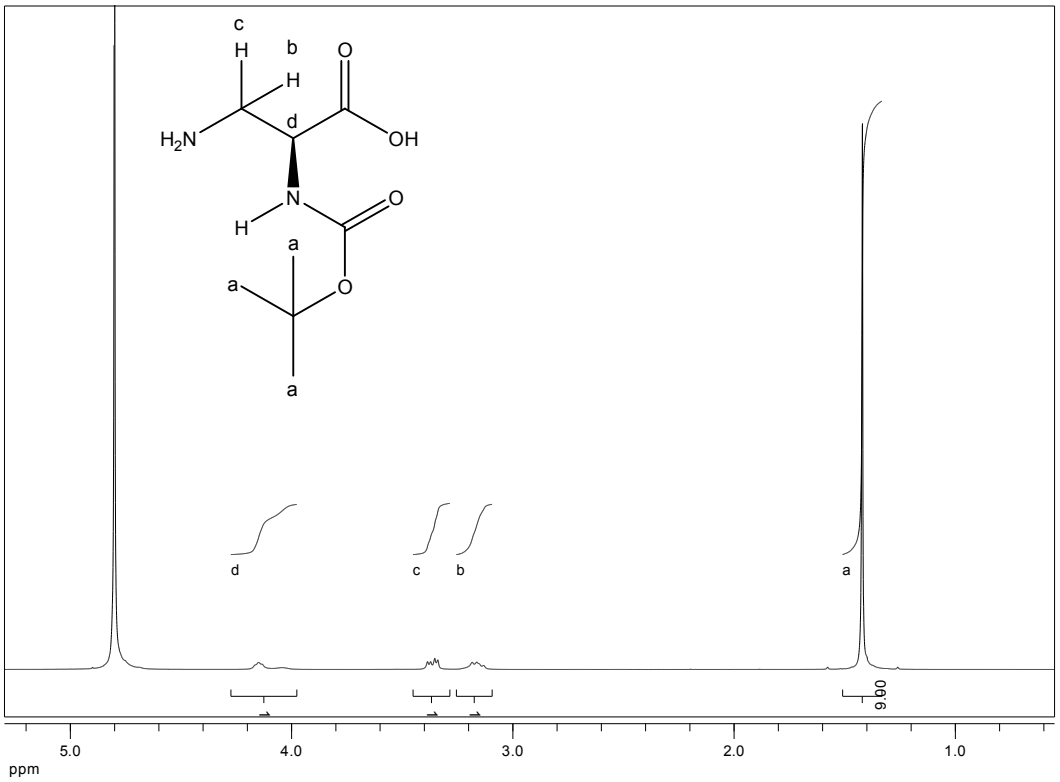

Figure 3.36 ^{1}H NMR spectrum of Boc-Dpr-OH (**15**). Solvent: D_2O.

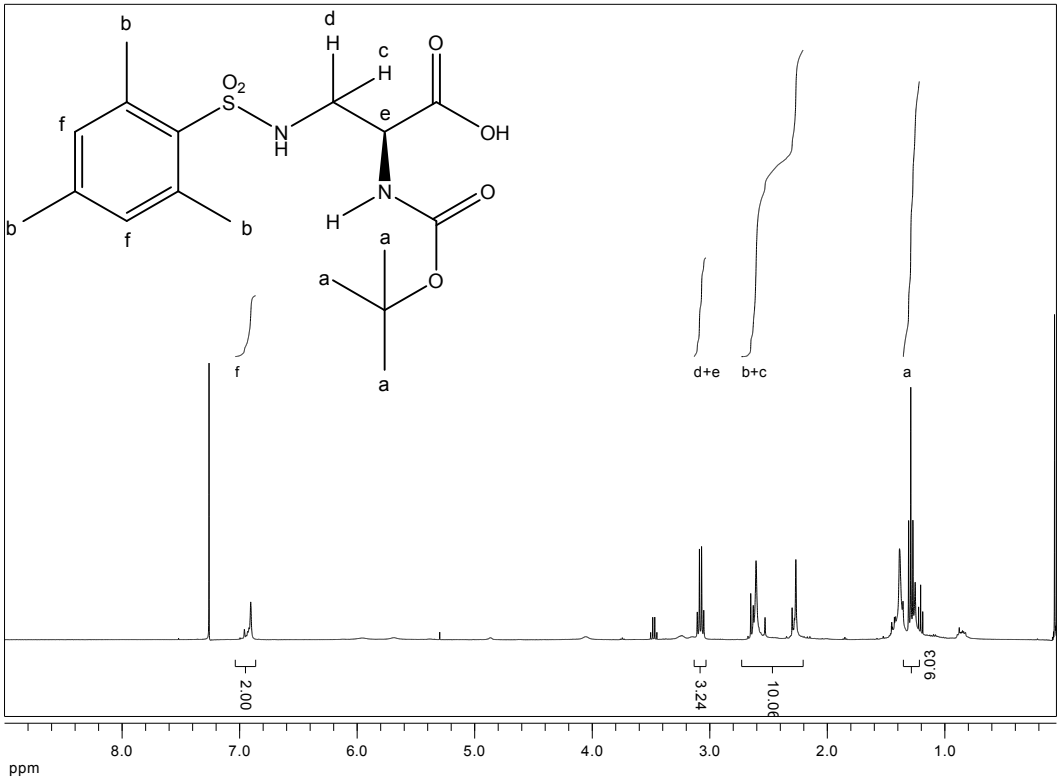

Figure 3.37 ^{1}H NMR spectrum of Boc-Dpr(Mes-SO_2)-OH (**16**). Solvent: $CDCl_3$.

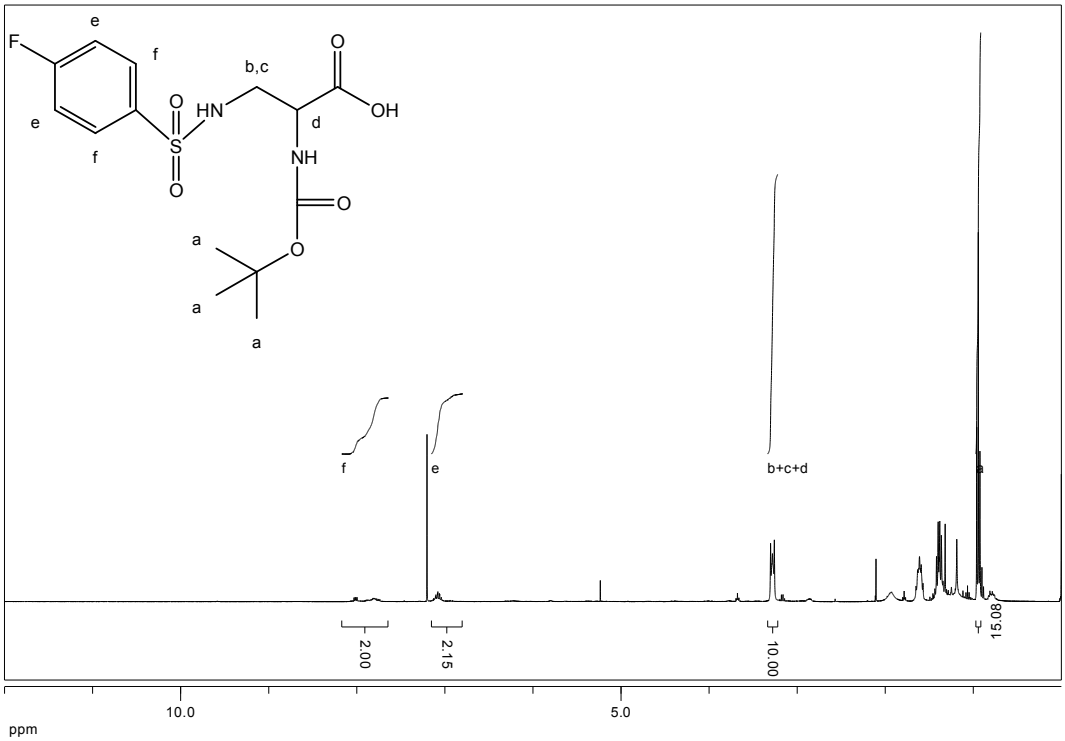

Figure 3.38 ^{1}H NMR spectrum of Boc-Dpr(F-Bn-SO_2)-OH (**17**). Solvent: $CDCl_3$.

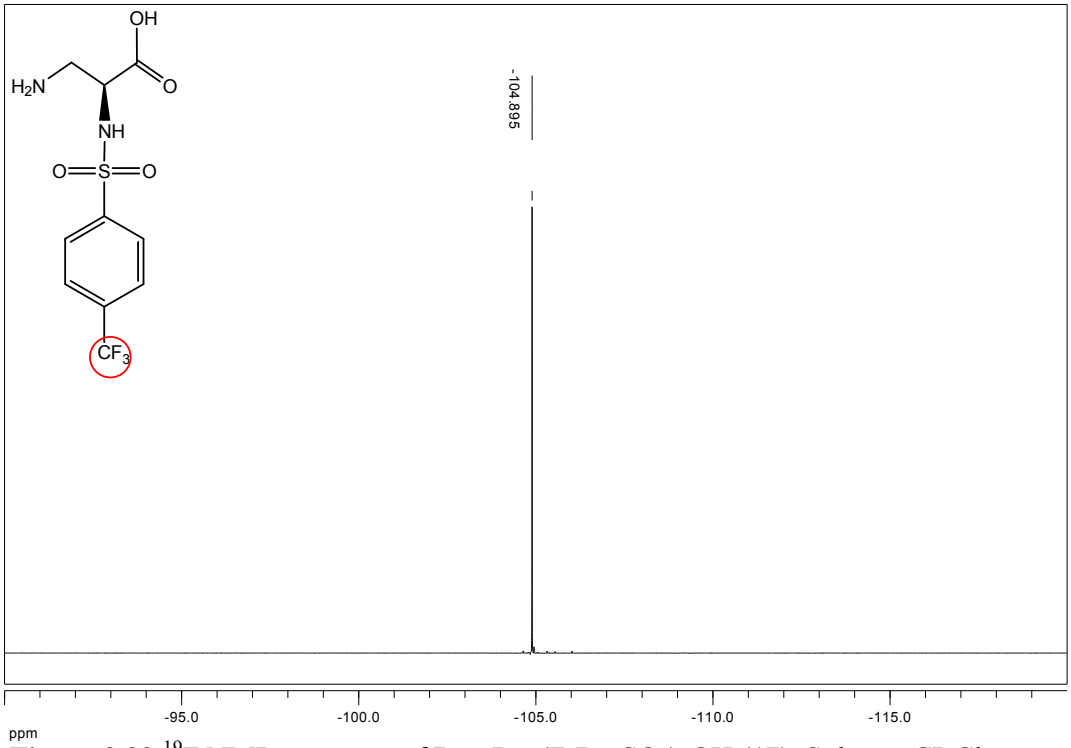

Figure 3.39 ^{19}F NMR spectrum of Boc-Dpr(F-Bn-SO_2)-OH (**17**). Solvent: $CDCl_3$.

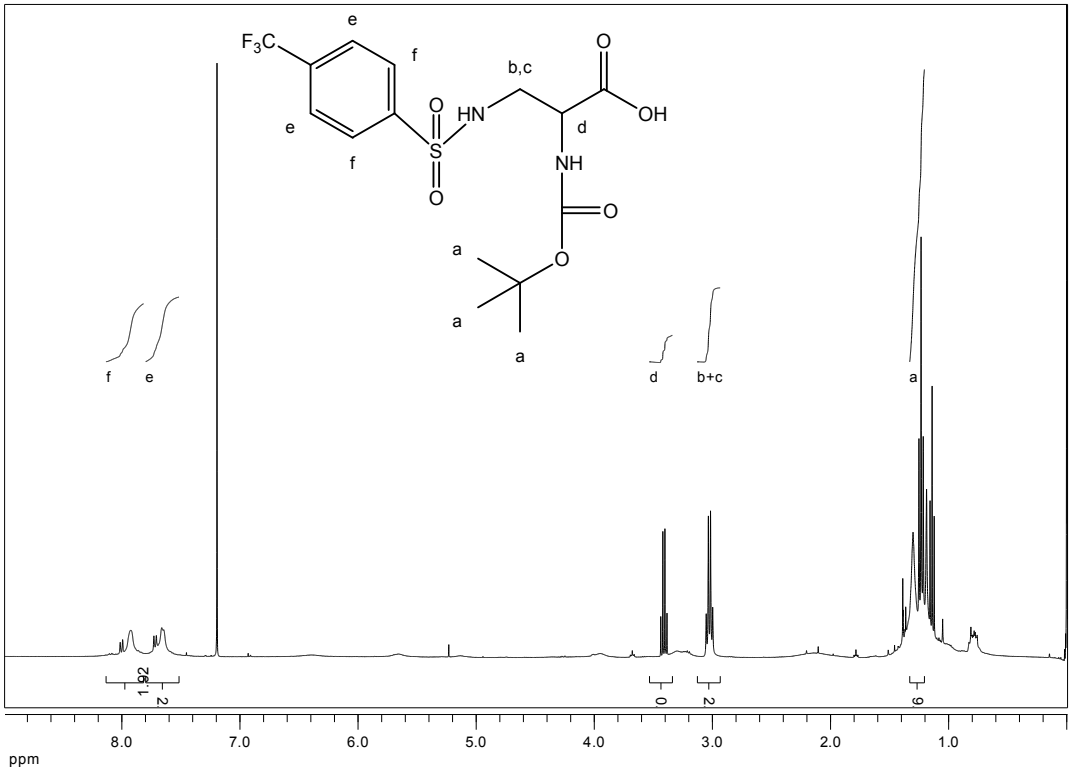

Figure 3.40 ^{1}H NMR spectrum of Boc-Dpr(CF_3-Bn-SO_2)-OH (**18**). Solvent: $CDCl_3$.

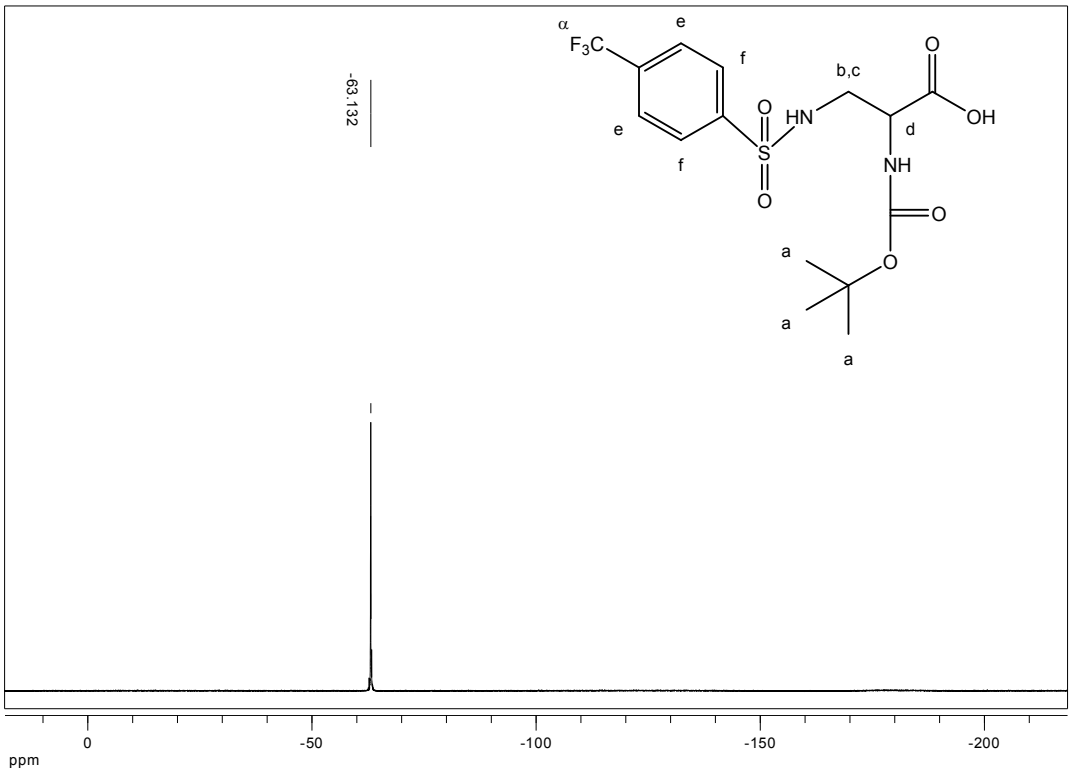

Figure 3.41 ^{19}F NMR spectrum of Boc-Dpr(CF_3-Bn-SO_2)-OH (**18**). Solvent: $CDCl_3$.

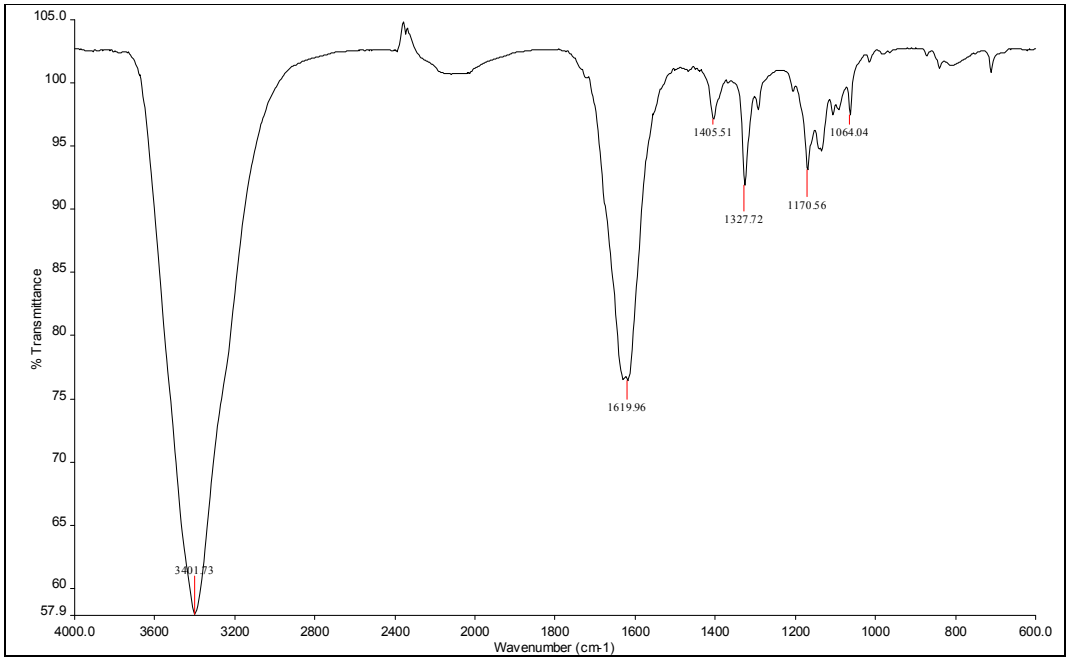

Figure 3.42 ATR spectrum of Boc-Dpr(C_3F_7C(=O))-OH (**19**).

Table 3. 3 Physical properties of N_β-substituted Asparagine and Dpr-OH moieties.

Molecule No.	Physical State	Melting Point (°C)	TLC, R_f (Butanol 1/ Toluene 1/ Acetic acid 1/ Water 0.5)	% Yield
Boc-Dpr-OH	White powder	-	0.20	70
16	Powder, yellowish white	110-116	0.95	80
17	Oil, clear	-	0.60	75
18	Powder, creamy white	118-122	0.65	65
19	Oil, clear	-	0.13	55

3.3. BIOLOGICAL EVALUATION

3.3.1. Introduction

Diaminopropionic acids have found wide use in biological research as well as pharmaceutics (**Chapter 1**). In our work, we have synthesized the Mes-SO_2-Ala-OH, the alanine moiety in SJ749 as well as the fluorinated analogs of this molecule where fluorinated moieties are located in N_α or N_β. The biological studies included the proliferation of A-172 and U-87 cell lines within the medium containing the fluorinated molecules, hence the will be stated as drugs, and drugs have caused any decrease in the proliferation, their cytotoxic effects on the cell lines mentioned performed by Tuğba Sağır.

3.3.2. Proliferation

Proliferation is basically the increase in the cell number by cell division. In this study, the proliferation assays of A–172 and U–87 cell lines and the effect of the fluorinated molecules synthesized were performed with WST-1 kit.

Based upon the reduction of the tetrazolium salt WST–1 to formazan by cellular dehydrogenases, the generation of the dark yellow colored formazan is measured at 420–480 nm and is directly correlated to cell number.

3.3.3. Cytotoxicity

The term cytotoxicity is defined as the degree to which an agent possesses a specific destructive action on certain cells (François Maniez 2005) . In another resource, drug cytotoxicity is defined as the release of LDH from LDH-leaking cells as a percentage of total LDH activity (Furusawa, Wu et al. 1998).

3.3.4. Biological Assays

The figures suggest that diaminopropionate derivatives 3-amino-N-[(2,4,6-trimethylphenyl)sulfonyl]-L-alanine (**8**), 3-amino-N-[(4-fluorophenyl)sulfonyl]-L-alanine (**10**), 3-amino-N-heptafluorobutanoyl-L-alanine (**14**), N_{α}-(4-fluorobenzene sulfonyl)-L-Asn-OH (**9**), N_{α}-Heptafluorobutyryl-L-Asn-OH (**13**), N_{α}t-Boc-L-Dpr-OH (**15**), and N_{β}-Heptafluorobutyryl- N_{α}t-Boc-L-Dpr-OH (**19**) are not toxic to any of the glioblastoma cell lines *in vitro*. The diaminopropionic moiety of SJ749 3-amino-N-[(2,4,6-trimethylphenyl)sulfonyl]-L-alanine (**8**) does not significantly inhibit the proliferation of A–172 cancer cells. So we can conclude that the molecules we have synthesized have the same non-toxic effect as our control group (**8**).

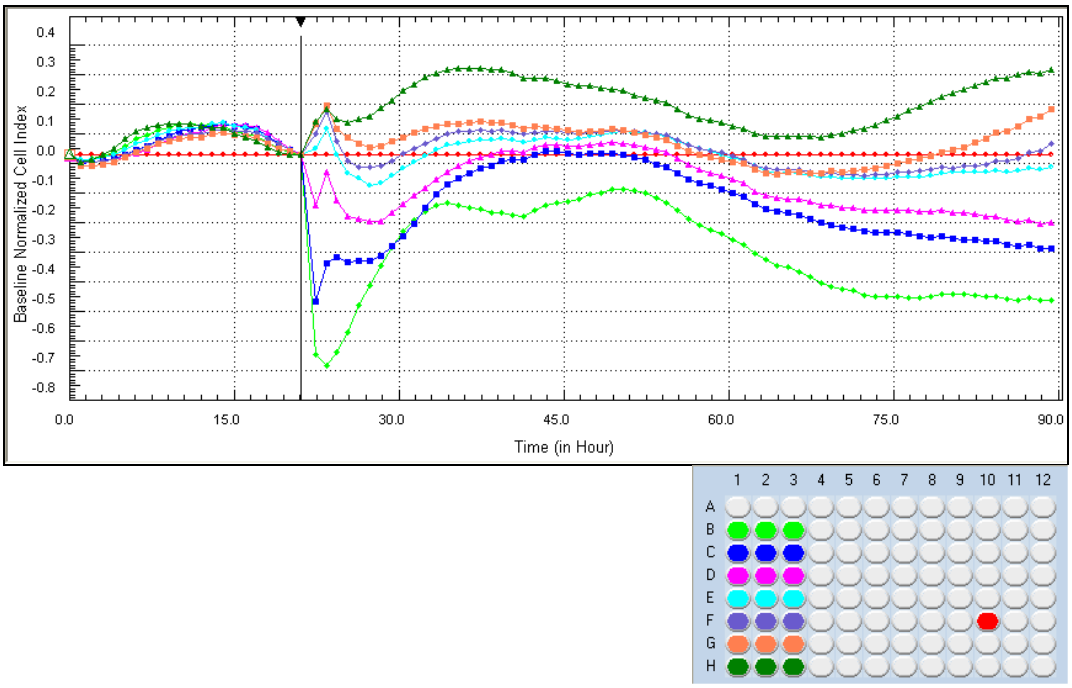

Figure 3.43 The determination of the cell index values of the effect of Mes-Ala-OH **(8)** on A-172 cell line xCelligence Real Time Cell Analysis System. The concentrations decrease from B to H. The concentrations are as follows: 100, 50, 25, 12.5, 6.25, 3.13, and 1.56 µM in series B, C, D, E, F, G, and H, respectively

In Figures 3.43, 3.44, 3.45, and 3.46 the most concentrated samples have cytotoxic effects on the cells whereas the lowest concentration 1.25 µM increases the cell index. The other results lie somewhere between these areas. Figures 3.47 and 3.48 show that (**8**), (**10**), and (**14**) do not increase cytotoxicity, instead it looks like these chemicals serve beter for the viability of the cells on which tests have been performed. Based on these results, we can conclude that molecules (**8**) and (**10**) as well as (**14**) do not have a significant cytotoxic effect on A-172 cell line.

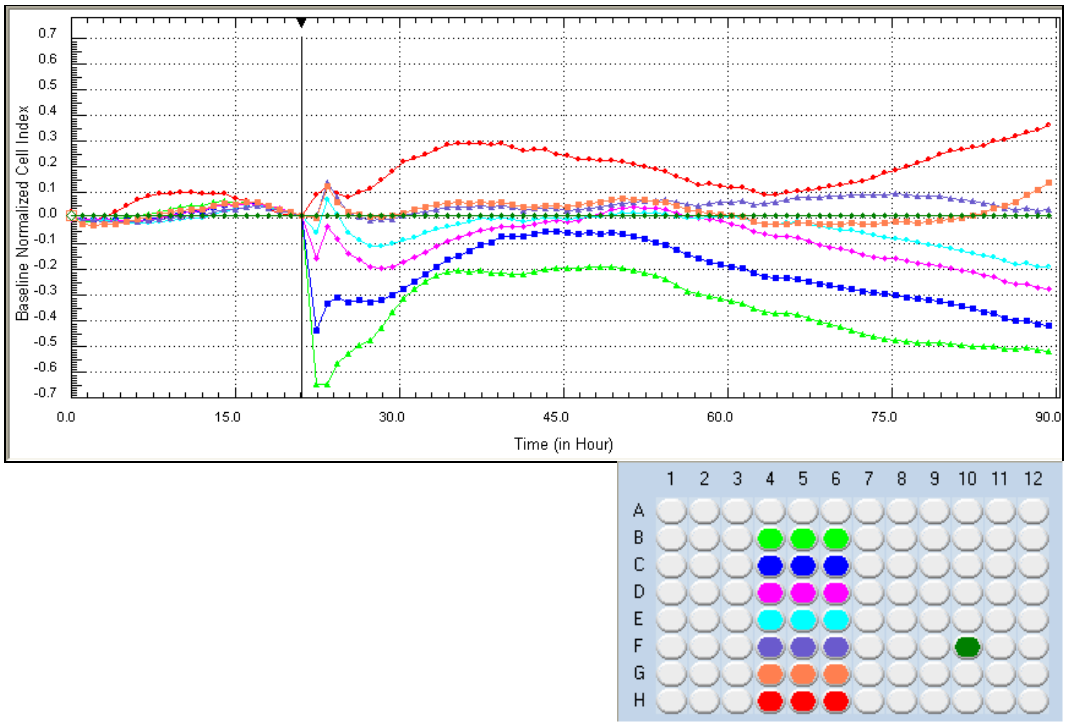

Figure 3.44 The determination of the cell index values of the effect of F-Bn-SO_2-Ala-OH **(10)** on A-172 cell line xCelligence Real Time Cell Analysis System.

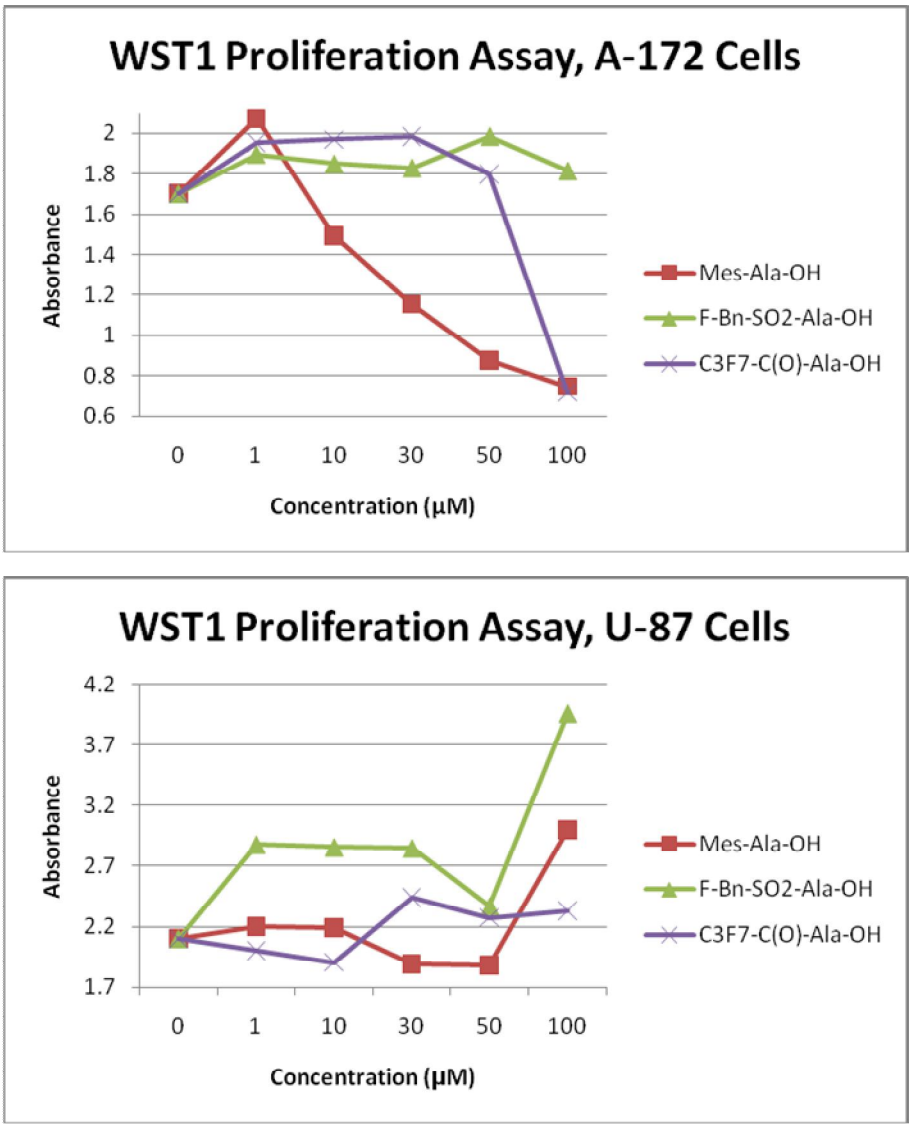

Figure 3.45 Proliferative effects of substituted diaminopropionic acid moieties – I: Molecules **(8)**, **(10)**, and **(14)** on **a)** A-172, **b)** U-87 cell lines after cells were exposed to the chemicals for 24 hours. Assays were performed on 96-well plates and findings were based on duplicate readings. The absorbance values were found by subtracting the reference absorbance at 690 nm from the absorbance values at 450 nm.

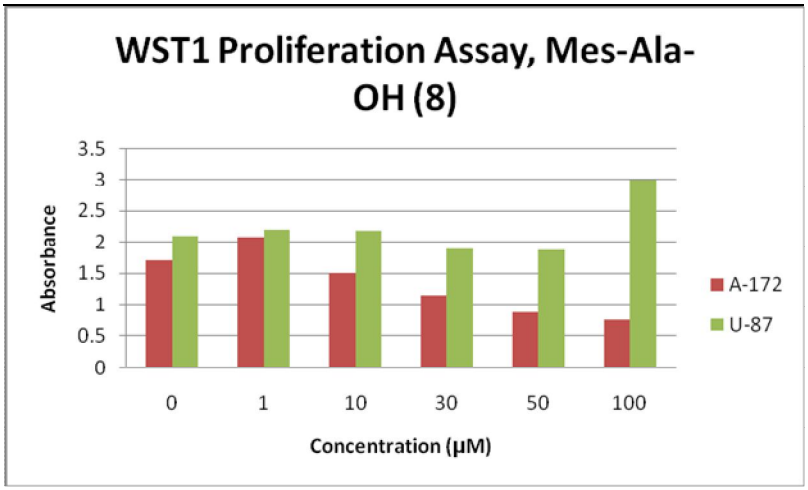

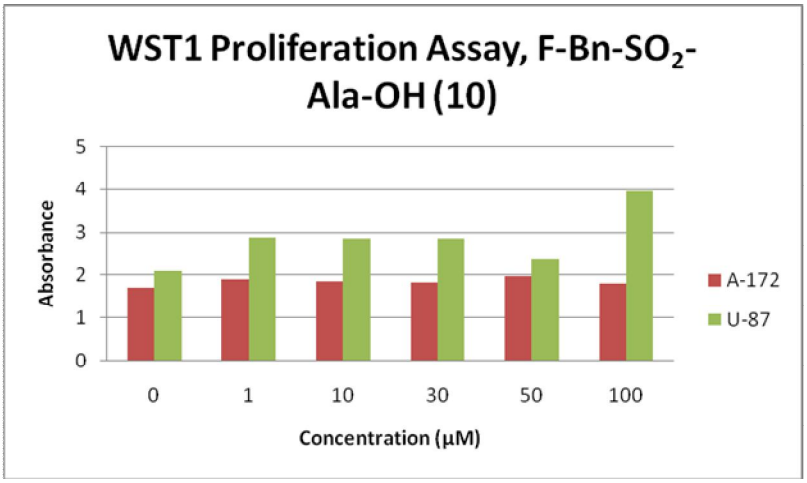

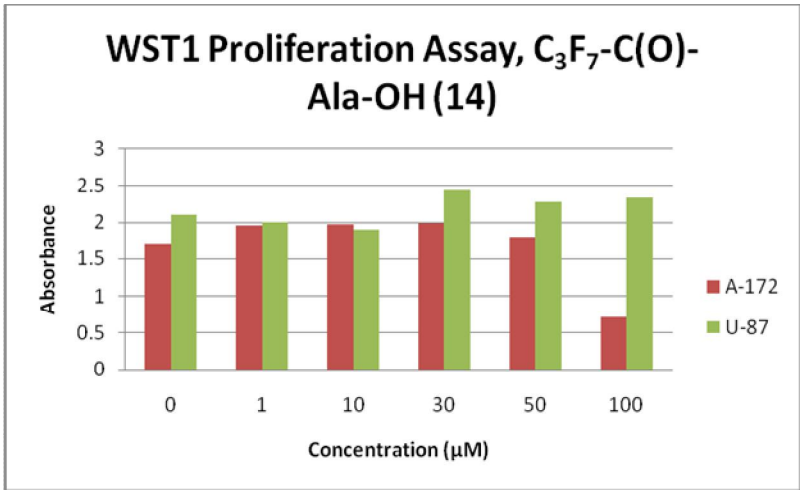

Figure 3.46 The comparison of the proliferative effects of substituted diaminopropionic acid moieties – I: Molecules **a) (8)**, **b) (10)**, and **c) (14)** on A-172 and U-87 cell lines after cells were exposed to the chemicals for 24 hours. Assays were performed on 96-well plates and findings were based on duplicate readings. The absorbance values were

found by subtracting the reference absorbance at 690 nm from the absorbance values at 450 nm.

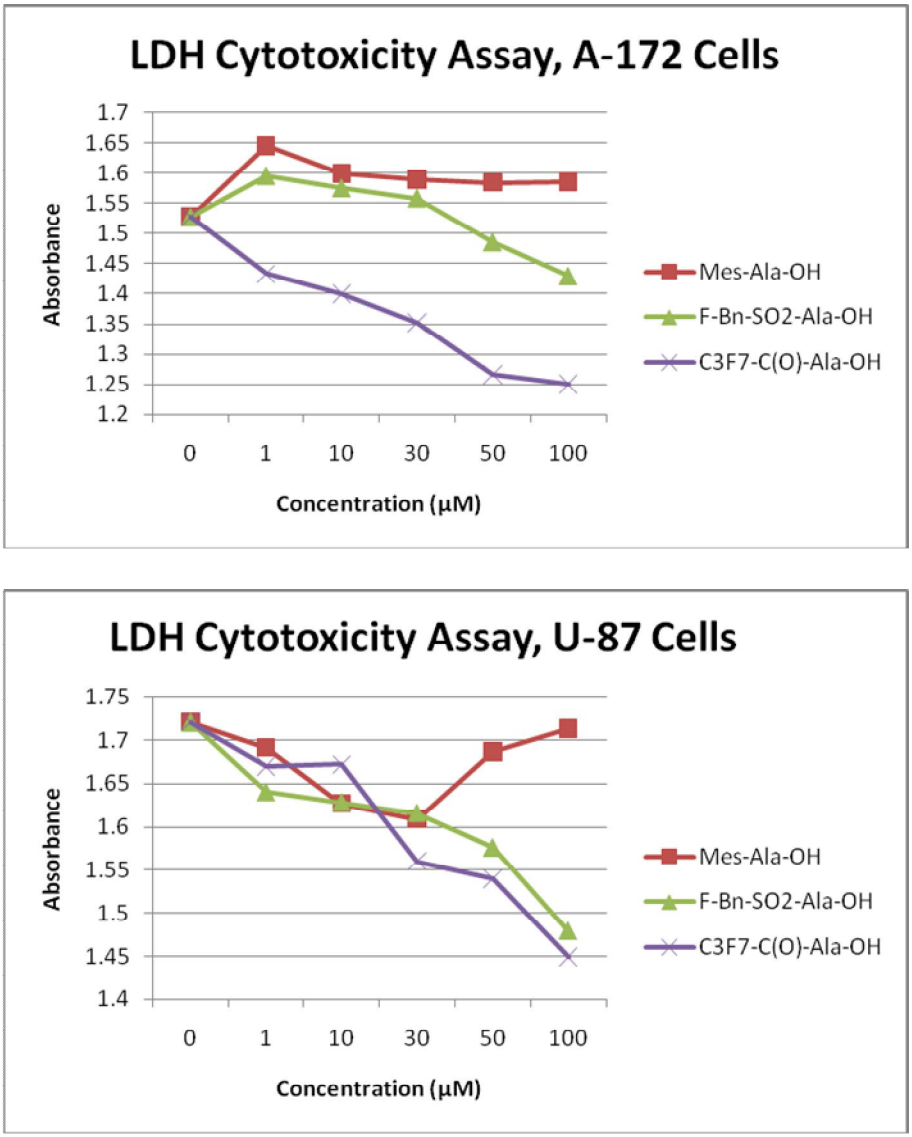

Figure 3.47 The evaluation of the cytotoxic effects of substituted diaminopropionic acid moieties – I: Molecules **(8)**, **(10)**, and **(14)** on **a)** A-172, **b)** U-87 cell lines after cells were exposed to the chemicals for 24 hours. Assays were performed on 96-well plates and findings were based on duplicate readings. The absorbance values were found by subtracting the reference absorbance at 690 nm from the absorbance values at 490 nm.

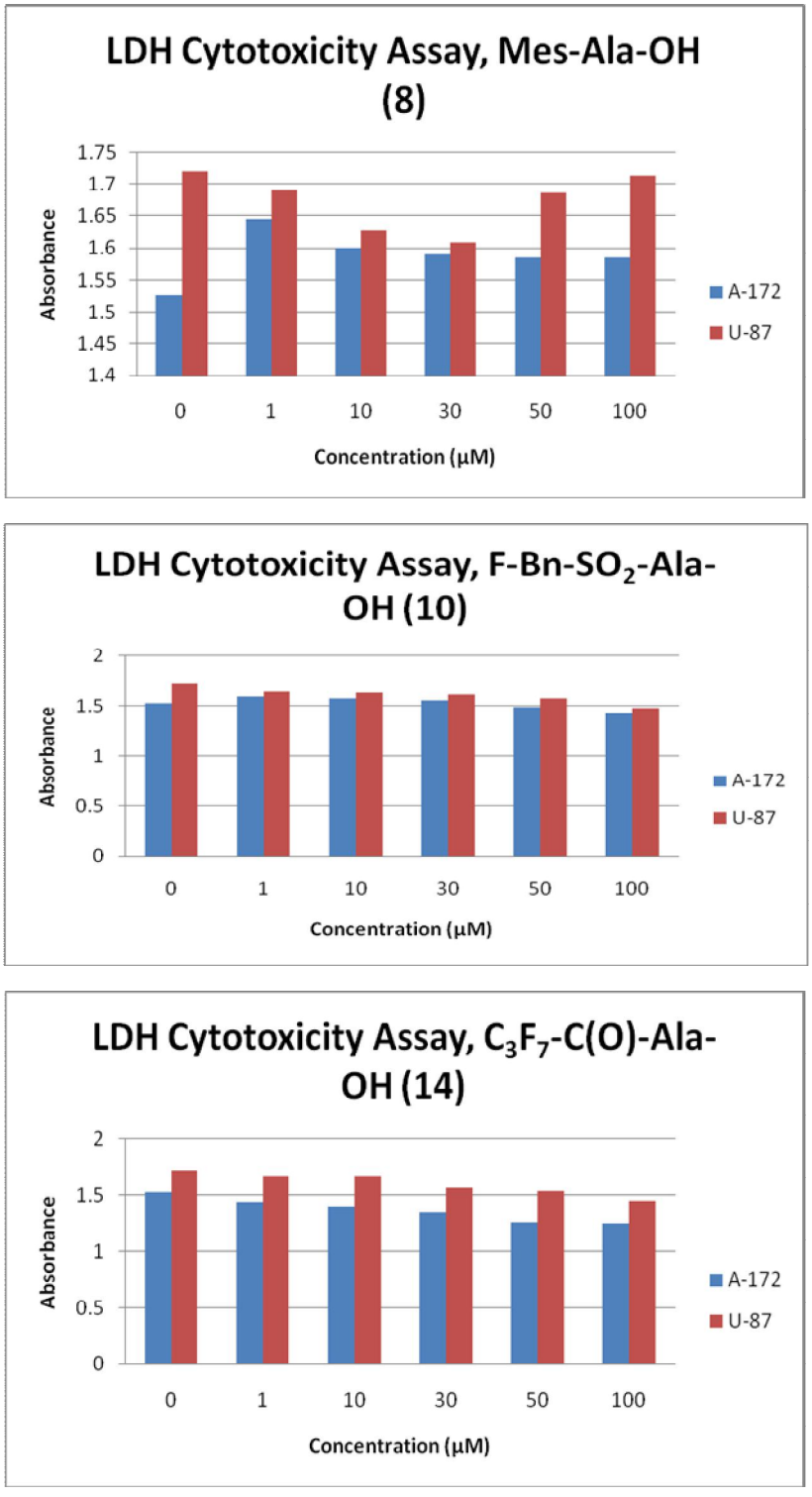

Figure 3.48 The comparison of the cytotoxic effects of substituted diaminopropionic acid moieties – I: Molecules **a) (8)**, **b) (10)**, and **c) (14)** on A-172 and U-87 cell lines after cells were exposed to the chemicals for 24 hours. Assays were performed on 96-well plates and findings were based on duplicate readings. The absorbance values were

found by subtracting the reference absorbance at 690 nm from the absorbance values at 450 nm.

The best values for the cytotoxicity of all three molecules in A-172 are observed at their lowest concentration 1 µM while the cytotoxicity decreases as the concentration in each molecule increases in A-172 cells. This is also the case for U-87 cells except that Mes-Ala-OH has an increasing cytotoxic effect as its concentration raises between 30 and 50 µM. Mes-Ala-OH might serve specific for also other types of integrins hence the cytotoxicity in U-87 cells increases along with its concentration, or it may not effect the cytotoxicity at all when we look at the overall graph of it. The inverse correlation between (**10**) and (**14**)'s cytotoxicities and concentrations suggests that these molecules might be serving as nutrients for the A-172 and U-87 cancer cell lines. That may be true because it is known that amino acids are constituents of cells

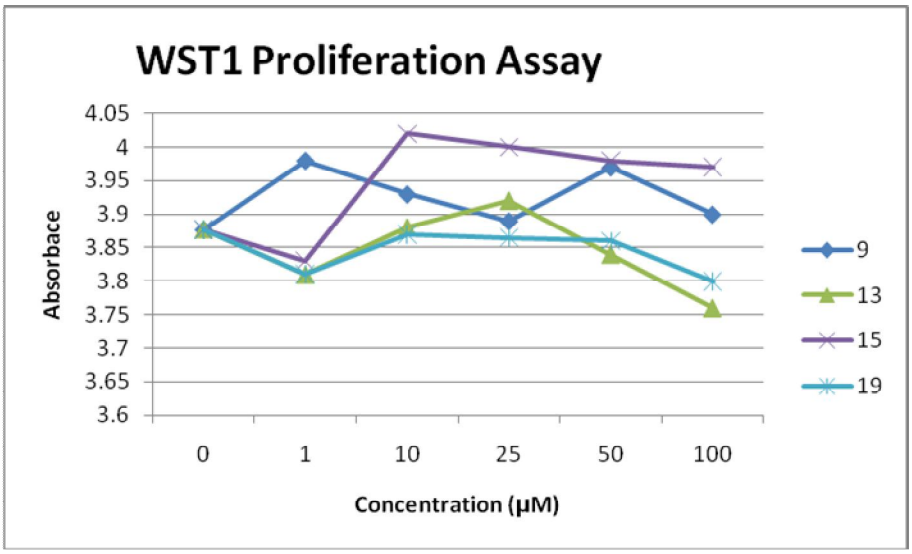

Figure 3.49 Proliferative effects of substituted diaminopropionic acid moieties – II: Molecules **(9)**, **(13)**, **(15)** and **(19)** on U-87 cell lines after cells were exposed to the chemicals for 24 hours. Assays were performed on 96-well plates and findings were based on duplicate readings. The absorbance values were found by subtracting the reference absorbance at 690 nm from the absorbance values at 450 nm.

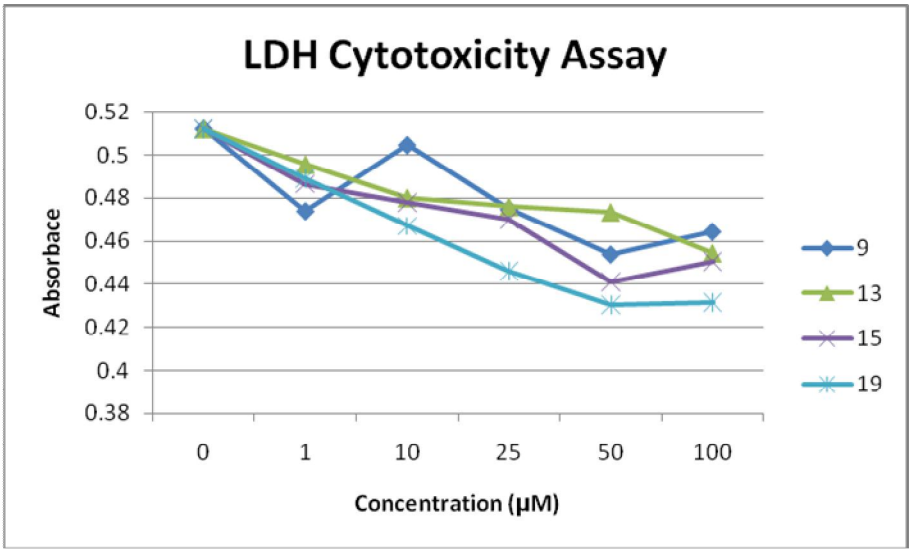

Figure 3.50 The evaluation of the cytotoxic effects of substituted diaminopropionic acid moieties – II: Molecules **(9)**, **(13)**, **(15)** and **(19)** on U-87 cell lines after cells were exposed to the chemicals for 24 hours. Assays were performed on 96-well plates and findings were based on duplicate readings. The absorbance values were found by subtracting the reference absorbance at 690 nm from the absorbance values at 490 nm.

Figures 3.49 and **3.50** show the proliferation and cytotoxicity graphs of chemicals **(9), (13), (15)** and **(19)** on U-87 cell line, respectively. Although all these chemicals decrease the proliferation generally least at their lowest concentration 1 µM and most at their highest concentration (**Figure 3.49**), the cytotoxicity graph on **Figure 3.50** suggests that the lowest concentration of these molecules serve as the best cytotoxic value on U-87 cells.

CHAPTER 4

CONCLUSIONS

Integrin family receptors, deemed as the moderators of cellular responses to cell proliferation, motility and differentiation, is one of the most promising topic in discovery of anti-cancer and anti-angiogenesis drugs. In this study, the spirocyclic intermediate on the way to the synthesis of SJ749 was synthesized as well as the alanine moiety and its fluorinated molecules followed by the evaluation of their biological activity. The alanine moiety Mes-SO_2-Ala-OH **(8)** was not found to be toxic. The fluorinated compounds synthesized were found not to be toxic on A-172 and U-87 astrocytoma cell lines either as expected. These results suggest that we need to have the full structures to inhibit the binding of integrin $\alpha 5\beta 1$ to fibronectin.

REFERENCES

Alberts, B. J., Alexander; Lewis, Julian; Raff, Martin; Roberts, Keith; Walter, Peter. *Molecular Biology of the Cell*, Garland Science, USA, 2002.

Archambaud, S., F. Legrand, K. Aphecetche-Julienne, S. Collet, A. Guingant and M. Evain. "Total Synthesis of (+)-Brefeldin C, (+)-nor-Me Brefeldin A and (+)-4-epi-nor-Me Brefeldin A", *European Journal of Organic Chemistry*, Vol. 7, pp. 1364-1380, January 2010.

Arnaout, M. A., B. Mahalingam, and J. P. Xiong. "Integrin structure, allostery, and bidirectional signaling", *Annual Review of Cell and Developmental Biology*, Vol. 21, pp. 381-410, November 2005.

Barczyk, M., S. Carracedo and D. Gullberg. "Integrins", *Cell and Tissue Research*, Vol. 339, No. 1, pp. 269-280, January 2010.

Englund, E. A., H. N. Gopi and D.H. Appella. "An efficient synthesis of a probe for protein function: 2,3-diaminopropionic acid with orthogonal protecting groups", *Organic Letters*, Vol. 6, No. 2, pp. 213-215, January 2004.

Ferrario, C. M. "Angiotensin I, angiotensin II and their biologically active peptides", *Journal of Hypertension*, Vol. 20, No. 5, pp. 805-807, May 2002.

Furusawa, S., J. Wu, , T. Fujimura, S. Nakano, S. Nemoto, M. Takayanagi, K. Sasaki and Y. Takayanagi. "Cepharanthine inhibits proliferation of cancer cells by inducing apoptosis", *Methods and Findings in Experimental and Clinical Pharmacology*, Vol. 20, No. 2, pp. 87-97, March 1998.

Grygorenko, O. O., I. V. Komarov and C. Cativiela. "A novel approach to 2,4-ethanoproline", *Tetrahedron-Asymmetry*, Vol. 20, No. 12, pp. 1433-1436, July 2009.

Gurrath, M. M., G.; H. Kessler, M. Aumailley and R. Timpl. "Conformation/activity studies of rationally designed potent anti-adhesive RGD peptides", *European Journal of Biochemistry* Vol. 210, No. 3, pp. 911-921, December 1992.

Heckmann, D. *Design and Synthesis of Selective Ligands for the α5β1 Integrin Receptor and Cyclic Peptides as Affinity Ligands for Factor VIII Purification*. Doktors der

Naturwissenschaften, Garching, Technische Universität München, 2007.

Huveneers, S., H. Truong, and H.J. Danen. "Integrins: signaling, disease, and therapy", *International Journal of Radiation Biology*, Vol. 83, No. 11-12, pp. 743-751, 2007.

Isanbor, C. and D. O'Hagan. "Fluorine in medicinal chemistry: A review of anti-cancer agents", *Journal of Fluorine Chemistry*, Vol. 127 No. 3, pp. 303-319, 2006.

Jones, M. L., M. T. Harper, E. W. Aitken, C. M. Williams, and A. W. Poole. "RGD-ligand mimetic antagonists of integrin alphaIIbbeta3 paradoxically enhance GPVI-induced human platelet activation", *Journal of Thrombosis and Haemostasis*, Vol. 8, No. 3, pp. 567-576, 2010.

Lapis, K. "Host defense peptides and peptidomimetics as new weapons for cancer treatment", *Magyar Onkológia*, Vol. 54, No: 1, pp. 47-58, 2010.

Le, Y., J. M. Wang, X. Liu, Y. Kong, X. Hou, L. Ruan, and H. Mou. "Biologically active peptides interacting with the G protein-coupled formylpeptide receptor", *Protein and Peptide Letters*, Vol. 14, No. 9, pp. 846-853, 2007.

Liu, F., A. G. Stephen, R. J. Fisher, and Burke, Jr. T. R. "Protected aminooxyprolines for expedited library synthesis: application to Tsg101-directed proline-oxime containing peptides", *Bioorganic and Medicinal Chemistry Letters*, Vol. 18, No. 3, pp. 1096-1101, February 2008.

Liu, Y., B. L. Oliveira, J. D. G. Correia, I. .C. Santos, I. Santos, B. Spingler and R. Alberto. "Syntheses of bifunctional 2,3-diamino propionic acid-based chelators as small and strong tripod ligands for the labelling of biomolecules with Tc-99m", *Organic and Biomolecular Chemistry*, Vol, 8, No. 12, pp. 2829-2839, June 2010.

Maglott, A., P. Bartik, S. Cosgun, P. Klotz, P. Rondé, G. Fuhrmann, K. Takeda, S. Martin, and M. Dontenwill. "The small alpha5beta1 integrin antagonist, SJ749, reduces proliferation and clonogenicity of human astrocytoma cells", *Cancer Research* Vol. 66, No. 12, pp. 6002-6007, June 2006.

Maniez, F. and Welsby, P. D. *L'anglais médical en situation : interrogatoire et examen clinique. Tome 2*, Elsevier Masson, Paris, France, 2005.

Mousa, S. A. "Anti-integrin as novel drug-discovery targets: potential therapeutic and diagnostic implications", *Current Opinion in Chemical Biology,* Vol. 6, No. 4, pp. 534-541, August 2002.

O'Connor, S. “Rational drug design, medicinal chemistry, planned serendipity and the impact of automation on the drug discovery process”, *The Journal of Automatic Chemistry*, Vol. 15, No. 1, pp. 9-12, January-February 1993.

Ojima, I. *Fluorine in Medicinal Chemistry and Chemical Biology*, Wiley-Blackwell, Chichester, U.K., April 2009.

Patrono, C. and B. Rocca. "The Future of Antiplatelet Therapy in Cardiovascular Disease", *Annual Review of Medicine,* Vol. 61, No. 1, pp.49-61, February 2010.

Pitts, W. J., J. Wityak, J. M. Smallheer, A. E. Tobin, J. W. Jetter, J. S. Buynitsky, P. P. Harlow, K. A. Solomon, M. H. Corjay, S. A. Mousa, R. R. Wexler, and Prabhakar K. Jadhav. "Isoxazolines as potent antagonists of the integrin alpha(v)beta(3)", *Journal of Medicinal Chemistry*, Vol. 43, No. 1, pp.27-40, December 1999.

Ruoslahti, E. and M. D. Pierschbacher. "Arg-Gly-Asp: a versatile cell recognition signal" *Cell*, Vol. 44, No. 4, pp. 517-518, July 1986.

Shanmugham, M. S. and J. D. White. "A new route to furanoeremophilane sesquiterpenoids. Synthesis of (+/-)-6 beta-hydroxyeuryopsin" *Chemical Communications*, Vol. 1, No. 1, pp. 44-45, January 2004.

Takagi, J. "Structural basis for ligand recognition by RGD (Arg-Gly-Asp)-dependent integrins", *Biochemical Society Transactions,* Vol. 32, No. Pt3, pp.403-406, June 2004.

Tamkun, J. W., D. W. DeSimone, D. Fonda, R. S. Patel, C. Buck, A. F. Horwitz, and R. O. Hynes. "Structure of integrin, a glycoprotein involved in the transmembrane linkage between fibronectin and actin", *Cell*, Vol. 46, No. 2, pp.271-282, July 1986.

Vagner, J., H. Qu, and V. J. Hruby. "Peptidomimetics, a synthetic tool of drug discovery", *Current Opinion in Chemical Biology* Vol. 12, No. 3, pp.292-296, June 2008.

Venkataramanarao, R., N. S. Sudarshan, and V. V. Sureshbabu. "Microwave assisted alcoholysis of isocyanates derived from N-alpha-[(9-fluorenylmethyl)oxy]carbonyl amino acids: Synthesis of N-Fmoc-N-^{1}-Z-/Boc-/Alloc-/Bsmoc-gem-diamines", *International Journal of Peptide Research and Therapeutics,* Vol. 13, No. 3, pp. 393-397, September 2007.

Wang YP, and R. Lai. "Insect antimicrobial peptides: structures, properties and gene regulation", *Dongwuxue.Yanjiu,* Vol. 31, No. 1, pp.27-34, February 2010.

Zaidel-Bar, R., S. Itzkovitz, A. Ma'ayan, R. Iyengar and B. Geiger. "Functional atlas of the integrin adhesome", *Nature Cell Biology*, Vol. 9, No. 8, pp. 858-867, August 2007.

Zhang, L.-h., G. S. Kauffman, J. A. Pesti and J. Yin. "Rearrangement of Nα-Protected l-Asparagines with Iodosobenzene Diacetate. A Practical Route to β-Amino-l-alanine Derivatives", *The Journal of Organic Chemistry*, Vol. 62, No. 20, pp. 6918-6920, October 1997.

Zheng, X., J. G. Cao, W. D. Meng and F. L. Qing. "Synthesis and anticancer effect of B-ring trifluoromethylated flavonoids", *Bioorganic & Medicinal Chemistry Letters*, Vol. 13, No. 20, pp.3423-3427, October 2003.